# 4/2011

# environment protection engineering

published quarterly

Wrocław 2011

*Editorial Office*

Faculty of Environmental Engineering
Wrocław University of Technology
Wybrzeże Wyspiańskiego 27, 50-370 Wrocław, Poland

*Publisher*

Wrocław University of Technology, Wybrzeże Wyspiańskiego 27, 50-370 Wrocław

Oficyna Wydawnicza Politechniki Wrocławskiej
Wybrzeże Wyspiańskiego 27, 50-370 Wrocław
http://www.oficyna.pwr.wroc.pl, e-mail: oficwyd@pwr.wroc.pl



Drukarnia Oficyny Wydawniczej Politechniki Wrocławskiej. Order No. 1169/2011.

CONTENTS

Environment Protection Engineering

Vol. 37 2011 No. 4

WOJCIECH M. BUDZIANOWSKI*

# $CO_2$ REACTIVE ABSORPTION FROM FLUE GASES INTO AQUEOUS AMMONIA SOLUTIONS: THE $NH_3$ SLIPPAGE EFFECT

Future deployment of $NH_3$-based $CO_2$ capture technology into coal-fired power plants will shift unwanted emissions from those currently comprising $SO_2$, $NO_X$ and particulate matter towards those comprising $NH_3$. This is due to volatility of ammonia. Therefore, the current paper aims at understanding of $NH_3$ slippage to flue gases from the $NH_3$-based $CO_2$ capture process and at identifying the opportunities to limit this unwanted slippage. The paper presents experimental and 2D modelling-based analysis of $CO_2$ reactive absorption from flue gases into aqueous ammonia solutions in a falling film reactor. The results enable one to characterise hydrodynamics of the falling film reactor, to analyse the effect of pH, pressure and temperature on $CO_2$ absorption and $NH_3$ slippage and to explain the role of migrative transport of ionic species in total mass transport. It was found that $NH_3$ slippage to the gaseous phase can be limited by alleviated operating temperatures, optimised pH, increased pressure and large $CO_2$ absorption fluxes which force negative enhancement of $NH_3$ mass transfer [16]. The $NH_3$ slippage under $CO_2$ capture conditions and under air stripping conditions is illustrated by experimental and simulation data. Finally, main approaches used for the integration of CCS systems into power plants are expounded.

## 1. INTRODUCTION

Recent atmospheric observations confirm that the concentration of $CO_2$ in the atmosphere has increased by nearly 30% for the last 150 years, with an accelerating trend in last years. The global mean concentration of $CO_2$ in 2005 was 379 ppm, leading to a radiative forcing of 1.66 $W \cdot mol^{-2}$. For the 1995–2005 decade, the growth rate of $CO_2$ in the atmosphere was 1.9 $ppm \cdot yr^{-1}$ and the $CO_2$ radiative forcing increased by 20%: this is the largest increase observed for any decade in at least the last 200 years. From 1999 to 2005, global $CO_2$ anthropogenic emissions from fossil fuel and cement production increased at the rate of roughly 3% by year [1].

*Faculty of Chemistry, Division of Chemical and Biochemical Processes, Wrocław University of Technology, WybrzeżeWyspiańskiego 27, Wrocław, Poland, e-mail: wojciech.budzianowski@pwr.wroc.pl

There are two major carbon reservoirs which comprise 99.90% of the total Earth's carbon, i.e. carbon rocks (limestone, chalk, dolomite) and organic-rich rocks (coal, oil, natural gas) [2]. Both those reservoirs are intensively exploited, e.g. in cement and energy production, respectively; leading to large anthropogenic emissions of $CO_2$ into the atmosphere. At the same time, Earth's plant-covered areas are severely limited due to the civilisation development and thus the remaining plants are unable to recycle all the emitted carbon back to organic-rich rocks or at least into the soil. Also, it must be noted that carbon rocks formation in deep oceans is a very slow process which requires absorption of atmospheric $CO_2$ into oceans. When Earth's temperature rises, the $CO_2$ solubility in water alleviates, which limits the role of oceanic $CO_2$ sink and can even the release of some $CO_2$ dissolved in oceans amplifying the initial global warming.

Therefore, it can be concluded that recent human activities such as uncontrolled exploitation of natural carbon reservoirs and reduction in atmospheric $CO_2$ recycle potentials by plants and oceans can contribute to net anthropogenic $CO_2$ emissions as it is clearly evidenced by recent atmospheric measurements [1]. $CO_2$ is the final product of numerous human activities which in large quantities accumulates in the atmosphere causing dangerous climate changes.

Consequently, urgent deployment of renewable and nuclear energy technologies is needed, while $CO_2$-intensive power plants must be integrated with carbon capture and sequestration (CCS). Therefore, the current paper provides modelling analysis of $CO_2$ separation from flue gases by using aqueous ammonia solutions in a falling film reactor. The study investigates complex phenomena of mass transfer, chemical reactions, electrochemistry and hydrodynamics in very simple but offering realistic operating conditions reactor geometry. Results of the simulation and experiments illustrate the problem of $NH_3$ slippage to the gaseous phase and discuss opportunities to limit this unwanted slippage.

## 2. MODELLING OF $CO_2$ ABSORPTION INTO AQUEOUS AMMONIA SOLUTIONS

Absorption of $CO_2$ into aqueous ammonia solutions has attracted attention as a potential CCS method for power plants relatively recently [3].

### 2.1. REACTION KINETICS AND THERMODYNAMICS

The most important liquid phase elementary chemical reactions in the $CO_2$–$NH_3$––$H_2O$ system are presented in Table 1.

Table 1

Elementary chemical reactions in the $CO_2$–$NH_3$–$H_2O$ system

| Equation | Process | No. |
|---|---|---|
| $CO_2 + NH_3 \longleftrightarrow NH_2COO^- + H^+$ | formation of ammonia carbamate | (1) |
| $CO_2 + OH^- \longleftrightarrow HCO_3^-$ | formation of bicarbonate by combination of $CO_2$ with hydroxyl ions | (2) |
| $HCO_3^- \longleftrightarrow CO_3^{2-} + H^+$ | formation of carbonate | (3) |
| $NH_3 + H_2O \longleftrightarrow NH_4^+ + OH^-$ | hydrolysis of ammonia | (4) |
| $H_2O \longleftrightarrow OH^- + H^+$ | dissociation of water | (5) |

Equations for reaction rates are summarised in Table 2.

Table 2

Rates of elementary reactions from Eqs. (1)–(5)

| No. | Kinetics | Source |
|---|---|---|
| (1) | $R_{(1)} = 1.66 \cdot 10^{11} \exp\left(\frac{-61000}{R^G T}\right) C_{CO_2} C_{NH_3}$ | [4] |
| (2) | $R_{(2)} = 4.32 \cdot 10^{10} \exp\left(\frac{-55420}{R^G T}\right) C_{CO_2} C_{OH^-}$ | [5, 6] |
| (3)–(5) | instantaneous reactions | [7] |

$CO_2$ absorbed in ammonia solutions forms ammonia carbamate being a dominant species at low $CO_2$ loadings and in presence of excess $NH_3$. For higher $CO_2$ concentrations and hence for lower free ammonia concentrations, the equilibria of ammonia carbamate are shifted to favour bicarbonate formation. This shift allows higher $CO_2$ loadings to be achieved in $NH_3$-based systems compared with MEA-based systems where $CO_2$ remains predominantly as a carbamate. Such observations have been confirmed by Mani et al. [8] based on $^{13}C$ NMR spectroscopy. However, the equilibria shifting towards bicarbonate requires higher pH in order to have higher concentrations of hydroxyl ions which promote bicarbonate formation (Eq. (2)). Carbamate formation is accompanied by $H^+$ generation which lowers pH and favouring hydrolysis of free ammonia. When free ammonia is completely hydrolysed pH decreases and bicarbonate formation may stop due to relevant equilibria shifting.

Modelling of reversibility of reactions (1)–(5) is based on reaction equilibrium constants [7]. The rate of physical dissolution of gaseous $CO_2$, $NH_3$, and $H_2O$ in aqueous solutions is relatively high. Therefore, equilibrium at the interface can be assumed. For $CO_2$ and $NH_3$ the Henry's law may be introduced:

$$CO_{2\,(g)} \longleftrightarrow CO_{2\,(l)}, \qquad P_{CO_2} = H_{CO_2} C_{CO_2} \tag{6}$$

$$NH_{3\,(g)} \longleftrightarrow NH_{3\,(l)}, \qquad P_{NH_3} = H_{NH_3} C_{NH_3} \tag{7}$$

## 2.2. GOVERNING EQUATIONS

$CO_2$ reactive absorption into a $NH_3$–$H_2O$ electrolyte solution in a falling film reactor is described by using 2D modelling. A simplified 2D model includes reaction kinetics, chemical reaction equilibria, interphase equilibria, diffusion of species and convection, following modern process modelling directions outlined in [9]. The governing equations of the model in a liquid phase are:

$$D_i \frac{\partial^2 C_i(x,z)}{\partial x^2} - w_z(z) \frac{\partial C_i(x,z)}{\partial z} = -\sum_{r=1}^{r=NR} R_r(C_i) \tag{8}$$

- boundary conditions:

$$C_i(x,0) = C_i^{IN} \tag{9}$$

$$-D_i \frac{\partial C_i(\delta,z)}{\partial x} = 0 \tag{10}$$

- volatile species:

$$-D_i \frac{\partial C_i(0,z)}{\partial x} = k_i^{GP}\left(P_i - H_i C_i\right) \tag{11}$$

- non-volatile species:

$$-D_i \frac{\partial C_i(0,z)}{\partial x} = 0 \tag{12}$$

Further, in order to enable an in-depth analysis of electrochemical engineering aspects a more detailed 2D axis-symmetric model is formulated. This model can describe migration of ionic species in a liquid phase. It also includes mass and momentum balance for the gaseous phase domain and hence it does not require mass transfer coefficients at the gas side. Main electrochemical aspects in the liquid phase arise from the mass and charge balance:

$$\nabla \cdot \left(D_i \nabla C_i - w C_i + v_i F m_i C_i \nabla \phi\right) = -\sum_{r=1}^{r=NR} R_r(C_i) \tag{13}$$

$$\nabla \cdot \left(\lambda^E \nabla \phi\right) = 0 \tag{14}$$

### 2.3. A FALLING FILM REACTOR

Falling-film reactors offer very simple geometries and well defined hydrodynamics which makes them to be well-suited for detailed kinetic studies. Besides, falling film reactors offer adjustable empty spaces and thus any crystallisation problems under highly concentrated and low temperature operating conditions can be limited. Furthermore, $CO_2$ separation processes under industrially relevant short contact times conditions usually do not approach equilibrium conditions due to limited reaction and mass transport rates. Hence reaction and mass transfer kinetics-oriented studies are of primary importance for detailed design of such gas–liquid reactors [10]. Figure 1 illustrates a falling film reactor utilised here for $CO_2$ separation from flue gases by aqueous ammonia solutions. The falling film reactor is well suited for aforementioned kinetic studies and can be operated in practical hydrodynamic conditions.

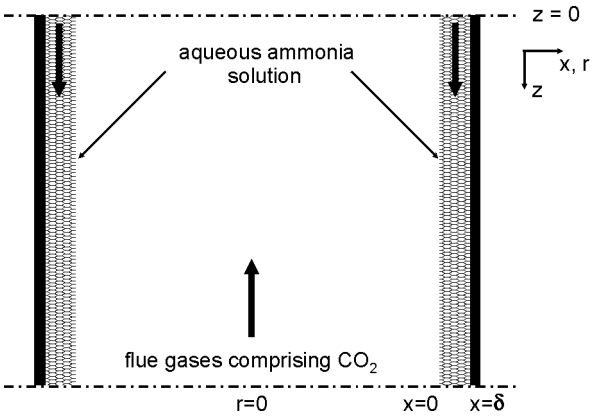


Fig. 1. Scheme of the falling film reactor

## 3. ANALYSIS OF THE $NH_3$ PROCESS

Among conventional $CO_2$ reactive processes, a monoethanolamine (MEA) process has been comprehensively studied and successfully used in chemical plants for $CO_2$ recovery. Although the MEA process is a promising method for the control of $CO_2$ emissions from massive discharging plants [11], it is a relatively expensive option. In addition, it has several major disadvantages including slow absorption rate, low solvent capacity, amine degradation by $SO_2$, $NO_2$, HCl, HF and $O_2$ from flue gases, high equipment corrosion rates, and high energy consumption during solvent regeneration (i.e. high heat of reaction compared with the $CO_2$-$NH_3$ system) [12].

In the MEA process $SO_2$ and $NO_X$ must be removed prior to $CO_2$ absorption. This preliminary costly removal might not be necessary when an aqueous ammonia solu-

tion is used which can capture all those acidic gases simultaneously with $CO_2$. The products of absorption of $CO_2$, $SO_2$ and $NO_X$ into aqueous ammonia solutions are ammonium bicarbonate, ammonium sulphate and ammonium nitrate, respectively, which are well known fertilizers for certain crops. Unfortunately, ammonia salts have high solubility in water. Their removal by, e.g. crystallisation followed by filtration or sedimentation, can be enhanced under the chilled $NH_3$ operating conditions (2–10 °C [13]) or by the addition of ethanol to aqueous ammonia solution which decreases solubility of salts [14]. Fertilisers from the $NH_3$ process offer great unexplored potential for cultivation of energy crops, i.e. biomass, which can tolerate fertilisers having lower quality and comprising some flue gas-derived impurities.

Further, an aqueous ammonia solvent is characterised in increased $CO_2$ absorption capacity of 1.2 kg $CO_2$/kg $NH_3$, while for MEA it is only 0.4 kg $CO_2$/kg MEA. There is little effect of oxidative degradation of ammonia as it comprises no carbon chains and thus it can offer improved solvent absorption/regeneration cycling. It has been shown [15] that $CO_2$ absorption fluxes into ammonia can be 3 times higher than those into MEA under similar conditions. Also in [14] it has been shown that aqueous ammonia solvent has very high $CO_2$ removal efficiency as compared with MEA or DGA solvents under similar operating conditions. Among major drawbacks of the $NH_3$ process one can indicate ammonia volatility which leads to the contamination of flue gases. All available methods directed at $NH_3$ removal [16] from diluted gases are costly. Therefore, to avoid ammonia slippage from the $NH_3$ process careful attention must be paid to all process design and operation aspects.

It should be emphasised that future deployment of $NH_3$-based $CO_2$ capture into power plants can change the composition of unwanted emissions from the energy-generating sector. Namely, $CO_2$ capture technologies using alkali aqueous solvents can offer simultaneous removal of $SO_2$, $NO_X$ and particulate matter (PM) thus those emissions will be reduced. However, $NH_3$-based $CO_2$ capture technologies can lead to large increase of $NH_3$ emissions [17] due to ammonia volatility. Therefore, the present study focuses on the opportunities for the reduction of $NH_3$ emissions in $NH_3$-based $CO_2$ capture systems. In this context, effects of ammonia volatility, falling film reactor hydrodynamics, pH, migration in electrolyte solutions, elevated pressure and temperature on the $NH_3$ process are analysed and discussed.

### 3.1. EFFECT OF AMMONIA VOLATILITY

Field tests of $CO_2$ capture into aqueous ammonia solutions indicate that a considerable ammonia slip to flue gases is frequently experienced under standard operating conditions. For instance Kozak et al. [18] have reported $NH_3$ contents in flue gases up to 2000 ppmv due to desorber instabilities, and for more stable operation the $NH_3$ slip has amounted up to 500 ppmv. Mathias et al. [19] have reported a smaller $NH_3$ slip from their absorber, i.e. 242 ppmv in flue gases. Current permissible limits in several countries allow release of flue gases comprising less than 10 ppmv $NH_3$. Therefore,

when utilising the $NH_3$ process, one must guarantee limited ammonia vaporisation to the gaseous phase.

$NH_3$ slippage to the gaseous phase can be reduced to meet the required level by controlling pH of the liquid, by making use of a negative enhancement of $NH_3$ transfer effect and by thorough process and reactor designs. pH of the liquid can be conveniently controlled by adjusting $NH_3$ content in water. Further, $NH_3$ transfer to the gaseous phase can be negatively enhanced in situations when $CO_2$ absorption flux is large enough to be able to substantially lower pH at the gas–liquid interface. Under the conditions of interfacial pH shift, $NH_3$ slippage can be limited even under total driving forces promoting $NH_3$ desorption [16].

Figure 2 shows $NH_3$ slippage under air stripping [20] experimental conditions. It can be observed that the $NH_3$ removal from the liquid is proportional to the stripping air flow rate. Such dependence is associated with gas–liquid phase equilibrium attained in the investigated conditions. Therefore, it can be concluded that the air-stripping process attains gas–liquid equilibrium at the investigated operating and geometrical ranges of parameters.

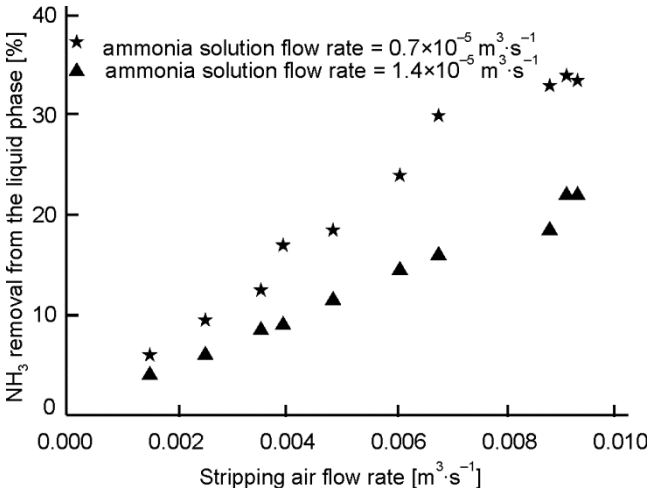


Fig. 2. $NH_3$ slippage under air stripping experimental conditions, the effect of air flow rate on $NH_3$ removal at 295 K, $P^{IN}_{CO_2} = 0$, $^{IN}_{NH_3} = 0$, $C^{IN}_{CO_2} = 20\ \text{mol}\cdot\text{m}^{-3}$, $C^{IN}_{NH_3} = 93\ \text{mol}\cdot\text{m}^{-3}$. Experimental data for the packed-bed counter-current stripper with packing height of 1 m and packing diameter of 0.1 m, 15 mm ceramic Raschig rings

Under $CO_2$ absorption conditions the phenomenon of $NH_3$ slippage is more complex. Figure 3 illustrates that the liquid concentration of free (i.e. undissociated) $NH_3$ decreases along the falling film reactor by means of two main mechanisms, i.e. by the reaction of $NH_3$ with $CO_2$ (Eq. (1)) and by $NH_3$ desorption to the gas. As it is seen,

under operating conditions utilising large $CO_2$ absorption flux, free $NH_3$ is completely reacted or desorbed within around 15 cm of the falling film reactor length. For comparison, when the desorption flux is switched off in the model and thus $NH_3$ is consumed solely by the aforementioned reactive mechanism, the required length is considerably prolonged to around 30 cm. The contribution of the two competing $NH_3$ consuming mechanisms strictly depends on process operating conditions [21]. It is expected that the contribution of $NH_3$ slippage can be substantially reduced by using process design approaches.

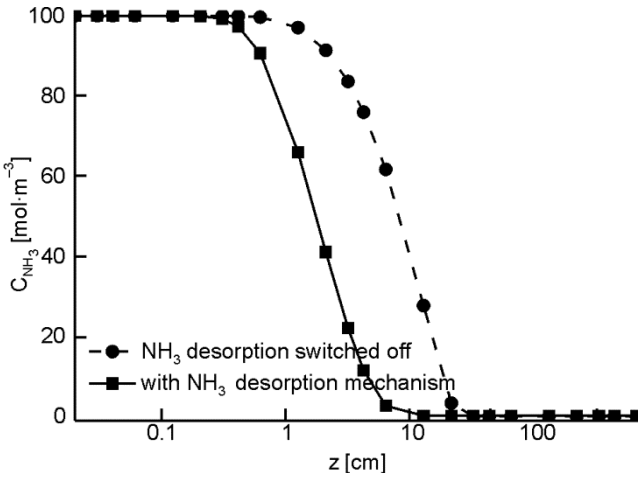


Fig. 3. $NH_3$ slippage under $CO_2$ absorption conditions, the effect of $NH_3$ desorption and reaction on $NH_3$ content in the liquid phase along the absorber at 288 K. $P^{IN}_{CO_2} = 10^4$ Pa, $P^{IN}_{NH_3} = 0/1$ Pa (without/with desorption), $C^{IN}_{CO_2} = 0$, $C^{IN}_{NH_3} = 100$ mol·m$^{-3}$. Simulations data from the simplified 2D model of the falling film reactor

The Henry's constant of ammonia is much lower than that of $CO_2$. $H_{NH_3}$ is typically of the order of 1 Pa m$^3$·mol$^{-1}$ while $H_{CO_2}$ typically amounts to the order of 2000 Pa·m$^3$·mol$^{-1}$. For instance, at $T$ = 288 K and $C_{NH_3}$ = 100 mol·m$^{-3}$ (free ammonia), the gaseous phase equilibrium partial pressure is 100 Pa $NH_3$, i.e. 1000 ppmv in flue gases (under atmospheric pressure) which means that free $NH_3$ can easily desorb to the gas since its desorption driving force is relatively large and shown in Fig. 2 gas–liquid equilibrium is likely. Further, $H_{NH_3}$ is a rising function of temperature; therefore lower temperatures should disfavour ammonia volatility. However, the dependence of $H_{NH_3}$ on $T$ is a relatively weak function, i.e. by decreasing temperature from 303 to 273 K, only a 5-fold drop in $H_{NH_3}$ is achieved. For instance, $NH_3$ partial pressure equilibrated with 100 mol·m$^{-3}$ of free $NH_3$ solution under 273 K is still around 40 Pa $NH_3$, i.e. 400 ppmv in flue gases (under atmospheric pressure). Consequently, new processes such as a chilled ammonia process [13] do not offer a complete solution to a $NH_3$

volatility problem and thus some additional $NH_3$ slippage limiting techniques are still necessary.

### 3.2. EFFECT OF PH ON MASS TRANSFER AND ON $NH_3$ SLIPPAGE

In practice, in $CO_2$ absorbers and solvent regenerators pH oscillates from 8,8 to 9,6 [12]. Ammonia slippage increases under high pH due to increased concentration of free $NH_3$ in the liquid. On the other hand, under lower pH $CO_2$ absorption is not enhanced by chemical reactions and thus $CO_2$ fluxes are degraded. Consequently, an optimum pH value should be found from economic evaluations of the whole $CO_2$ capture system. An optimum $NH_3$ content in water depends on $CO_2$ loading, $CO_2$ content in flue gases, temperature and pressure; however reasonable values can oscillate around 5%.

### 3.3. EFFECT OF HYDRODYNAMICS

In a falling film reactor, the liquid flow is solely driven by gravity while the gas flow is mainly driven by application of an external pressure, whereas gravity does virtually play no role. From present hydrodynamic analysis of the falling film reactor it can be deduced that liquid can be entrained by gas, especially for thin liquid films and large gas to liquid velocity ratios.

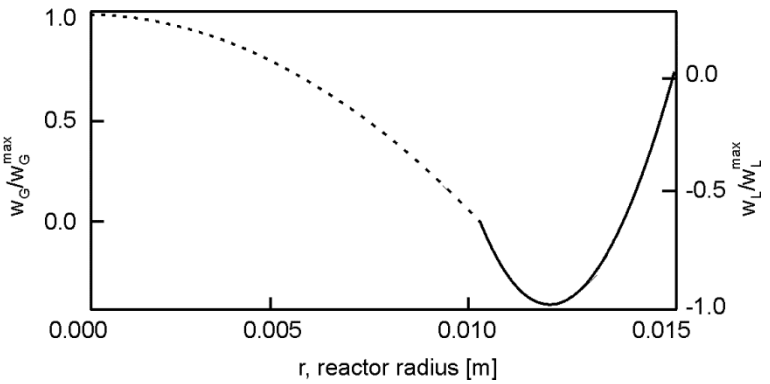


Fig. 4. Gas and liquid axial velocity profiles in a falling film reactor: dashed line – gaseous phase, solid line – liquid phase; $w_L$ – liquid velocity, $w_G$ – gas velocity, $w^{max}$ – maximum velocity in a relevant film. Simulation data from the detailed 2D axis-symmetric model of the falling film reactor

Figure 4 illustrates results of simulation for a vertical falling film reactor (cf. Fig. 1). The gas flows in an upward direction and its velocity at the gas–liquid interface is substantially decreased compared with the bulk gas velocity. The liquid phase velocity profile is more complex. Under the operating conditions shown in Fig. 4 liquid en-

trainment is exhibited, at least close to the gas–liquid interface. At the gas–liquid interface velocity discontinuity is observed (note that the scales are different in Fig. 4). At the wall, liquid velocity approaches 0 due to the domination of friction forces. Consequently, maximum liquid velocity is attained somewhere in between the interface and the wall. This hydrodynamic effect is very disadvantageous for $CO_2$ absorption fluxes since the velocity of saturated interfacial liquid is alleviated and hence its exposure time to the gas is prolonged. In contrast, this hydrodynamic effect can be beneficial for limiting $NH_3$ slippage, especially under the conditions of simultaneous large $CO_2$ absorption fluxes which can shift the equilibria at the gas–liquid interface towards complete consumption of free volatile ammonia.

It is expected that reactors with larger gas channels and of simpler geometry such as falling film reactors with thin liquid films can provide conditions for high $CO_2$ removal, low $NH_3$ slippage, ability to operation under high-pressure and to cope with salts crystallisation.

### 3.4. EFFECT OF MIGRATIVE SPECIES TRANSPORT

A $NH_3$–$CO_2$–$H_2O$ solution is a weak electrolyte and thus comprises numerous ionic species. Simulations conducted with the detailed 2D axis-symmetric model provide some interesting insights into the $NH_3$ process in this regard. Accordingly, apart from diffusive and convective motions involved, ionic species can also undergo migrative motion. According to the Nernst–Planck equation, migrative fluxes tend to reduce electrical potential gradients which arose here from diffusion of species (Eqs. (13), (14)). Such gradients of electrical potential can be formed when species substantially differ in diffusivities and when mass transfer fluxes are large. For instance, from the products of reaction in Eq. (1), $H^+$ cations have 3-fold higher diffusivity than carbamate anions. Hence, under a large $CO_2$ absorption flux, faster diffusion of $H^+$ from the gas–liquid interface creates small gradient of the electrical potential. In this electric field, carbamate anions formed diffuse and migrate in the same direction but $H^+$ cations migrate and diffuse in the opposite one. This effect arises from the same direction of diffusion for all species produced in the liquid film due to $CO_2$ absorption and the opposite directions of migration of ions with negative and positive valences, i.e. anions and cations, within the electric field. Consequently, the transport of a carbamate anion (which carries $CO_2$ and bounded $NH_3$) is enhanced by its migrative motion and thus $CO_2$ transport is favoured by a migrative mechanism from the interface to the liquid bulk. In a similar way, the migrative mechanism favours the transport of $NH_4^+$ from the liquid bulk to the gas–liquid interface beneficially facilitating ammonia transport. The above conclusions can also be deduced from Eq. (13) taking into account relevant valences of anions and cations as well as concentration and potential gradients formed in $CO_2$ absorption into aqueous $NH_3$. The migrative transport can only have indirect effect on $NH_3$ slippage since $NH_3$ is not an ionic species.

### 3.5. EFFECT OF ELEVATED PRESSURE

Elevated pressure affects vapour–liquid equilibria. It increases absorption fluxes and it alleviates desorption fluxes of both $CO_2$ and $NH_3$. Namely, under elevated pressure conditions partial pressures of $CO_2$ and $NH_3$ are increased by a factor comparable with a compression ratio applied. Increased partial pressures enhance $CO_2$ absorption and beneficially degrade $NH_3$ slippage. High pressures can be attained by e.g. the integration of an absorber with a gas turbine. High pressures are necessary in a desorber unit (ca. 15 MPa) also with the aim to limit ammonia vaporisation from the hot regenerated liquid. Thus the $NH_3$ process is well suited for all pressurised combustion or IGCC power systems.

### 3.6. EFFECT OF TEMPERATURE

Experimental data on the effect of temperature on $NH_3$ slippage under air stripping operating conditions is shown in Fig. 5. Increase in temperature facilitates $NH_3$ slippage due to decreased $NH_3$ solubility in water, i.e. $H_{NH_3}$ increases with temperature.

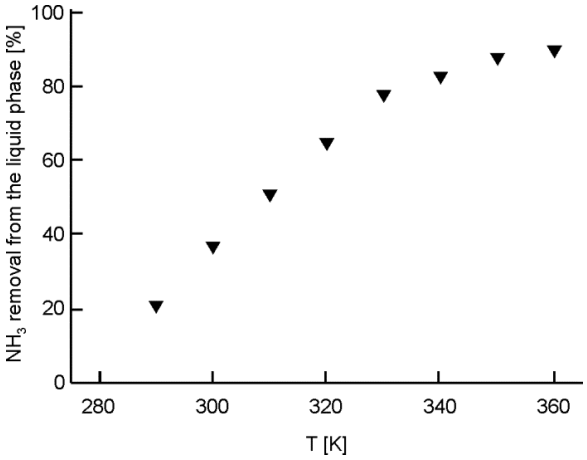


Fig. 5. Effect of temperature on $NH_3$ slippage under air stripping experimental conditions; $T = 296$ K, $P^{IN}_{CO_2} = 0$, $P^{IN}_{NH_3} = 0$, $C^{IN}_{CO_2} = 20\ \text{mol}\cdot\text{m}^{-3}$, $C^{IN}_{NH_3} = 93\ \text{mol}\cdot\text{m}^{-3}$, aqueous ammonia solution flow rate = $1.4\times10^{-5}\ \text{m}^3\cdot\text{s}^{-1}$, stripping air flow rate = $6.7\times10^{-3}\ \text{m}^3\cdot\text{s}^{-1}$. Experimental data from the packed-bed counter-current stripper with the packing height of 1 m and packing diameter of 0.1 m utilising 15 mm ceramic Raschig rings

Again, the thermal behaviour of $NH_3$ slippage under $CO_2$ capture conditions is a bit more complex than under air striping conditions. Semi-batch $CO_2$ absorption experiments [12] indicate that the net amount of $CO_2$ absorbed decreases upon increasing temperature. This result arises from the decreased solubility of $CO_2$ at higher temperatures since $H_{CO_2}$ increases upon increasing $T$. On the other hand, higher tem-

peratures tend to increase diffusivities of species and reaction rates. Besides, under $CO_2$ capture conditions pH can strongly vary along the reactor due to $CO_2$ absorption.

A thermal process control is a powerful tool in combating $NH_3$ slippage [22–24]. However, a process utilising chilled $NH_3$ [13] seems to be relatively expensive. Namely, the chilled $NH_3$ process requires chilling of flue gases including the condensation of water, chilling of regenerated ammonia from a desorber and chilling of an absorber itself. The costs of chilling can be reduced in power plants having unlimited access to large cold water resources such as rivers or lakes.

### 3.7. EFFECT OF INTEGRATION INTO POWER PLANTS

Integration of $CO_2$ capture systems into power plants necessitates advanced management of energy and mass flows in order to reduce the CCS-induced power plant efficiency drop penalty. Besides, for the $NH_3$ process the aspect of limited $NH_3$ slippage must be considered. Integration can benefit from the following measures:

- recirculation of flue gases back to combustion chambers which improves cycle efficiency and beneficially enriches $CO_2$ in flue gases [25],
- thermal integration of processes [26–30],
- utilisation of processes and apparatuses which enable one to reduce exergy losses (large losses are typically linked with heaters, fans, compressors and reactors),
- high-pressure $CO_2$ separation,
- optimising pressure and other parameters of steam supplied to a desorber,
- optimising stripper operation and its configuration,
- integration of CCS with more sophisticated energy technologies such as fuel cells [31, 32] or bioenergies [33, 34].

More specifically, the $NH_3$ process can benefit from highly reactive solvents such as $NH_3$, simultaneous removal of acidic gases ($SO_2$ and $NO_X$) and PM and direct integration of a desorber with a heat recovery steam generator unit (HRSG). The $NH_3$ process offers a reduction in regeneration energy requirements due to the higher loading capacity of an aqueous ammonia solution, the lower heat of reaction, and the lower heat of vaporisation when compared with standard MEA solutions.

## 4. CONCLUSIONS

Deployment of $NH_3$-based $CO_2$ capture into coal-fired power plants would shift unwanted emissions from those currently comprising $SO_2$, $NO_X$ and particulate matter towards those comprising $NH_3$ which necessitates research efforts directed at limiting $NH_3$ slippage from $NH_3$-based $CO_2$ capture power systems. The presented experimental and 2D simulation data of the $NH_3$ process characterised the hydrodynamics of the

falling film reactor, determined the effect of pH, pressure and temperature on $CO_2$ absorption and explained the role of migrative transport of ionic species in total mass transport. It was found that $NH_3$ slippage could be limited by alleviated operating temperatures, optimised pH, increased pressure and large $CO_2$ absorption fluxes, which forced negative enhancement of $NH_3$ mass transfer to the gaseous phase. $NH_3$ slippage under $CO_2$ capture conditions and under air stripping conditions were illustrated by simulation and experimental data. Approaches used in the integration of CCS systems into power plants were expounded.

## SYMBOLS

CCS – carbon capture and sequestration
$E$ – activation energy, $J \cdot mol^{-1}$
HRSG – heat recovery steam generator
$K$ – chemical equilibrium constant, $mol \cdot m^{-3}$ or, $m^3 \cdot mol^{-1}$ or, $mol^2 \cdot m^{-6}$
$k^{GP}$ – mass transfer coefficient in the gaseous phase,, $mol \cdot m^{-2} \cdot s^{-1} \cdot Pa^{-1}$
$M$ – molecular mass of species, $kg \cdot mol^{-1}$
MEA – monoethanolamine
PM – particulate matter
$R$ – reaction rate, $mol \cdot m^{-3} \cdot s^{-1}$
$C$ – molar concentration in liquid phase, $mol \cdot m^{-3}$
$D$ – molecular diffusivity, $m^2 \cdot s^{-1}$
$F$ – Faraday's constant, $A \cdot s \cdot mol^{-1}$
$H$ – Henry's constant, $Pa\ m^3 \cdot mol^{-1}$
$m$ – mobility of ion, $s \cdot mol \cdot kg^{-1}$
$P$ – pressure or partial pressure, Pa
$r$ – radial coordinate, m
$R^G$ – universal gas constant, $J \cdot mol^{-1} \cdot K^{-1}$
$T$ – temperature, K
$v$ – valence of ion
$w$ – velocity, $m \cdot s^{-1}$
$w_Z$ – $z$ component of velocity vector **w**, $m \cdot s^{-1}$
$x$ – space coordinate, m
$\delta$ – film thickness, m
$\lambda$ – thermal conductivity, $J \cdot mol^{-1} \cdot s^{-1} \cdot K^{-1}$
$\lambda^E$ – electrical conductivity, $S \cdot mol^{-1}$
$\varphi$ – electric potential in the electrolyte, V
$G$ – gaseous phase
$i, j$ – compound
$L$ – liquid phase
$r$ – reaction
z – space or axial coordinate, m

GREEK SYMBOLS

$\delta$ film thickness, m
$\lambda$ thermal conductivity, $J \cdot mol^{-1} \cdot s^{-1} \cdot K^{-1}$
$\lambda^E$ electrical conductivity, $S \cdot mol^{-1}$
$\varphi$ electric potential in the electrolyte, V

SUBSCRIPTS AND SUPERSCRIPTS

$G$ gaseous phase
$i, j$ compound
$L$ liquid phase
$r$ reaction

ACKNOWLEDGEMENTS

The author gratefully acknowledges the financial support from Wrocław University of Technology under grant No. S 10040/Z0311.

REFERENCES

[1] FORSTER P., RAMASWAMY V., ARTAXO P., BERNTSEN T., BETTS R., FAHEY D.W., HAYWOOD J., LEAN J., LOWE D.C., MYHRE G., NGANGA J., PRINN R., RAGA G., SCHULZ M., VAN DORLAND R., *Changes in atmospheric constituents and in radiative forcing*, [In:] *Climate Change 2007: The Physical Science Basis. Contribution of Working Group I to the Fourth Assessment Report of the Intergovernmental Panel on Climate Change*, Cambridge University Press, Cambridge, 2007.
[2] FLORIDES G.A., CHRISTODOULIDES P., *Global warming and carbon dioxide through sciences (Review),* Environ. Int., 2009, 35, 390.
[3] OLAJIRE A.A., Energy, 2010, 35, 2610.
[4] PUXTY G., ROWLAND R., ATTALLA M., Chem. Eng. Sci., 2010, 65, 915.
[5] PACHECO M.A., ROCHELLE G.T., Ind. Eng. Chem. Res., 1998, 37, 4107.
[6] PINSENT B.R.W., PEARSON L., ROUGHTON F.J.W., Transactions of the Faraday Society, 1956, 52, 1512.
[7] BUDZIANOWSKI W.M., KOZIOŁ A., Chem. Proc. Eng., 1999, 20, 485.
[8] MANI F, PERUZZINI M, STOPPIONI P., *$CO_2$ absorption by aqueous $NH_3$ solutions: speciation of ammonium carbamate, bicarbonate and carbonate by 13C NMR study*, Green Chemistry, 2006, 8, 995 –1000.
[9] ZARZYCKI R., *Diffusive methods in the description of environmental processes – historical overview*, [In:] *Modern Achievements in the Protection of Atmospheric Air*, A. Musialik-Piotrowska, J.D. Rutkowski (Eds.), Polskie Zrzeszenie Inżynierów i Techników Sanitarnych, 2010, 407–410 (in Polish).
[10] BUDZIANOWSKI W.M., Rynek Energii, 2009, 83(4), 21.
[11] GREER T., BEDELBAYEV A., IGREJA J. M., GOMES J. F., LIE B., Environ. Technol, 2010, 31 (1), 107.
[12] YEH J.T., RESNIK K.P., RYGLE K., PENNLINE H.W., Fuel Process. Technol., 2005, 86, 1533.
[13] GAL E., *Ultra cleaning combustion gas including the removal of $CO_2$*, Patent No. WO2006022885, 2006.

[14] PELLEGRINI G., STRUBE R., MANFRIDA G., Energy, 2010, 35, 851.
[15] LIU J., WANG S., ZHAO B., TONG H., CHEN C., Energy Proc., 2009, 1, 933.
[16] BUDZIANOWSKI W.M., KOZIOL A., Chem. Eng. Res. Des., 2005, 83, 196.
[17] KOORNNEEF J., RAMIREZ A., VAN HARMELEN T., VAN HORSSEN A., TURKENBURG W., FAAIJ A., Atmos. Environ., 2010, 44, 1369.
[18] KOZAK F., PETIG A., MORRIS E., RHUDY R., THIMSEN D., Energy Proc., 2009, 1, 1419.
[19] MATHIAS P.M., REDDY S., O'CONNEL J.P., Energy Proc., 2009, 1, 1227.
[20] HUANG H., XIAO X., YAN B., Desalin. Water Treatment, 2009, 8, 109.
[21] SUN B.C., WANG X.M., CHEN J.M., CHU G.W., CHEN J.F., SHAO L., Ind. Eng. Chem. Res., 2009, 48, 11175.
[22] KOTHANDARAMAN A., NORD L., BOLLAND O., HERZOG H.J., MCRAE G.J., Energy Proc., 2009, 1, 1373.
[23] BUDZIANOWSKI W.M., KOZIOŁ A., Chem. Proc. Eng., 2001, 22, 301.
[24] BUDZIANOWSKI W.M., KOZIOŁ A., Chem. Proc. Eng., 2000, 21, 741.
[25] BUDZIANOWSKI W.M., Rynek Energii, 2010, 88(3), 151.
[26] ROMEO L.M., ESPATOLERO, S., BOLEA I., Int. J. Greenh. Gas Con., 2008, 2, 563.
[27] BUDZIANOWSKI W.M., MILLER R., Environ. Prot. Eng., 2008, 34(4), 17.
[28] BUDZIANOWSKI W.M., MILLER R., Int. J. Chem. React. Eng., 2009, 7, A20.
[29] BUDZIANOWSKI W.M., MILLER R., Can. J. Chem. Eng., 2008, 86, 778.
[30] BUDZIANOWSKI W.M., MILLER R., Chem. Proc. Eng., 2009, 30, 149.
[31] BUDZIANOWSKI W.M., Int. J. Hydrogen Energ., 2010, 35, 7454.
[32] BUDZIANOWSKI W.M., Rynek Energii, 2009, 82 (3), 59.
[33] GAJ K., KNOP F., TRZEPIERCZYŃSKA I., Environ. Prot. Eng., 2009, 35 (4), 73.
[34] VALDEZ-VAZQUEZ I., POGGI-VARALDO H.M., Renew. Sust. Energ. Rev., 2009, 13(5), 1000.

Environment Protection Engineering

Vol. 37 2011 No. 4

JOANNA ĆWIKŁA*, KRYSTYNA KONIECZNY**

# TREATMENT OF SLUDGE WATER WITH REVERSE OSMOSIS

Considering the increasingly stringent requirements on the quality of treated wastewater introduced into surface or ground water, it is reasonable to reduce the loads of biogenic compounds produced already at wastewater treatment plants in sludge treatment processes because sludge water produced in such treatment brings into the process cycle up to 20% more of nitrogen and phosphorus load. The paper presents the results of sludge water treatment in a reverse osmosis process. The concentration of biogenic compounds in sludge water was successfully reduced by 95%. The tests were made using a pilot installation and laboratory installation. The concentrate produced in the reverse osmosis was treated by precipitating nitrogen and phosphorus compounds in form of struvite $(NH_4)Mg(PO_4)\times 6H_2O$ that can be next used as a fertiliser.

## 1. INTRODUCTION

Removal of biogenic compounds containing nitrogen and phosphorus from wastewater for many years has been at the focal point of both, researchers and end users. The issue has become especially vital after Poland's accession into the European Union and the adaptation of sewage treatment legislation with the EU standards. The Ordinance of the Minister of Environment valid from 2006 (and earlier from 2004) on the conditions to be fulfilled for discharging sewage to surface or ground water and on the substances especially harmful for the aquatic environment is setting forth that the permitted quantity of total nitrogen discharged to the environment with treated sewage for wastewater treatment plants with the ENI value of over 100 000 is only 10 mg N/dm$^3$ or that the achieved reduction level should be at least 85%. The permitted value for wastewater treated at such plants was laid down at 1.0 mg/dm$^3$ for phosphorus. The requirements were the consequence of adaptation Polish legislation with the EU solutions, in particular Directive 91/271/EEC of 21 May 1991 concerning urban wastewater treatment and Directive 98/15/EC of 27 February 1998 amending

*Przedsiębiorstwo Wodociągów i Kanalizacji Sp. z o.o., ul. Rybnicka 47, 44-100 Gliwice, Poland.

**Silesian University of Technology, Faculty of Energy and Environmental Engineering, ul. Akademicka 2A, 44-100 Gliwice, Poland, e-mail: krystyna.konieczny@polsl.pl

Directive 91/271/EEC with respect to certain requirements established in Annex I thereof.

One should underline that the previous national requirements in this field provided that the permitted total nitrogen content in treated wastewater should not exceed 30 mg/dm$^3$ and 5 mg/dm$^3$ for phosphorus (Ordinance of the Minister of Environmental Protection, Natural Resources and Agriculture of 5.11.1991, Jol No. 116, item 503). Considering such low permitted concentration thresholds for N and P elements, it has become necessary to find efficient methods of removing biogenic compounds from sewage by methods other than conventional nitrification-denitrification systems.

Significant amounts of sludge are produced as a result of implementing new, advanced sewage treatment technologies. Sludge undergoes, respectively, the stabilisation and dewatering process at the treatment plant. The sludge water produced in such processes is in most cases recycled directly to the process cycle. Many researchers, therefore, have become interested in seeking alternatives to reduce nitrogen and phosphorus loads generated already at the treatment plants as the removal of biogenic compounds from the internal process streams substantially decreases the nitrogen and phosphorus load flowing into the treatment plant's main process [1].

Studies at wastewater treatment plants have revealed that the nitrogen and phosphorus load returned with the sludge water produced in sludge treatment processes may account for up to 20–30% of the general load of biogenic compounds directed to biological reactors [2–4]. The C/N ratio is improved in the main process by removing nitrogen from the side streams, thus enhancing denitrification efficiency. It is an especially attractive solution for the existing plants that are being upgraded for the purpose of carrying out or intensifying the biological removal of biogenic compounds.

There are significant issues involved in the treatment of water from digested sewage sludge dewatering such as: very high concentration of total nitrogen (occurring predominantly in the form of ammonium nitrogen), high concentration of phosphorus compounds and suspended solid and marked variations in the concentration of contaminants.

High concentrations of nitrogen and phosphorus compounds is the effect of processes occurring in mesophile sludge digestion – a hydrolysis of polyphosphates gathered in the cells of the bacteria responsible for the biological sewage dephosphatation process and the intensive proteins ammonification process.

## 2. CHARACTERISTICS OF SLUDGE WATER AND ITS TREATMENT METHODS

The following are the key parameters evaluated for sludge water [5]

- COD 500–10 000 mg $O_2$/dm$^3$,
- $BOD_5$ 150–1000 mg $O_2$/dm$^3$,
- ammonium nitrogen 300–1000 mg N– $NH_4^+$/dm$^3$ (TKN typically 966 mg/dm$^3$ [2]),

- phosphorus 30–100 mg P/dm$^3$,
- suspended solid = 400–13000 mg/dm$^3$,
- dissolved gases, including $H_2S$,
- heavy metals.

Irrespective of the broad range of potential contaminant concentrations in sludge water of various treatment plants, one should be aware that its composition in one particular plant may vary from day to day. The loads introduced with recirculated sludge water for particular plants may also differ, what is shown in a list provided as an example in Table 1 for several treatment plants in Poland [6].

Table 1

Average estimated loads of contaminants introduced with recirculated sludge water at wastewater treatment plants [5]

| Parameter | Loads [%] | | | | |
|---|---|---|---|---|---|
| | Białystok | Ełk | Łomża | Suwałki | Olsztyn |
| $BOD_5$ | 3.5 | 26.0 | 0.47 | erv | 3.5 |
| COD | 6.5 | 31.0 | 4.8 | 2.4 | 1.0–4.5 |
| Total nitrogen | 9.7 | 43.3 | 5.8 | 19.6 | 4.1–8.6 |
| Ammonium nitrogen | 12.0 | 40.0 | 6.9 | 16.7 | 4.4–10 |
| Total phosporus | 4.8 | 28.6 | 6.8 | 15.8 | 4.0–6.6 |
| Phosphates | 5.7 | 27.8 | 7.2 | 15.3 | 3.9–7.8 |
| Suspended solid | 6.0 | 42.7 | 0.06 | 6.7 | 0.6–4.1 |

In connection with the above, when analysing the operation of a specific plant it becomes necessary to identify how much such composition may vary, or alternatively, which determinations may exhibit the highest fluctuations of results as such data is indispensable for deciding what treatment process for such water will be most appropriate in a particular case.

In general, sludge water can be treated with methods falling into two groups: biological processes and physiochemical processes. The following methods are most widespread for physiochemical processes:

- chemical precipitation,
- hot air degassing,
- stripping,
- ion exchange.

Each of the methods – both biological and physiochemical one, has its advantages and disadvantages and many factors are decisive in choosing a specific one. Choosing the right method depends on the quality and variation of the treated water composition, available funds as well as the conditions existing at the site. For instance, ammonia stripping with water steam will prove cost-effective if waste heat is available, whereas such costs will be substantial if such heat has to be produced particularly for

this method. If the high concentrations of ammonium nitrogen are also accompanied by the high concentrations of phosphorus compounds, the precipitation method (e.g. struvite crystallisation) may offer more benefits as compared to stripping because it allows one to remove both biogenic elements at the same time.

On the other hand, a certain disadvantage of new, unconventional biological methods is, most generally, that they focus more on removing nitrogen compounds, and their goal at the same time is not to remove phosphorus. The fact is also weighty that such methods are not conventional; therefore wastewater treatment plant researchers and environmental engineering designers are not familiar with them too well. The physiochemical methods, though, have been in use at the chemical industry for many years and are well known.

The paper focuses on the feasibility of reducing a load of biogenic compounds in sludge water using a combined method – reverse osmosis (RO) and then the precipitation of struvite from a concentrate in reverse osmosis. In practise, the RO process has been employed for treating run-offs from landfill sites (so-called leachates). Up till now the process has not, however, been used for sludge water at treatment plants. This is because the further handling of the concentrate has not been solved yet (in the case of leachate it is recycled to landfill sites where it gradually concentrates as water is evaporating naturally). Precipitation of ammonium and magnesium phosphate allows one not only to treat a concentrate from biogenic contaminants but also supplies a product usable as a fertiliser [7]. The advantage of concentrating contaminants before their precipitation in such case is that the tanks and equipment used will require smaller volumes and throughputs. Moreover, the precipitation of the struvite sludge itself from the tanks should also be easier as compared to the precipitation method used directly for raw sludge water. It was also expected when choosing this method that the struvite crystals produced would be more regular than when precipitating this compound from unconcentrated solutions, and hence the struvite sludge will feature better sedimentation properties. A simple operation of a reverse osmosis installation and resistance to any installation startups and shutdowns was also of importance when choosing such a method. In addition, the installation is also easy to operate as the driving force of the process is pressure gradient. Similarly, any change in the amount of the medium treated is not any problem – modular design of the device enables changes to its processing capacity by increasing or decreasing the area of the membrane applied (by adding or removing the installation modules).

## 3. CHARACTERISTICS OF REVERSE OSMOSIS

Reverse osmosis, also referred to as hyperfiltration, serves for separating water (solvent) from the solute having small molecular mass. Single- and multivalent ions and low-molecular organic compounds are separated in this process. RO process is the opposite of natural osmosis phenomenon where the solvent is spontaneously passing

through a semipermeable membrane. If the membrane separates the solution from the solvent or separates two solutions with different concentration, then the solvent is flowing towards the solution having a higher concentration. External pressure equalising the osmotic flow is called osmotic pressure characteristic of a specific solution. If a hydrostatic pressure builds up at the solution side exceeding the osmotic pressure, the solvent will permeate from the more concentrated solution to the more diluted one, therefore in the direction opposite than in the osmosis process. This process has been termed reverse osmosis [8].

The amount of water (solvent – $F_w$) passing through a semipermeable membrane characterised by $L_p$ permeability ($cm^3/(cm^2 \cdot s \cdot Pa)$) can be calculated from the following formula [8]:

$$F_w = L_p (P - \pi).$$

The hydraulic performance of the process is directly proportional to the difference between the external pressure $P$ and the osmotic pressure $\pi$ [9].

The amount of the solute ($F_s$) passing through the membrane depends on the constant permeability of the solute B (cm/s) though, and the difference in concentrations $\Delta C$ for the solutions separated with the membrane:

$$F_s = B\Delta C.$$

The hydraulic performance of the process is measured with so-called membrane permeability ($L_p$) determined with the following formula:

$$L_p = \frac{V_r}{tS_m\Delta P},$$

where $V_r$ – solution volume, $t$ – time, $S_m$ – membrane surface area, $\Delta P$ – pressure drop at both sides of the membrane [10].

Transmembrane pressure (TMP) used in reverse osmosis is higher than in an ultrafiltration (UF) and microfiltration (MF) processes (3,5-10 MPa) [11], and the solvent (water) affinity to the membrane material plays a predominant role for choosing a membrane, whereas membrane pores are much less important as the separation mechanism is of the solving and diffusion nature [12,13].

## 4. EXPERIMENTAL

Sludge produced in the Central Wastewater Treatment Plant in Gliwice is introduced to mezophilic methane fermentation and next the dewatering process on Roediger–Pasavant belt filter presses is performed. The sludge water produced during the

dewatering is recycled to the biological part of the plant and directed to the activated sludge chambers. The following parameters were evaluated for investigated sludge water: pH, COD, $BOD_5$, ammonium nitrogen, nitrate nitrogen, total nitrogen, total phosphorus, phosphates, suspended solid, conductivity, calcium, magnesium. All analyses were made according to standards presented in Table 2. Studies were carried out between January 2005 and March 2009.

Table 2

Variations in sludge water composition in January 2005–March 2009

| Parameter | Method of determination (Norm) | Average | Minimum | Maximum |
|---|---|---|---|---|
| pH | PN–C-04540/01:1990 | 7.58 | 7.3 | 8.0 |
| COD, mg $O_2/dm^3$ | PN–ISO 15705:2005 | 435.5 | 79.5 | 869.0 |
| $BOD_5$, mg $O_2/dm^3$ | PB-5.4-01/23 publ. 02. 02.01.07 | 99.8 | 40 | 220 |
| Ammonium nitrogen, mg $N–NH_4/dm^3$ | PN–ISO 5664:2002 | 603.3 | 416 | 887 |
| Nitrates nitrogen, mg $N–NO_3/dm^3$ | PB-5.4-01/09 publ. 02. 02.01.07 | 5.48 | 0.5 | 24.3 |
| Total nitrogen, mg $N/dm^3$ | PB-5.4-01/04 publ. 04. 02.02.09 PB-5.4-01/09 publ. 02. 02.01.07 PN–EN 25663:2001 PN–C-04576/14:1973 | 652.9 | 438.0 | 896.7 |
| Total phosphorus, mg $P/dm^3$ | PB-5.4-01/08 publ. 02. 02.01.07 | 27.8 | 4.67 | 114.0 |
| Phosphates, mg $PO_4^{3-}/dm^3$ | PB-5.4-01/08 publ. 02. 02.01.07 | 194.5 | 13.8 | 349.0 |
| Suspended solids, $mg/dm^3$ | PN–EN 872:2005 +Apl:2007 | 91.5 | 14.4 | 292.4 |
| Conductivity, µS/cm | PN EN 27888:1999 | 5863 | 4299 | 9699 |
| Calcium, mg $Ca^{2+}/dm^3$ | PB-5.4-01/32 publ. 03. 02.02.09 | 55.0 | 21.8 | 130.0 |
| Magnesium, mg $Mg^{2+}/dm^3$ | PB-5.4-01/32 publ. 03. 02.02.09 | 20.0 | 12.5 | 57.8 |

The next step of the studies focused on the treatment of sludge water by the reverse osmosis process. The studies were performed using two installations: Osmonics' laboratory installation and a pilot installation supplied by the Pall Poland with a disk tube (DT) module mounted. Composite membranes were used for the studies in both cases marked with BW 30 symbol by the Pall Poland. The final step of the studies covered the treatment of the condensate from RO process via struvite crystallization.

The evaluation of produced crystals was made with the use of a Novex optic microscope magnified 40 and 100 times.

*Pilot installation*. The membrane cushions of the pilot installation comprised two composite membrane disks with a spacing inner layer. They were sealed with a patented technique so as the filtered medium did not contact other materials (e.g. bonding agents for membrane). The total surface area of membranes in the installation was 6.8 $m^2$ (160 "cushion" membranes with the surface area of 0.0425 $m^2$ each).

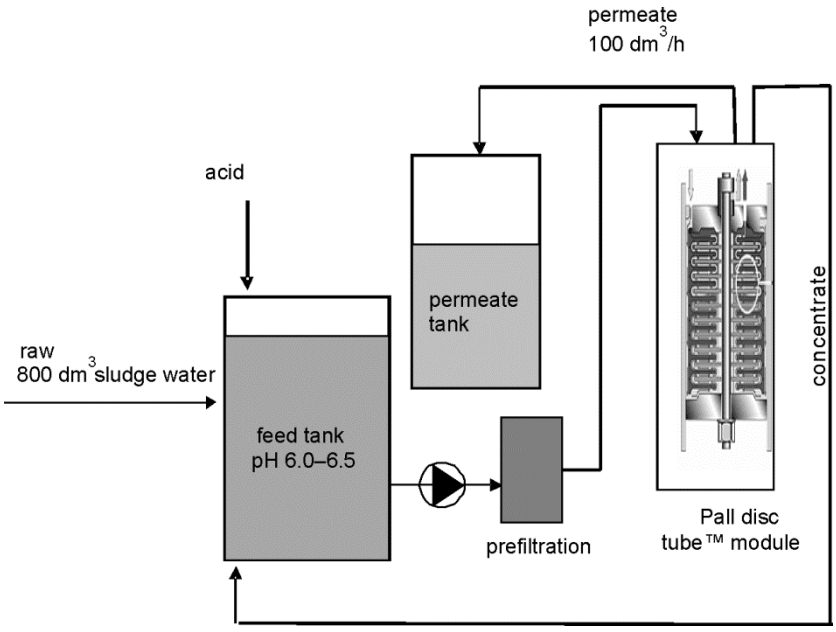


Fig. 1. Simplified working principle of the pilot installation

A sample of 800 $dm^3$ of sludge water was tested (Fig. 1). It was directed onto the membrane module under an initial pressure of 1.6–1.8 MPa, thus reaching the permeate flow of 100 $dm^3$/h. The RO concentrate was returned to the feed tank and its concentration gradually increased. The studies were continued until 75% of the initial volume of feed was purified (i.e. for approx. 8 h). A constant intensity of permeate flow was maintained during the experiment and the intensity was adjusted by increasing operating pressure. When the feed concentration reached 25% of its initial volume, the working pressure had to be increased to 2.1–2.2 MPa to maintain the permeate stream of 100 $dm^3$/h.

After ca. 5–10 min, as only the condensation process was stabilized, the feed and permeate samples were collected in order to determine their physicochemical composition.

*Osmonics laboratory installation.* The surface area of the tested membrane was 0.013m$^2$, being much smaller than that for the pilot installation. Nevertheless, the efficiency of retention of the ammonium nitrogen turned out to be comparable to that in the pilot installation. As the area of the tested membrane was small, the intensity of permeate flow was much smaller as compared to that in the pilot installation. Thus the sample was not concentrated in this case and instead the experiment was focused on seeking optimum process parameters such as:

- pH (in the range of 5.5–7.2, adjusted by addition of 0.1 M HCl)
- temperature (from 22 °C to 39 °C, its self-heating was obtained by shutting off the feed cooling)
- pressure (2.0, 2.5 and 3.0 MPa),
- water flow rate through the module (1.2 and 3 m/s).

Pressure and feed flow rate were adjusted by using a pump and appropriate RO module valves opening.

Most of experiments (except from the part focused on the influence of pressure on the process efficiency) were carried out under the pressure of 2.0 MPa. Permeate samples for physicochemical analysis were collected after stabilization of the process conditions, i.e. ca. 15 minutes after every change in the process set up.

The volume of the feed introduced to every process was equal to 10 dm$^3$ and it was decreasing during the process run by the amount of collected permeate (depending on the number of collected permeate samples, the final volume of the concentrate varied from 8 to 9 dm$^3$). The initial concentration of ammonium nitrogen in the feed varied insignificantly within 580–615 mg/dm$^3$.

*Condensate treatment*. The premliminary tests of struvite precipitation from sludge water (feed) and from concentrated water (concentrate) were made. The tests were made in two series:

- for samples prepared with distilled water, $NH_4H_2PO_4$ and $MgCl_2 \cdot 6H_2O$,
- for actual raw and concentrated sludge water.

The same quantities of $NH_4H_2PO_4$ and $MgCl_2 \cdot 6H_2O$ were dissolved in different amounts of water in the first case, thus producing solutions with the same load but different concentrations. 2 dm$^3$ of water for the diluted solution was used and 0.5 dm$^3$ for the concentrated one.

The content of ammonium nitrogen, phosphates and magnesium in raw and concentrated sludge water was determined in the first case. Next, $K_2HPO_4$ and $MgCl_2 \cdot 6H_2O$ were added in stoichiometric amounts, necessary for struvite precipitation.

Precipitation was performed after adjusting pH of the solutions to 9.0 with NaOH [14]. The results of such preliminary studies are given in Table 3.

Table 3

Results of preliminary tests for struvite precipitation efficiency[a]

| Parameter | Prepared sludge water | | | | | |
|---|---|---|---|---|---|---|
| | Prepared sludge water (feed) | | | Concentrated sludge water | | |
| | Series 1 | | | | | |
| | P1 | P2 | Red % | P1 | P2 | Red % |
| $PO_4$ | 2830 | 69 | 97.6 | 11350 | 151 | 98.7 |
| $N–NH_4$ | 420 | 42 | 90 | 1630 | 170 | 89.6 |
| | Series 2 | | | | | |
| | P1 | P2 | Red % | P1 | P2 | Red % |
| $PO_4$ | 2850 | 15 | 99.5 | 11340 | 11 | 99.9 |
| $N–NH_4$ | 450 | 40 | 91.1 | 1635 | 187 | 88.6 |
| | Actual sludge water | | | | | |
| | Sludge water (feed) | | | Concentrated sludge water | | |
| | Series 3 | | | | | |
| | P1 | P2 | Red. % | P1 | P2 | Red % |
| $PO_4$ | 241 | 5 | 97.9 | 10085 | 10 | 99.9 |
| $N–NH_4$ | 665 | 322 | 51.6 | 1456 | 192 | 86.8 |
| | Series 4 | | | | | |
| | P1 | P2 | Red. % | P1 | P2 | Red % |
| $PO_4$ | 3792 | 12 | 99.7 | 11428 | 10 | 99.9 |
| $N–NH_4$ | 769 | 271 | 64.8 | 1578 | 232 | 85.3 |
| | Series 5 | | | | | |
| | P1 | P2 | Red. % | P1 | P2 | Red % |
| $PO_4$ | 6013 | 39 | 99.4 | 14245 | 279 | 98 |
| $N–NH_4$ | 735 | 107 | 85.4 | 1542 | 136 | 91.2 |

[a]P1 – solutions prior to adding $MgCl_2 \cdot 6H_2O$, P2 – solutions after adding $MgCl_2 \cdot 6H_2O$ and struvite crystallisation.

## 5. DISCUSSION OF RESULTS

The results of the study of the composition of sludge water (Table 2) show very strong fluctuations in concentrations of contaminants affected by the seasons of the year as well as the procedures taken in the sludge treatment process. Slightly higher concentrations of phosphorus compounds are observed during the biomass growth of filamentous bacteria (e.g. in spring). This, most likely, is caused firstly by efficient biological dephosphatation induced by this group of bacteria in a biological reactor and, secondly, by a release of phosphates collected in the bacterial cells during sludge digestion. When the higher doses of coagulant for phosphorus precipitation from

wastewater (e.g. PIX) are used at the plant, however, the quantity of this element in sludge water is lower, as well. The loading of digestion chambers with sludge significantly affects ammonium nitrogen concentrations in sludge water. The above findings point out that the concentrations of contaminants in sludge water are not constant parameters even for one specific plant, which makes it even more difficult to choose a single optimum treatment process. The results of studies of the pilot installation are given in Table 4. Results of selection of optimum parameters such as pH, temperature, pressure and water flow speed through the module are presented in Figs. 2–4.

Table 4

Results of studies of the pilot installation

| Parameter | Method of determination (Norm) | I series | | II series | | III series | |
|---|---|---|---|---|---|---|---|
| | | N | P | N | P | N | P |
| pH | PN–C-04540/01:1990 | 6.5 | 5.1 | 6.9 | 5.7 | 7.1 | 5.9 |
| COD, mg $O_2$/dm$^3$ | PN–ISO 15705:2005 | 444 | 13.9 | 204 | 8.8 | 320 | 8.7 |
| $BOD_5$, mg $O_2$/dm$^3$ | PB-5.4-01/23 publ.02, 02.01.07 | 240 | 4 | 95 | 2 | 140 | 14 |
| N–$NH_4$, mg/dm$^3$ | PN–ISO 5664:2002 | 490 | 12 | 474 | 22 | 533 | 28 |
| N–$NO_3$, mg/dm$^3$ | PB-5.4-01/09 publ.02, 02.01.07 | 8.4 | 1.5 | 3.15 | 1.5 | 10.9 | 0.55 |
| Total N, mg N/dm$^3$ | PB-5.4-01/04 publ.04, 02.02.09 PB-5.4-01/09 publ.02, 02.01.07 PN–EN 25663:2001 PN–C-04576/14:1973 | 541 | 15 | 477 | 26 | 555 | 32 |
| Total P, mg P/dm$^3$ | PB-5.4-01/08 publ.02, 02.01.07 | 19.5 | 0.6 | 15.1 | 0.64 | 17.0 | 1.4 |
| $PO_4^{3-}$, mg/dm$^3$ | PB-5.4-01/08 publ.02, 02.01.07 | 61.7 | 1.7 | 46.4 | 2.0 | 49.7 | 4.4 |
| Suspended solids, mg/dm$^3$ | PN–EN 872:2005 +Apl:2007 | 51 | 2.0 | 36 | 0.8 | 49 | 1.6 |
| Conductivity, µS/cm | PN EN 27888:1999 | 6701 | 153 | 3109 | 264 | 5282 | 371 |
| Calcium, mg $Ca^{2+}$/dm$^3$ | PB-5.4-01/32 publ.03, 02.02.09 | 53 | 0.5 | 28 | 1.1 | 42 | 2.3 |
| Magnesium, mg $Mg^{2+}$/dm$^3$ | PB-5.4-01/32 publ.03, 02.02.09 | 21 | 2.1 | 5 | 1.4 | 14 | 1.7 |
| Chrome, µg Cr/dm$^3$ | PN EN ISO 15586:2005 | 10.7 | <2 | 3.3 | <2 | 3.1 | <2 |
| Zinc, µg Zn/dm$^3$ | PN ISO 8288:2002 | 120 | 7.4 | 32.3 | 3.6 | 57.1 | 8.2 |
| Cadmium, µg Cd/dm$^3$ | PN EN ISO 15586:2005 | 2.62 | <0.4 | <0.4 | <0.4 | 0.45 | <0.4 |
| Manganese, µg Mn/dm$^3$ | PN EN ISO 15586:2005 | 328 | 4.55 | 118 | 2.20 | 150 | 10.2 |
| Copper, µg Cu/dm$^3$ | PN EN ISO 15586:2005 | 10.1 | <1.5 | 6.3 | 1.5 | 6.8 | <1.5 |
| Nickel, µg Ni/dm$^3$ | PN EN ISO 15586:2005 | 56.5 | 3.2 | 26.2 | 3.9 | 27.1 | 4.7 |
| Lead, µg Pb/dm$^3$ | PN EN ISO 15586:2005 | 2.61 | 1.35 | 1.07 | 1.01 | 0.50 | 0.36 |

It was confirmed that sludge water can be treated by the method of reverse osmosis. The process efficiency was very high, as 95% reduction in biogenic compounds was achieved. The reduction level for N and P compounds differed insignificantly according to the feed quality.

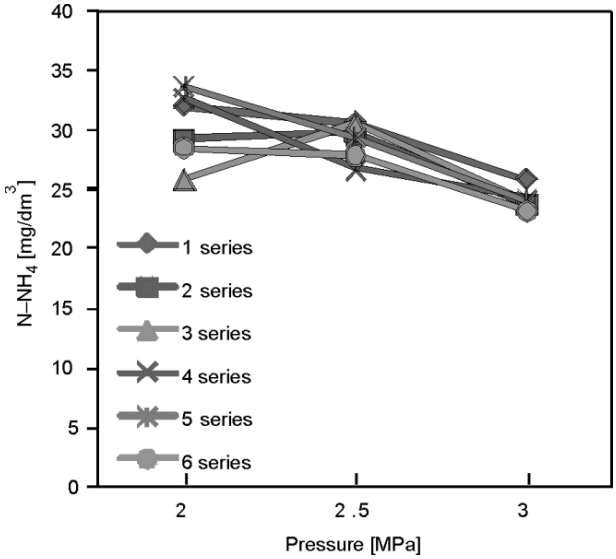


Fig. 2. Pressure dependence of the N–$NH_4$ content in permeate using the Osmonics module and BW 30 membranes; $T$ = 22 °C, flow speed 2 m/s, N–$NH_4$ in feed: 600 mg/dm$^3$

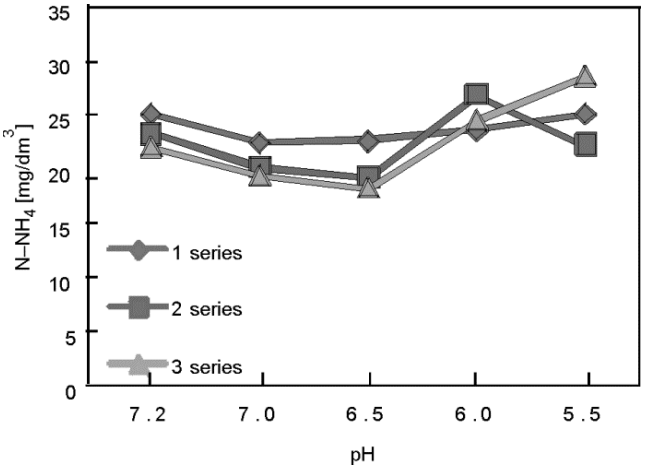


Fig. 3. Dependence of the N–$NH_4$ content in permeate on pH of feed using the Osmonics module and BW 30 membranes; $\Delta P$ = 2 MPa, $T$ = 22 °C, flow speed 2 m/s, N–$NH_4$ in feed 605 mg/dm$^3$

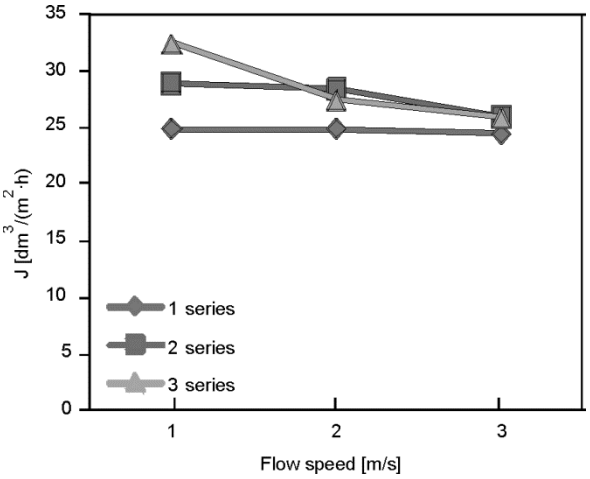


Fig. 4. Dependence of the volumetric flux of permeate on the flow rate through the Osmonics module in the RO process using the BW 30 membrane; $\Delta P$ = 2 MPa, pH = 7.0, $T$ = 22 °C, N–$NH_4$ in feed 590 mg/dm$^3$

The content of ammonium nitrogen in the permeate however, never exceeded 30 mg/dm$^3$, and 1.5 mg/dm$^3$ for general phosphorus, i.e. the permeate composition was similar in this respect to standard urban sewage (Table 4). Additional load brought to the treatment plant with permeate will, therefore, not be significant from the process point of view.

Optimum working conditions for the reverse osmosis were identified: the highest reduction in ammonium nitrogen content was reached for the feed with pH of 6.5 (Fig. 3) under the pressure of 3 MPa. (Fig. 2). However, considering the energy consumption and fouling intensity observed for the higher pressure, its the lower value, i.e. 2 MPa was found to be efficient enough to provide satisfactory treatment effect.

A higher intensity of permeate flow was accomplished for feed flowing via the membrane at a lower flow rate (Fig. 4). The reasons would be both turbulent flow for higher flow rate disturbing the convection motion to the membrane and/or torrential growth of flow losses under higher flow rate leading to the decrease of the process driving force.

The concentrate produced in the reverse osmosis was purified by precipitating ammonium and phosphorus compounds in a form of struvite $(NH_4)Mg(PO_4)\times 6H_2O$ (Table 4). The appropriate amount of magnesium ions and phosphates had to be added to the concentrate for this purpose. It is also important that by concentrating the contaminants, the tank and the equipment to be used in actual conditions will feature dimensions and capacities much smaller than when using this technology straightforward for untreated sludge water.

Sedimentation properties of the sludges precipitating from concentrated solutions were better than those of the sludges precipitating from raw sludge water: the

precopitates were falling quicker and the occurence of other types of crystals produced in sludges was found in the microscopic image (optical microscope Novex, magnified 40× and 100×). Sludges from the concentrated samples were drying quicker than the those from the samples imitating raw sludge water. Similar reduction values for ammonium nitrogen were obtained from the concentrated and diluted solution. The tests made for actual solutions also differed with regard to the composition of crystals, however, it is necessary to select appropriate process conditions to intensify struvite precipitation considering unsatisfactory reduction in ammonium nitrogen content as compared to the prepared solutions.

Regular, romboidally-shaped crystals along with thin needles and X-shaped forms occured in all the cases. The proportions of various crystal forms in sludges differed, however: forms with regular shapes were prevalent in respect of X-shaped forms for the concentrated solutions and regular forms for the actual solutions were lower in numbers.

The admixtures of other compunds, disturbing the struvite crystallisation process, were probably present in the actual solutions. It is therefore recommened to determine the elemental composition of the sludges produced, which could help to conclude if other crystals than struvite occur in sludges.

The studies have not been completed, yet and they are being continued to produce a series of repeatable results and to select appropriate parameters for the process performed.

## 6. CONCLUSIONS

The studies have shown that the treatment of sludge water with the reverse osmosis method is feasible and its efficiency is very high. The concentrate produced in the process can be treated by the precipitation of struvite sludge. The sludge can be used in agriculture as a good quality fertiliser. The RO module is simple to operate and its installation is resistant to changes in contaminant concentrations in the feed. Breaks in the module usage do not affect the efficiency of the method. There is an opportunity to implement this process for wastewater treatment plants where it can be used for limiting the concentration of biogenic loads from external process streams, thereby achieving higher efficiency of nitrogen and phosphorus removal in biological reactors.

## REFERENCES

[1] STROUS M., VAN GERVVEN E., ZHENG P., KUENEN J.G., JETTENM S.M., Water Res., 1997, 31 (8), 1955.

[2] CONSTANTINE T., SHEA T., JOHNSON B., *Newer approaches for treating return liquors from anaerobic digestion*, IWA Spec. Conf. Nutrient Management in Wastewater Treatment Processes and Recycle Streams, Cracow, 2005, 455–464.

[3] CAFFAZ S., LUBELLO C., CANZIANI R., SANTIANNI D., A*utotrophic nitrogen removal from anaerobic supernatant of Florence's WWTP digesters, Newer approaches for treating return liquors from anaerobic digestion*, IWA Spec. Conf. Nutrient Management in Wastewater treatment Processes and Recycle Streams, Cracow, 2005, 397–406.
[4] MASŁOŃ A., TOMASZEK J.A., Environ. Prot. Eng., 2007, 33 (2), 175.
[5] MALEJ J., MAJEWSKA A., BOGUSKI A., Rocznik Ochr. Środ., 2002, 4, 11.
[6] MYSZOGRAJ S., Inż. Ochr. Środ., 2008, 11 (2), 219.
[7] BRIDGER G., CEEP Scope Newsletter, 2001, 43, 3.
[8] KOŁTUNIEWICZ A.B., DRIOLI E., *Membranes in Clean Technologies. Theory and Practice*, Wiley, Weinheim, 2008.
[9] MAJEWSKA-NOWAK K., Ochr. Środ., 2007, 2, 21.
[10] KOWAL A., ŚWIDERSKA-BRÓŻ M., *Purification of Water*, PWN, Warsaw, 2009, p. 311–312 (in Polish).
[11] CHERYAN M., *Ultrafiltration and Microfiltration Handbook*, Technomic Publ. Comp., Lancaster, 1998.
[12] NOWORYTA A., TRUSEK-HOŁOWNIA A., *Membrane Separations*, Agencja Wyd. ARGI, Wrocław, 2001 (in Polish).
[13] NARĘBSKA A., *Membrany i membranowe techniki rozdziału*, Wyd. Uniw. Mikołaja Kopernika, Toruń, 1997.
[14] JAFFER Y., CLARK T.A., PEARCE P., PARSONS S.A., Water Res., 2002, 36, 1834.

Environment Protection Engineering

Vol. 37 2011 No. 4

WOJCIECH DĄBROWSKI*

# RATIONAL OPERATION OF VARIABLE DECLINING RATE FILTERS

An approximate solution to the system of equations governing the flow distribution among variable declining rate (VDR) filters results in flow rates through filters being elements of a geometrical progression. Based on this approximation, it was deduced how to operate a plant in order to keep the same flow rates through VDR filters for various total head losses of flow. These principles of operation were carefully verified using the accurate di Bernardo mathematical model of VDR filter plants. It was deduced that the longest filter runs result from such an operation of a plant for which the ratio of the highest to the average flow rates through a filter and simultaneously the affordable total head loss of flow through the plant are the highest.

## 1. INTRODUCTION

In the forty years since the first application of the variable declining rate (VDR) control system [1], many existing plants have been installed with orifices to replace expensive and sometimes unreliable mechanical flow rate controllers. VDR filters are especially popular in South America, but several water treatment plants using the VDR control system operate successfully in the U.S.A., and in the European Community.

The idea of declining filtration might be advantageous in further application of activated carbon, either by itself or as one of filter media layers. A longer time is required for filtration in the case of a clogged activated carbon filter. This longer time facilitates improved adsorption of soluble organic compounds. However, if granular activated carbon (GAC) filters follow conventional sand or sand–anthracite filters the GAC media often requires backwashing to avoid high bacteriological content in filtrate, before any significant clogging of carbon is observed [2]. So far it is difficult to

*Water Supply and Environmental Engineering Institute, Cracow University of Technology, ul. Warszawska 24, 31-135 Cracow, Poland, e-mail: wdabrow@pk.edu.pl

judge how effectively the VDR system of operation will compete with mechanical flow controllers, as this second type of a flow control system can also be constructed to operate under a declining flow rate in a more manageable fashion than that offered by orifices installed at the outflows from the filters. However, it is evident that variable declining rate (VDR) filters are an economically reasonable solution for all treatment plants unable to meet the water quality demands or those poorly controlled. Moreover, it has been shown several times that the quality of filtrate produced by filters operated under this system is at least as good as that obtained under a constant filtration velocity [3–8]. Thus, it is easy to understand why this invention has spread rapidly in countries where increasing water demands exist but still low financial capabilities. VDR filters offer some advantages as an increase in plant capacity, longer filter runs or a decrease in the total head loss in the system. If only one of these factors is chosen for maximization, it limits or excludes making use of other opportunities. Therefore, a proper design of a VDR filter system is best approached as an optimisation problem.

Optimisation theory is a powerful tool which deals with hundreds or even thousands of decision variables, especially when linear problems are concerned. In the case of retrofitting a plant with a VDR filter control system there are only a few operation parameters to be optimised. Therefore major difficulty results from a lack of comprehensive knowledge about relations existing between them. However, there are several prospective methods of computing hydraulic control systems of VDR filters. An approximate solution to di Bernardo's [9, 10] mathematical model is used here to elaborate several relationships between filters operating in a bank. Most of these relationships have been found to be useful in an optimisation procedure proposed for the hydraulic control system of a VDR filter plant. It was assumed that an existing water treatment plant is equipped with hydraulic flow rate controllers (orifices) located at the outflow pipe from each of the filters [10, 11]. The maximum available head loss, the ratio of the maximum to the mean flow rate, the flow rate through the whole plant and the filter media are assumed to be fixed. The coefficients characterizing the friction created by orifices, the ratio of maximum $q_{max}$ to average $q_{avr}$ flow rates through the filter units, the height of water surface fluctuation above filter media $h_0$, and the value of the total head loss of flow through the system $H$ are decision variables. The goal is to minimize the frequency of backwash subject to the constraints imposed on the decision variables by the total plant capacity, affordable head loss of flow through the system, and the highest admissible flow rate through a clean filter.

## 2. FLOW CONTROL SYSTEM

Variable declining rate filters are equipped with identical orifices installed at inflows or outflows from all filters. The operation of such a filter plant is based on co-

operation between head losses created by linear laminar flow through filter media with head loses of turbulent flow through orifices and transitional flow through the drainage [11, 12]. The operational parameters of the flow control system should be selected in such a way to restrict flow through the freshly backwashed filters mostly by head losses of flow through orifices. However, for the most significantly clogged filter, waiting for backwash, this head loss should be negligible in comparison with the head loss of flow through the filter media. The principles of the VDRF plant operation are described elsewhere [10–18]. The following assumptions were made:

- there are at least four filters in a bank,
- all filters are identical,
- inflows are located below the lowest water surface above the filter media,
- head losses in piping are negligible in comparison with those created by filter media,
- orifices are located at outflows from filters.

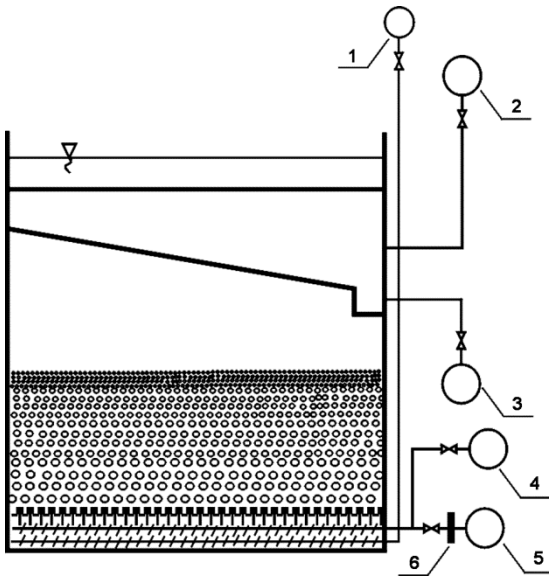


Fig. 1. The place of installation of an orifice:
1 – air, 2 – raw water, 3 – wastewater, 4 – backwash water, 5 – filtrate, 6 – orifice

Under these assumptions the unconfined water surface level is the same above all filters in any moment of time. This level rises in time due to clogging of filter media, to drop down quite rapidly after restoring the most recently backwashed filter to service. The place of installing orifices controlling flow rates through filters is presented in Fig. 1. Examples of patterns of water and flow rates are presented in Figs. 2, 3.

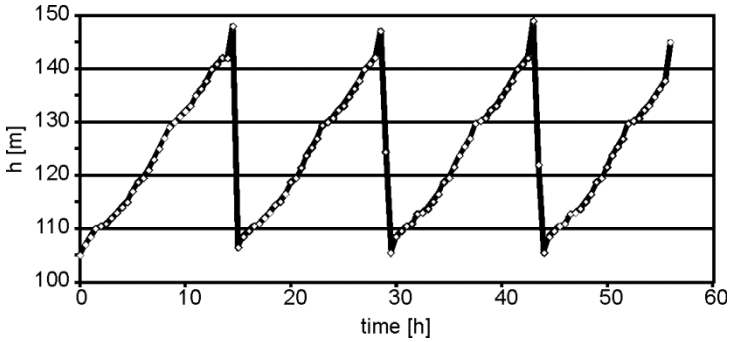


Fig. 2. An example of water table fluctuations at the pilot VDR filter plant constructed at the Cracow University of Technology

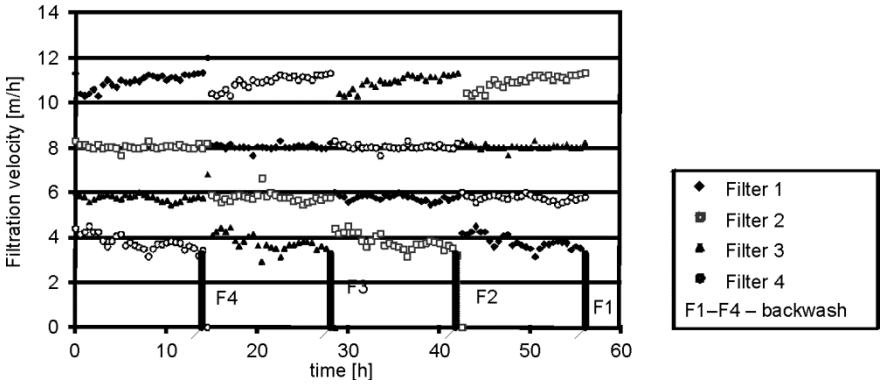


Fig. 3. An example of flow rates recorded at the pilot VDR filter plant constructed at the Cracow University of Technology

## 3. EQUATIONS

Di Bernardo [9, 10] proposed a model of the variable declining rate filter control system under the following assumptions:

1. All flow rates vary only at time of and just after a backwash of one filter, thus they remain essentially constant between subsequent backwashes in a plant.

2. The period of a backwash of one of the filters is so short that the hydraulic resistances of the filters remaining in service are not visibly affected by clogging during this period (the resistance of a filter $i$ is recognized to be the same before and after the backwash of a filter $z$).

Di Bernardo [9, 10] compared theoretical results obtained by his model with experimental data collected from a pilot plant as well as from a full-scale filtration plant and he received strong support for his theory. Dąbrowski [11] found the Di Bernardo model to give results similar to those produced from the set of equations elaborated by

Arboleda et al. [16] and summarized di Bernardo's model in a set of $z + 1$ Eqs. (1)–(3). Mackie et al [12] proved the solution to the system of Eqs. (1)–(3) to be close to results of computations based on the unit bed element (UBE) [19] model of a filter plant

- $z - 1$ equations

$$\frac{H - h_0 - c_2 q_{i+1}^n}{q_{i+1}} = \frac{H - c_2 q_i^n}{q_i} \tag{1}$$

- 1 equation

$$H - h_0 = c_1 q_1 + c_2 (q_1)^n \tag{2}$$

- 1 equation

$$Q = \sum_{i=1}^{i=z} q_i \tag{3}$$

where: $c_1$ is a proportional coefficient characterizing the resistance of clean medium, $c_2$ – coefficient of turbulent head losses, $H$ – total head loss of flow through the plant just before a backwash, $h_0$ – height of water surface increase between backwashes, $i$ – number of a filter in a bank, $n$ – exponent of turbulent and transitional head loss created by orifices and drainage, $q_i$ – flow rate through $i$th unit, $q_i = q_1$ for $i = 1$, etc., $Q$ – total flow rate through the system, $z$ – number of filters in a bank.

Equations (1) does not account for compressing of deposit in filter media, which is an easily visible phenomenon in the case of increasing [20] and less visible for decreasing [21] of coagulated water suspension filtration velocity. However, extensive pilot plant experiments [22] proved that the di Bernardo model [10] was surprisingly accurate for modelling filter plants following chemical pretreatment and flocculators. There are $(z - 1)$ equations (1) and two single Eqs. (2), (3) where $z$ is the number of filters in a bank.

Three approximate solutions to the system of Eqs. (1)–(3) were elaborated [11] and tested in comparison with accurate numerical solutions and with experimental data. Approximation (4) to Eq. (1) was definitely of the worst accuracy but still gave quite acceptable results:

$$\frac{q_{i+1}}{q_i} = 1 - \frac{h_0}{H} \tag{4}$$

According to this approximation flow rates through filters are elements of a geometrical progression. Obviously approximated Eq. (4) to Eq. (1) may be applied only as long as the parameters of a filter plant operation $H$, $h_0$, $z$, $c_1$, $c_2$, $q_1$ ..., $q_i$ ..., $.q_z$ are in the range commonly used in water filtration practice. Beyond this range the substitution of Eq. (1) by Eq. (4) may result in unexpectedly high errors of calculations.

## 4. BASIC RULES

Some general properties of VDR filters developed from a solution to the set of Eqs. (2)–(4) give an idea which particular parameters should be considered in optimisation of filter runs. Since Eq. (4) is a rough approximation to Eq. (1), thus all the conclusions developed here were carefully verified in numerical experiments by rigorous solution to the set of Eqs. (1)–(3). The theory developed here is limited to a reconstruction of an existing plant, so the coefficient $c_1$, describing the hydraulic resistance of a clean porous medium against the flow, is given. The head loss $H$, height of water table fluctuations over the filters $h_0$, and the turbulent head loss coefficient $c_2$ are adjusted in calculations to meet the required optimisation goals. However, prior to formulation of the optimisation problem, some properties of the solution to the system of Eqs. (2)–(4) are summarized. These properties will be used later in search for a special family of solutions to the set of Eqs. (1)–(3) for which flow rates through filter units remain almost the same when parameters of a filter plant operation change according to basic rules defined in the next paragraph.

## 5. PROPERTIES OF THE SOLUTION TO THE SYSTEM OF EQUATIONS (2)–(4)

Prior to formulation of the optimisation problem, some properties of the solution to the system of Eqs. (2), (3), (4) are summarized. Property 1 follows directly from Eq. (4).

Theorem 1. The ratio of $q_{i+1}/q_i$ does not depend on the number $i$ of a filter in a bank. If the values of $H$ and $h_0$ are the subject of change in such a particular way that $h_0/H$ is the same each time the ratio $q_{i+1}/q_i$ remains constant.

From this statement and from Eqs. (2), (3) a practical rule for management of VDR control systems may be directly deduced.

Theorem 2. In order to receive the same flow rates through all filters in a plant $q_1$, ..., $q_i$, ..., $q_z$ for any feasibly chosen new values of the total head loss of flow through a plant before a subsequent backwash $H$, parameters of the plant operation $c_2$, $h_0$ should be adjusted according to the following rules:

1) $h_0$ is to be calculated for a new value $H$ directly from a constant (equal to the previous) value of the quotient $h_0/H$.

2) The coefficient characterizing the orifice $c_2$ is to be calculated from Eq. (2) in order to give the same $q_1$.

Finally, a whole family of solutions to the set of Eqs. (2)–(4) characterized by the same total plant capacity $Q$ and the same flow rates $q_i$ through all filters is obtained.

Such a family of solutions is presented in Fig. 4 based on a rigorous numerical solution to the system of Eqs. (1)–(3) supplied with the same data $c_1$, $Q$, $z$, $n$ as given in di Bernardo's [9, 10] example of calculations for a pilot plant – see Table 1. In these computations, the ratio of $q_1/q_{avr}$ was imposed to be equal to 1.3. The flow rates now refer to 1 m$^2$ of a filter (hydraulic load), so consequently, the following dimensions are in use: $H$ [m $H_2O$], $q$ [m/day], $Q$ [m/day], $c_1$ [(m $H_2O$)/(m/day)], $c_2$[(m $H_2O$)/(m/day)$^n$].

Table 1

Coefficients $c_1$, $c_2$, $n$ of Eq. (2) measured by Di Bernardo [9], [10] for a pilot and a full scale plants[a]

| Scale of the plant | Number of filters | $c_1$ [(m $H_2O$)/(m/day)] | $c_2$ [(m $H_2O$)/(m/day)$^n$] | $n$ |
|---|---|---|---|---|
| Pilot plant | 4 | 0.00145 | 0.00050 | 1.22 |
| Full scale plant | 4 | 0.00150 | 0.0000026 | 1.90 |

[a]The coefficients $c_1$, $c_2$ were predicted for $q_i$ referred to 1 m$^2$ (hydraulic load, [m$^3$/(m$^2$·day)] simplified to [(m/day)]).

The curves $q_i(H)$ in Fig. 4 fit perfectly with the horizontal straight lines expected here in spite of the fact that they are not received from the rough approximation (4), but from the precise numerical solution [11] to the set of Eqs. (1)–(3). Fifty different values of $H$ were chosen, then $h_0$, $c_2$ calculated according to the points 1, 2 of the theorem 2 and finally $q_i$ computed from the system of Eqs. (1)–(3). The set of Eqs. (1)–(3) was solved by the most precise of the methods described elsewhere [11]. In this method, each value of $q_i$ is bounded both from the upper and the lower side but these limits are so close to each other that they are denoted by single lines in Fig. 4.

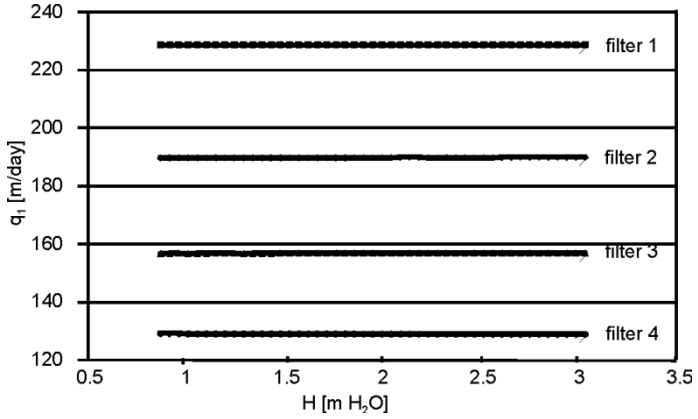


Fig. 4. Distribution of the flow rate vs. $H$ for a family of solutions calculated according to property 1 for $Q$ = 704 m/day, $q_1/q_{avr}$ = 1.3, and for the same data $c_1$, $n$ as for the pilot plant experiments (Table 1 after [9, 10])

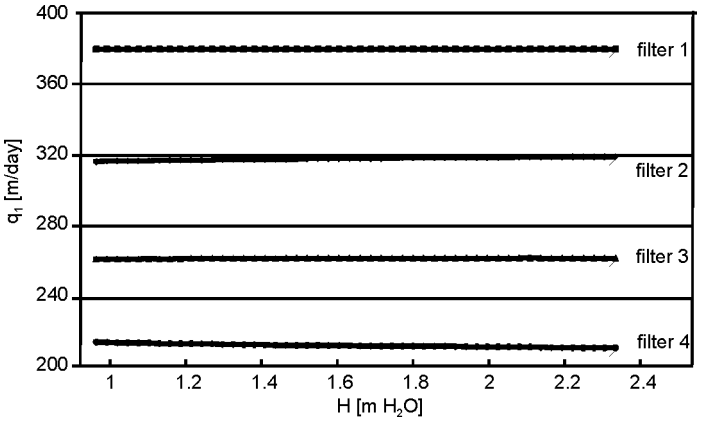


Fig. 5. Distribution of the flow rate vs. $H$ for a family of solutions calculated according to property 1 and for $c_1$, $n$ the same as given in Table 1 for the full scale water treatment plant and for $q_1/q_{avr} = 1.3$, $Q = 4q_{avr} = 1168$ m/day

The same refers to Fig. 5 but this time the inclinations of the curves $q_i(H)$ from straight horizontal lines are more visible due to a high value of exponent $n$ describing head losses $c_2 q_i^n$ created by drainages and orifices.

The next property refers only to the family of solutions to the system of Eqs. (2)–(4) defined by Theorems 1 and 2.

Theorem 3. According to Eqs. (2), (4) and to Theorem 1, the flow rate through a clean filter $q_1$ and the total capacity of the plant $Q$ remain the same for various coefficients $c_2$ if simultaneously:

1) the lowest water table level $H - h_0$ varies linearly with $c_2$ according to Eq. (2):

$$H - h_0 = c_1 q_1 + c_2 (q_1)^n$$

2) the highest water table level $H$ before a backwash depends proportionally on $c_2$;

$$H = \frac{c_1 q_1 + c_2 (q_1)^n}{1 - \dfrac{h_0}{H}} \tag{5}$$

3) the water level increase between backwashes $h_0$ fulfils a linear dependence:

$$h_o = \frac{\left(c_1 q_1 + c_2 (q_1)^n\right)\dfrac{h_0}{H}}{1 - \dfrac{h_0}{H}} \tag{6}$$

Theorem 3 is illustrated in Figs. 6–9 computed as previously from an accurate solution to Eqs. (1)–(3) for $c_1$, $z$, $n$, $Q$ listed in Table 1 as predicted for a full scale plant and for $q_1/q_{avr} = 1.3$.

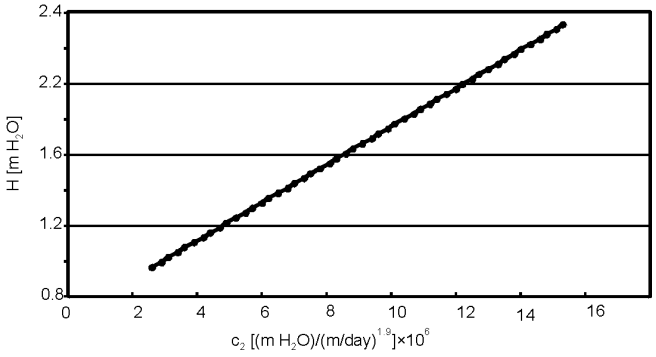


Fig. 6. Total head loss $H$ as a function of $c_2$ for data presented in Fig. 5

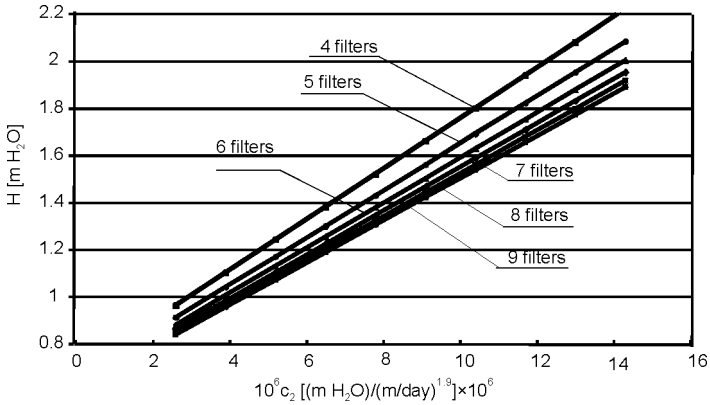


Fig. 7. Head loss $H$ as a function of $c_2$ (for $c_1$, $n$ as for the full scale treatment plant reported in Table 1) in comparison with the head loss computed for more filters operating with the same $q_{avr} = Q/z = 292$ m/day, $q_1/q_{avr} = 1.3$

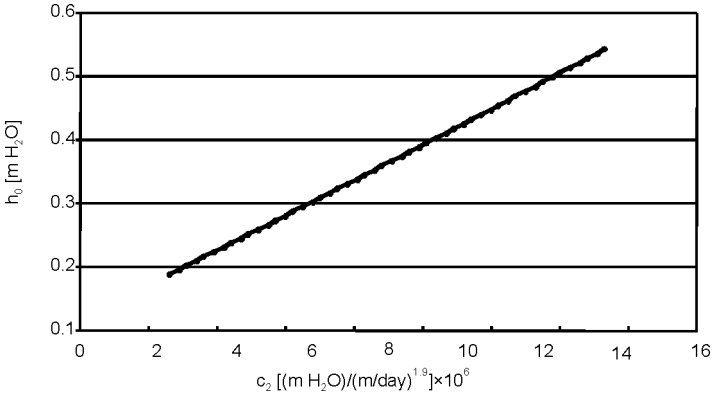


Fig. 8. The highest water table fluctuation $h_0$ over the filters, computed as a function of $c_2$ for the same data as the calculations presented in Fig. 5

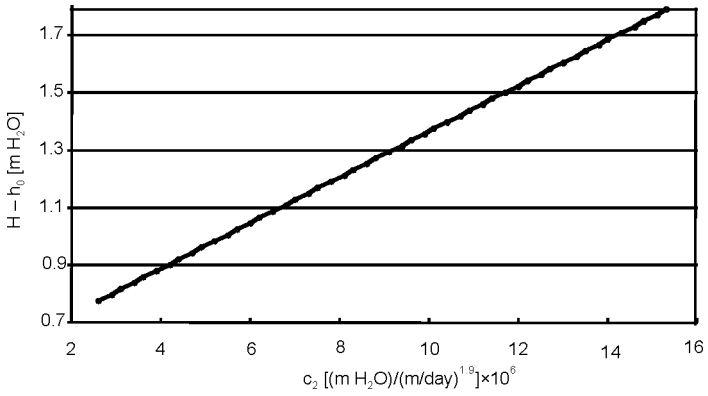


Fig. 9. Head loss $H - h_0$ calculated as a function of $c_2$ for the same data as in Figs. 5, 6

The next theorem refers to the resistance of hydraulic porous media $c_{1z}$ to flow just before its backwash. As the total head loss of flow through the plant is equal to $H$ just before each of backwashes, $c_{1z}$ is defined by:

$$H = c_{1z}\, q_z + c_2 \left(q_z\right)^n \tag{7}$$

Equation (7) is introduced for the most clogged filter $z$ operated with the flow rate $q_z$.

Theorem 4. For a family of solutions to the set of Eqs. (2)–(4) constructed according to the points 1, 2 of Theorem 2 (so characterized by the same values of flow rates $q_1$, ..., $q_i$, ..., $q_z$) the hydraulic resistance $c_{1z}$ of the most clogged filter media just before its backwash depends linearly on the constant $c_2$ being proportional to the turbulent head losses in the drainage and orifices:

$$c_{1z} = \frac{c_1 q_1 + c_2 q_1^n - \left(1 - \dfrac{h_0}{H}\right) c_2 q_z^n}{q_z \left(1 - \dfrac{h_0}{H}\right)} \tag{8}$$

The family of solutions to the system of Eqs. (4), (2), (3) calculated according to the instructions given by Theorems 1–3 have almost identical flow distribution $q_1$, ..., $q_i$ ..., $q_z$ between filters in a bank and a constant ratio $h_0/H$. Equation (8) results directly from the definition of $c_{1z}$ (7) and from Eqs. (2), (6). Theorem 4 is illustrated in Figs. 10, 11 constructed as previously from fifty accurate solutions to the set of Eqs. (1)–(3). The data for these computations are the same as those listed in Table 1, with $q_1/q_{avr} = 1.3$ in this instance. It may be seen that the resistance $c_{1z}$ is almost a linear function of $c_2$. However, the ratio of $c_{1z}/H$ as a function of $c_2$ shows some unlinearity as presented in Fig. 12, constructed from the solutions to the system of Eqs. (1)–(3) for 50 different values of $c_2$.

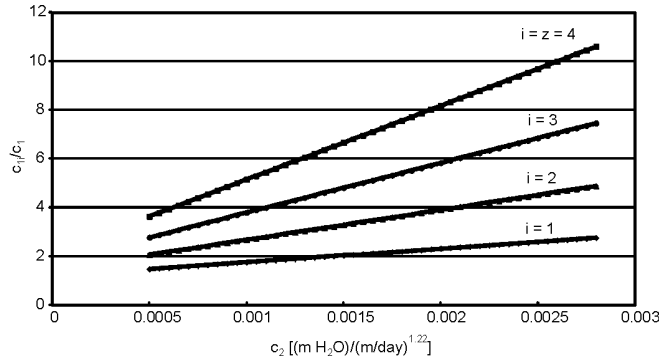


Fig. 10. Relative resistance $c_{1i}/c_1$ of four filters before backwashing calculated as a function of $c_2$ for $Q$ = 704 m/day, $q_1/q_{avr}$ = 1.3, and for $c_1$, $n$ the same as for the pilot plant (see Table 1) ; the most clogged filter 4

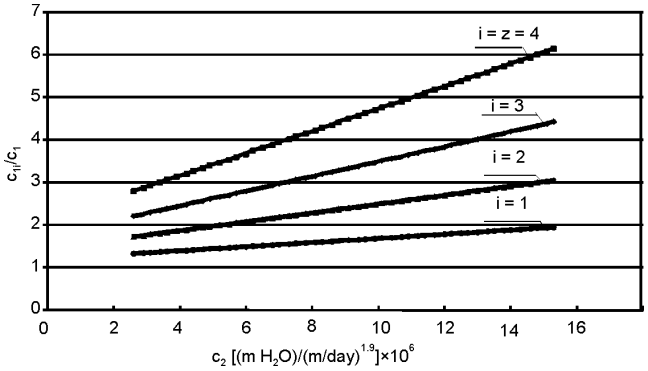


Fig. 11. Resistance of four filters as a function of $c_2$ for the same $n$, $c_1$ as for the full scale plant reported in Table 1, and for $q_1/q_{avr}$ = 1.3, $Q = 4q_{avr}$ = 1168 m/day

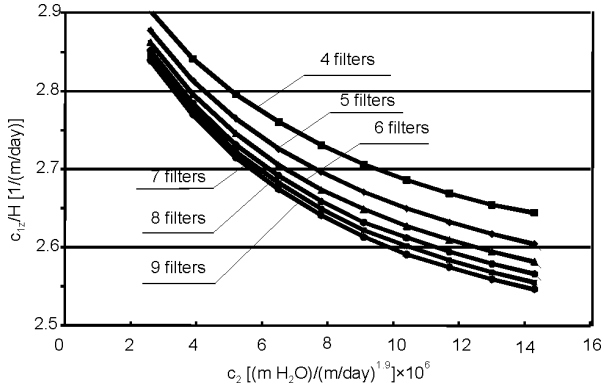


Fig. 12. Some nonlinearity of the ratio $c_{1z}/H$ as a function of $c_2$ according to computations based on a precise numerical solution to the system of Eqs. (1)–(3) and subject to the same $Q$, $q$, $c_1$, $n$ as for Figs. 5–9, 11

## 6. OPTIMISATION PROBLEM

It is assumed that the highest resistance of porous media to flow corresponds to the largest volume of water passing through a filter. This usually reasonable assumption is not always valid as the depth bed filtration theory gives a complex picture of the head loss increase with time and filtration velocity impacts a pattern of deposit distribution in depth. However, in most optimisation tasks it is not possible to avoid some simplifications. It is believed that the substitution of a problem on the longest filter run by the problem on the highest media resistance to flow $c_{1z}$ at the end of this run is acceptable in many technical applications. Concluding the objective function is defined by the equation

$$\mathrm{Max}c_{1z} = \frac{H - c_2 q_z^n}{q_z} \tag{9}$$

The constraints include the set of Eqs. (4), (2), (3) and some limits imposed to the total available head loss of flow $H$ and the ratio of flow rate $q_1$ to the average flow rate $q_{\mathrm{avr}}$:

$$H \le H_{\max} \tag{10}$$

$$\frac{q_1}{q_{\mathrm{avr}}} \le D \tag{11}$$

where: $H_{\max}$ – the highest available head loss of flow through a plant limited by its construction, $D$ – limit imposed on the ratio $q_1/q_{\mathrm{avr}}$ because of required filtrate quality.

The formulated optimisation problem will be solved in two steps. First it will be shown that for all families of solutions to the set of Eqs. (4), (2), (3) characterized by flow rate distribution $q_1$, ..., $q_i$, ..., $q_z$ for which $q_1/q_{\mathrm{avr}} = D$ the highest hydraulic resistance to flow of the most clogged filter $c_{1z}$, just before its backwash, refers to the highest coefficient $c_2$. For this value of $c_2$ the total head loss of flow through the plant $H$ reaches $H_{\max}$. In the latter step, it will be proved that any solution being outside of these families of solutions for which $q_1/q_{\mathrm{avr}} = D$ refers to a lower value of $c_{1z}$, than received simultaneously for $q_1/q_{\mathrm{avr}} = D$ and for $H = H_{\max}$.

## 7. SOLUTIONS

The solution to the optimisation problem inside of the family of fixed values of $q_1$, ..., $q_i$, ..., $q_z$, for which $q_1/q_{\mathrm{avr}} = D$ results directly from theorems 1–4. As the parameters $c_2$, $H$, $h_0$ have to be adjusted through Eqs. (2), (5), (6) resulting in the required $Q$, $q_1/q_{\mathrm{avr}}$, the same $h_0/H$ and $q_z$, so the resistance of the filter media $z$ in Eq. (8) linearly depends on $c_2$ and is the highest for the value of $c_2$ for which $H = H_{\max}$. This might be intuitively expected.

The family of solutions defined by the points 1–3 fulfilling Theorem 3 refers to the highest acceptable value of $q_1$. There are also solutions to the set of Eqs. (4), (2), (3) fulfilling constrains (10), (11) but not belonging to this family. These solutions satisfy required plant capacity $Q$ for some lower values of the largest flow rate $q_1^*$, and for different flow rate distributions $q_1^*, ..., q_i^*, ..., q_z^*$ among the filters. To make this text clear, the same notations are used as previously to describe $h_0$, $q_1$, ..., $q_i$, ..., $q_z$, $c_2$, $c_{1z}$ when they refer to the solutions of the set of Eqs. (4), (2), (3) being a subject to the restriction $q_1/q_{avr} < D$, and not belonging to the family of fixed $q_1$, ..., $q_i$, ..., $q_z$, for which $q_1/q_{avr} = D$. However, in this case they are denoted additionally by an asterisk, thus $q_1^* < q_1$. As the filter media is known in advance and all comparisons between the results of calculations will be done for the same arbitrarily chosen head loss $H$ before a subsequent backwash in a plant, there is no reason to use the asterisk * to distinguish $c_1$ and $H$ for separate families of solutions.

Let us take into account two different solutions to the system of Eqs. (4), (2), (3), both satisfying the same plant capacity for the same available head loss $H$. The second of these solutions $q_1^*, ..., q_i^*, ..., q_z^*, c_2^*, h_0^*$ refers to $1 < q_1/q_{avr} < D$. At the end of a filter run, the resistance of the most clogged porous media may be described by the equation:

$$c_{1z}^* = \frac{H - c_2^*(q_z^*)^n}{q_z^*}, \qquad c_{1z} = \frac{H - c_2 q_z^n}{q_z} \tag{7*}$$

We shall investigate the relations between $c_2$, $q_z$, and $c_2^*$, $q_z^*$ in advance to confront $c_{1z}$ with $c_{1z}^*$. For further discussion it is useful to have a closer look at the relations between $h_0$, $H - h_0$ and $h_0^*$, $H - h_0^*$. According to approximation (4) both flow rate distributions $q_1$, ...,$q_i$, ...,$q_z$ and $q_1^*, ..., q_i^*, ..., q_z^*$ consist of elements of geometric progression giving an identical plant capacity $Q = q_1 + ... + q_i + ... + q_z = q_1^* + ... + q_i^* + ... + q_z^*$. Bearing in mind that by definition the flow rate $q_1^*$ is lower than $q_1$ obviously $q_z^*$ must be higher than $q_z$. Moreover from Eq. (4) $h_0^* < h_0$. As both solutions (with and without the asterisk) refer to the same available head loss $H$, thus $H - h_0^* > H - h_0$, which means that the turbulent head loss coefficients $c_2$ and $c_2^*$ fulfil the inequality $c_1 q_1^* + c_2^* \left(q_1^*\right)^n > c_1 q_1 + c_2 \left(q_1\right)^n$. Keeping in mind that from the definition of $q_1$ any value of $q_1^*$ is lower than $q_1$, it is obvious that $c_2^* > c_2$. All the necessary items of information on the relations between $c_2^*, c_2$ and $q_z, q_z^*$ have been collected $(c_2^* > c_2, q_z^* > q_z)$, and finally the expectation that $c_{1z}^*$ is lower than $c_{1z}$ may be confirmed by discussing the equation:

$$c_{1z} = \frac{H}{q_z} - c_2(q_z)^{n-1}, \qquad c_{1z}^* = \frac{H}{q_z^*} - c_2^*(q_z^*)^{n-1} \tag{7**}$$

Concluding, the highest hydraulic resistance of filter media before backwashing should be sought among the family of solutions $q_1$, ... $q_i$, ... $q_z$, $c_2$, $h_0$, subject to $q_1/q_{\text{avr}} = D$. Finally, the highest value of $c_{1z}$ (and hopefully the longest filter run) refers to $H = H_{\max}$ and to $q_1/q_{\text{avr}} = D$.

## 8. PRACTICAL ASPECTS

A possible application of equations and theorems discussed here is now presented in an optimisation example calculated for a four-filter plant. The conditions assumed are those of di Bernardo [9, 10] for a full scale plant (see Table 1): According to the theorems developed in the previous paragraphs, the highest resistance of the media before a backwash occurs if simultaneously the ratio of $q_1/q_{\text{avr}}$ and $H$ reach their maximum values.

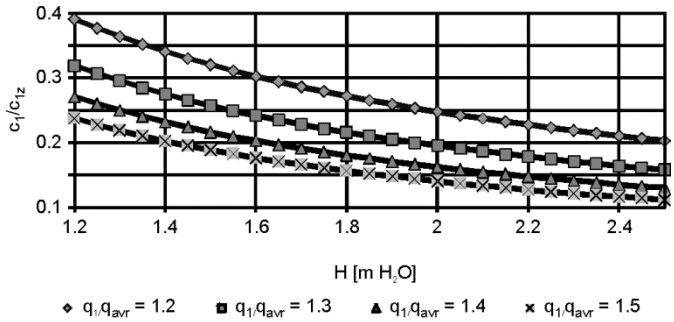


Fig. 13. The ratio of $c_1/c_{1z}$ as a function of $H$ and $q_1/q_{\text{avr}}$ for an optimisation example

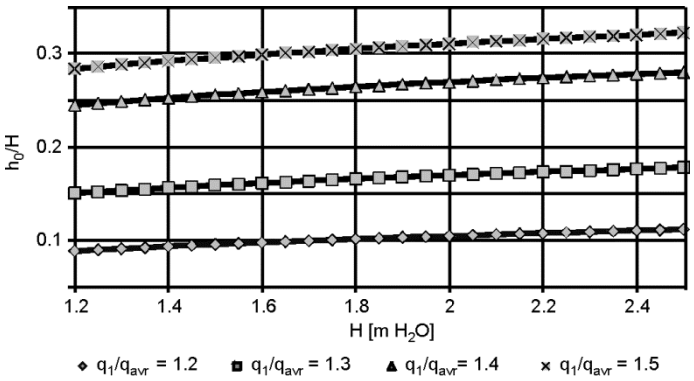


Fig. 14. Values of $h_0/H$ as a function of $q_1/q_{\text{avr}}$
and to some extent also a function of $H$ (data the same as for Fig. 11)

Usually $q_1/q_{avr}$ is limited by technological reasons and $H$ mainly by the construction of a plant. This simple optimisation rule was tested many times in numerical calculations. Examples of such tests are presented in Figs. 13 and 14. Each of lines in these figures was constructed from 50 points obtained from an accurate numerical solution to the set of Eqs. (1)–(3). A full system of equations was used again to verify the optimisation approach developed based on the approximated model described by the set of Eqs. (4), (2), (3). Coefficients $c_1$, $n$ and the plant capacity are the same as in di Bernardo's [10] full scale experiments. Values $h_0$, $c_2$ were adjusted in such a way that the same $Q$ and $q_1/q_{avr}$ were obtained for different values of $H$ varying from 1.2 to 2.5 m. From Figure 13 it can be seen that the resistance of the filter media $z$ increases as $q_1/q_{avr}$ increases (for the same $H$) and behaves analogously if $H$ increases for the same $q_1/q_{avr}$ . The value of $h_0/H$ remains almost constant for all computations referring to the same $q_1/q_{avr}$ (Fig. 14).

## 9. CONSTANT VERSUS VARIABLE RATE FILTRATION

To evaluate the advantage resulting from using the VDR control system, as opposed to the constant flow rate system, two filter plants consisted of $z = 4$ identical filter media, producing the same amount of filtrate, and operated with the same total head loss $H$ were compared. The ratio of $c_{1z}$ (CRF)/$c_{1z}$(VDRF) was calculated and shown in Fig. 15.

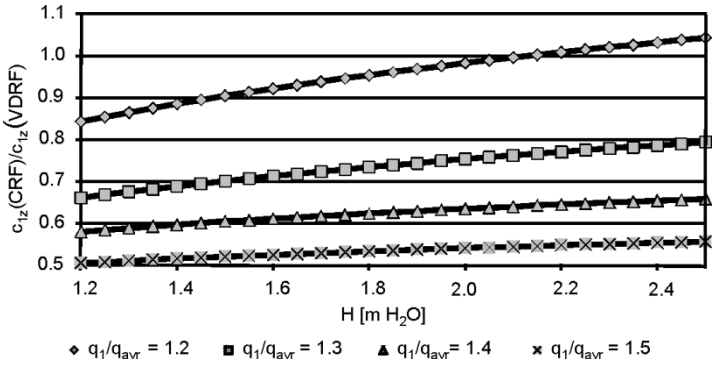


Fig. 15. Ratio of the filter media resistances before a backwash $c_{1z}$ (CRF)/$c_{1z}$(VDRF), representative of Constant rate and variable declining rate filter operation, respectively

Here $c_{1z}$(CRF) presents the hydraulic resistance of the constant rate filter (CRF) media $z$ just before the backwash and $c_{1z}$(VDRF) resistance of the variable declining rate filter (VDRF) media $z$. The resistance $c_{1z}$(CRF) was calculated as equal to $(H - 0.2\text{ m})/q_{avr}$, on the assumption that the head loss of flow through the filter drainage and an open flow rate controller (at the end of the filter run) is equal to 0.2 m $H_2O$.

For $q_1/q_{avr} = 1.1$ the resistance of the clogged filter media is usually higher in a CFR system than it is in a VDR one. Therefore it is possible that no profit would result from VDR control system and these results are not included in Fig. 15. For $q_1/q_{avr} = 1.2$ VDR control system results in higher hydraulic resistance $c_{1z}$ of filter media $z$ for $H < 2.0$ m. Higher the ratio $q_1/q_{avr}$, lower the ratio $c_{1z}$(CRF)/$c_{1z}$(VDRF) is and more profitable is the VDR operation system. However, the ratio $q_1/q_{avr}$ is to be restricted because of the filtrate quality. A limit of 1.3 or more commonly 1.5 is imposed on this ratio on a rule of thumb but pilot plant experiments should be used to verify these limits for a given case. In such pilot experiments particles counting is much more reliable than turbidity measuring.

## 10. THE MOSTLY CLOGGED FILTER

Till now only the maximum ratio of $q_1/q_{avr}$ was concerned as a significant factor of the filtrate quality to be determined experimentally. However, the turbidity of filtrate produced by the dirtiest filter may be of crucial concern. The product $h_{media}q$ is sometimes recognized as a representative parameter for filtrate quality relating to given raw water, pretreatment, and porous media. By $h_{media}$ head loss created by filter media is created. The flow rates $q_z$ (four filters) obtained according to precise solution to the set of Eqs. (1)–(3) are denoted by circles in Fig. 16 in comparison with a monogram $q_z/q_{avr}$ constructed as a function of $h_0$/H from Eq. (12):

$$\frac{q_z}{q_{avr}} = \frac{z\left(1-\frac{h_0}{H}\right)^{(z-1)}}{\frac{h_0}{H}\left(1-\left(1-\frac{h_0}{H}\right)^{z}\right)} \tag{12}$$

resulting directly from approximation (4) and from the formula for a sum of geometrical progression elements $q_1$ ..., $q_i$ ..., $q_z$. The general monogram can be applied to any VDR water filtration plant but it is based on rough approximation (4), so the points denoted by circles do not lay exactly on the line developed for a four filter plant. Each of these points represents a value of $q_z/q_{avr}$ computed from the set of Eqs. (1)–(3) for tests in which $q_1/q_{avr} = 1.1$, 1.2, 1.3, 1.4 and 1.5. For these particular tests $q_z$ versus $h_0$/H are presented in Fig. 16. If for instance a total available head loss $H$ in this plant is equal to 2.2 m, $h_0 = 0.61$ m, and $q_1 = 438$ m/day $= 1.5q_{avr}$ was chosen experimentally it is advisable to verify also the quality of filtrate collected from the mostly clogged filter ($c_{1z} = c_1/0.12$, see Fig. 13) operated with $q_z = 0.58q_{avr} = 0.58q_1/1.5$ = 169 m/day (Fig. 16). If the filtrate quality is poor, it is a question of economy whether it is reasonable to improve pretreatment or whether a lower $H$, rather than the maximum available value, should be considered. In general, optimising of chemical

treatment should be attempted first as it has usually a tremendous impact on both filtration quality and length of a filter run.

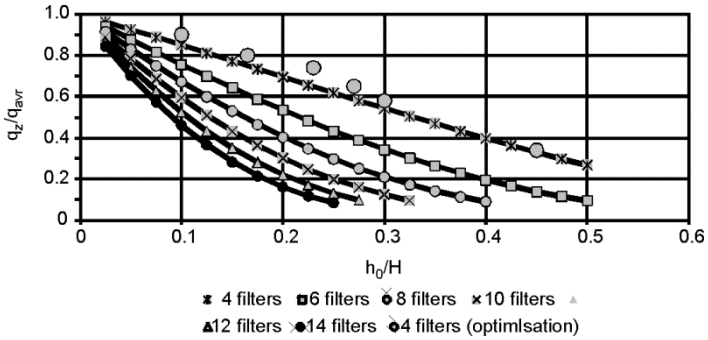


Fig. 16. Monogram for primary values $q_z$ in comparison with some points obtained from an optimisation example

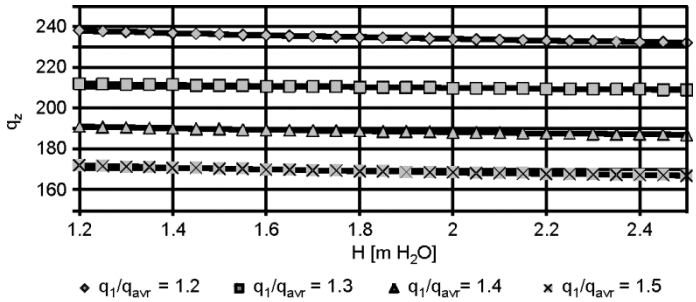


Fig. 17 Almost constant values of $q_z$ versus $H$ calculated for an optimisation example

## 11. FINAL REMARKS

The theorems presented in the paper and the optimisation approach to operation of a VDR filter plant were developed from the set of Eqs. (4), (2), (3) but verified by numerical solutions to the set of Eqs. (1)–(3), which does not include a simplified Eq. (4). The data from a pilot and a technical scale treatment plants reported by di Bernardo [9, 10] were used for verification of the findings. However, this verification is still limited and partially numerical, so a pilot plant was constructed at the Cracow University of Technology [24] to carry out empirical tests. The results of experiments confirming the theory presented here and advantages of application of the optimisation approach to both a pilot and a full-scale treatment plants will be described in the next paper.

## 12. CONCLUSIONS

Approximation (4) has been found to be useful in deducing some approximate linear relationships between the parameters of a VDRF hydraulic control system. Based on this approximation, it has been shown that the highest resistance of filter $z$ media before backwashing is related to the highest available head loss of flow through a plant and to the turbulent resistance of orifices adjusted to obtain as high a flow rate through a clean filter as technologically possible. The deduced properties of the solution to the system of equations governing VDR filter plants have been verified in comparison with numerical solutions, which in turn have been compared with literature experimental data.

It is expected that the longest duration of filter runs is related to the highest resistance of the filter media just before the backwash. In conclusion, the theoretical considerations presented here led to a more efficient filter plant operation method based on an increase of both the water table level above filter media and the ratio of maximum to average flow rates to the highest acceptable values.

Perhaps the best solution to optimisation problems is a pilot plant experiment taking into consideration some of the linear relations developed in the present paper (Theorems 1–4). Such a pilot plant and calculations would have to take into account any possible changes in the water temperature in summer and winter [25].

### SYMBOLS

| | | |
|---|---|---|
| $c_1$ | – | proportional coefficient characterizing the resistance of a clean medium |
| $c_2$ | – | coefficient of turbulent head losses |
| $c_{1z}$ | – | resistance of filter media $z$ before a backwash |
| $c_{1z}$(CRF) | – | resistance of filter media $z$ for constant flow rate control system |
| $D$ | – | constant value |
| $H$ | – | total head loss of flow through the plant just before a backwash |
| $h_{\text{media}}$ | – | head loss of flow through filter media just before its backwash |
| $h_0$ | – | the height of water surface increase between backwashes |
| $i$ | – | number of a filter in a bank |
| $n$ | – | exponent of turbulent head loss |
| $Q$ | – | total flow rate through the system |
| $q_i$ | – | flow rate through a filter i |
| $q_{\text{avr}}$ | – | mean value of flow rate through a filter $q_{\text{avr}} = Q/z$ |
| z | – | number of the filters in a bank |

### ACKNOWLEDGEMENTS

This work was sponsored by the Polish National Foundation as a part of the project 1235/T09/2005/28.

REFERENCES

[1] CLEASBY J.L., J. Am. Water Works Assoc., 1969, 61 (4), 181.
[2] DĄBROWSKI W., ZIELINA M., KUŁAKOWSKI P., SPACZYŃSKA M., *Evaluation of sorption into granular activated carbon by UV absorbance*, 5th Int. Conf. Hydro-Science and Engineering, September 18–12 2002, Warsaw, on CD.
[3] DI BERNARDO L., CLEASBY J.L., J. Environ. Eng. Div., 1980, 106, 1023.
[4] HILMOE D.J., *A comparison of constant rate and declining rate direct filtration of a surface water supply*, Thesis presented to Iowa State University, in partial fulfilment of the requirements for the MSci. degree, 1983.
[5] HILMOE D.J., CLEASBY J.L., J. Am. Water Works Assoc., 1986, 78 (12), 26.
[6] CLEASBY J.L., Water Sci. Technol., 1993, 27 (10), 151.
[7] MACKIE R.I., DĄBROWSKI W., ZIELINA M., Environ. Prot. Eng., 2007, 33 (4), 27.
[8] CORNWELL D.A., BISHOP M.M., DUNN H.J., J. Am. Water Works Assoc., 1984, 76 (12), 55.
[9] DI BERNARDO L., *A rational method to the design of declining rate filters*, 4th World Filtration Congress, Ostend, Belgium, 1986 (manuscript).
[10] DI BERNARDO L., Filtration Separation, 1987, Sept./Oct., 338.
[11] DĄBROWSKI W., Acta Hydroch. Hydrob., 2006, 34 (5), 442.
[12] MACKIE R.I., DĄBROWSKI W., ZIELINA M., Environ. Prot. Eng., 2003, 29 (1), 45.
[13] AKGIRAY O., SAATÇI A.M., Water Sci. Technol., 1998, 38(6), 89.
[14] SAATÇI A.M., J. Environ. Eng., 1989, 115 (2), 462.
[15] CHAUDHRY F.H., J. Environ. Eng., 1987, 113 (4), 852.
[16] ARBOLEDA J., GIRALDO R., SNEL H., J. Am. Water Works Assoc., 1985, 77 (12), 67.
[17] CLEASBY J.L., DI BERNARDO L., J. Environ. Eng. Div., 1980, 106,1043.
[18] DROŻDŻ J., Gaz, Woda i Technika Sanit., 1979, 55 (4), 108.
[19] MACKIE R.I., ZHAO Q., Water Res., 1999, 33 (3),794.
[20] DĄBROWSKI W., *A discussion of controversies regarding deep bed filtration for water treatment*, Filtech – Int. Conf. Exhibition for Filtration and Separation Technology, 2005, 11–13 October., Rhein-Main-Hallen Wiesbaden, Germany, Vol.1, I-394–401.
[21] DĄBROWSKI W., Arch. Hydro-Eng. Environ. Mechanics, 1993, 40 (1/2),135.
[22] ZIELINA M., *Theoretical and Empirical Investigations into Water Rapid Filters of Variable Declining Rate*, Thesis presented to the Environmental Engineering Department, Cracow University of Technology, in the partial fulfilment of the requirements for the degree of PhD, Cracow, 2002.
[23] ZIELINA M., DĄBROWSKI W., MACKIE R.I., *Empirical verification of an optimisation approach to a VDR filter plant operation*, 5th Int. Conf. Hydro-Science and Engineering, 1992, September 08–12, Warsaw (on CD).
[24] ZIELINA M., DĄBROWSKI W., *Principles of Designing and Operating Rapid Filter Plants Which Are Not Supplied with Flow-Rate Regulators*, Monograph 293, the Cracow University of Technology, 2003, Cracow (in Polish).
[25] DĄBROWSKI W., MACKIE R.I., Arch. Hydro-Eng. Environ. Mechanics, 1994, 41 (3–4), 37.

Environment Protection Engineering

Vol. 37 2011 No. 4

WOJCIECH GOLIMOWSKI*, AGNIESZKA GRACZYK-PAWLAK*

# INFLUENCE OF ESTERIFICATION OF WASTE FATS PROCESS PARAMETERS ON AGRICULTURAL BIOFUEL PRODUCTION FACILITIES

The paper presents the influence of esterification process parameters in waste fats on their level of reaction. Raw materials contained: frying rapeseed oil, animal lard, methyl alcohol and potassium hydroxide as a catalyst, necessary for reaction in non-pressure conditions. Esterification was carried out at 35–40 °C and 60–65 °C in two separate esterificators differing from one another with mixing systems. It has been established that in terms of contents of non-reactants allowed the obtained product meets the European EN 14214 standard, determining the quality of biodiesel.

## 1. INTRODUCTION

In search of alternative fuels, Szlachta [1] pointed at methyl esters of higher fatty acids, their properties being close to those of motor oil. In the nineties, a research was conducted in Poland on capabilities to produce biofuels by farmer producers out of raw rapeseed oil [2], based on the technology of low-temperature transesterification [3]. From the moment of publishing the information on a prototype low-efficiency installation for fuel production [4], there has been an increasing interest among farmers. In 2007, a rapid increase in rape prices [5] along with a decrease in oil prices caused the farmers to seek other inexpensive sources to produce methyl esters.

Walisiewicz-Niedbalska and Podkówka [6] proposed to utilize frying oils and animal fats for biofuels production for own use. Research conducted by Sulewski et al. [7], Wang et al. [8], Leong et al. [9], Predojević [10], Phan [11] have shown that methyl esters from frying oils from various sources have similar properties. Animal fats are solid at room temperature due to high content of saturated fatty acids [12]. As shown in the studies performed by Tashtoush et al. [13], Wyatt'a et al. [14], Golimoski and Nowak [15] biofuels made from animal fats as well as frying oils have sim-

*Institute of Technology and Life Sciences, Poznań, ul. Biskupińska 67, 60-463 Poznań, Poland; corresponding author W. Golimowski, e-mail: wojgolim@ibmer.waw.pl

ilar properties as diesel fuel, except for their freezing point, which takes positive values. Biodiesel, based on frying oil, is manufactured on industrial scale in Austria, where it contributes to 1.5% of fuel's national supply [16]. In Denmark, the Daka company produces biodiesel from animal fats [17].

The analyses of waste fats-based biofuel properties performed so far, in most cases did not determine the presence of free glycerol and unreacted particles. According to Strenziok and Wickboldt [18], an excessive presence of these particles can cause serious damage to the engine. A research conducted by Golimowski et al. [19] on the production of biofuels based on low-temperature esterification technology from refined rapeseed oil as well as from fresh animal lard, has shown increased participation of di- and triglyceride in the ester phase. This proves low reaction level of triglycerides.

The study aimed at evaluating the influence of the reaction environment and the kind of raw materials on the occurrence of glycerol groups in methyl esters of higher fatty acids. Present knowledge provides no information on the quality of waste fat-based biofuels, manufactured in homesteads for own use.

## 2. MATERIALS AND METHODS

Raw materials used in the research were waste rapeseed oil (FO) and animal lard (AL), which went rancid on behalf of bad storage. Substrates necessary for esterification were methyl alcohol with molar part of 6 to 1 and a 2% addition of potassium hydroxide. 8 kg of raw materials were used for one trial.

Table 1

Physical and chemical properties of materials used

| Parameters | FO | AL |
|---|---|---|
| Acid value, mg KOH·g$^{-1}$ | 2.6 | 7.3 |
| Thickness at 20 °, kg·m$^{-3}$C | 912 | 915 |
| Kinematic viscosity at 40 °C, mm$^{2}$·s$^{-1}$ | 53.99 | 42.63 |
| Combustion temperature, °C | 242 | 244 |
| Calorific value, MJ·kg$^{-1}$ | 38.9 | 39.1 |

Physicochemical properties of the materials were described and compared to those of food fats. The results obtained are given in Tables 1 and 2. In the next stage of the study, frying oil and animal fats underwent the esterification process, which was carried out in two separate esterificators: hydraulically mixed (EH) and mechanically mixed (EM) at 35–40 °C and 60–65 °C after mixing the substrates for 30 minutes. Post-reactive product was placed in sedimentation columns for 24 h, where it distributed into two phases: ester phase and glycerol phase. After two weeks, the concentra-

tion of unreacted particles and free glycerol in the ester phase was determined using the gas chromatography (Clarus 600, PerkinElmer). The measurement was performed in accordance to the Polish standard PN-EN 14105, regarding free and total glycerol and mono-, di-, triglycerides.

Table 2

The contribution of fatty acids [%]

| Fatty acids | Systematic name of the acid | Carbon number | Measurement results | | Rapeseed oil [20] | Lard [21] |
|---|---|---|---|---|---|---|
| | | | FO | AL | | |
| Saturated | tetradecanoic | 14:0 | – | 2.28 | 0.06 | 0.58 |
| | pentadecanoic | 15:0 | – | 0.25 | – | – |
| | hexadecanoic | 16:0 | 5.45 | 26.79 | 4.5 | 22.77 |
| | heptadecanoic | 17:0 | – | 0.75 | – | – |
| | oktadecanoic | 18:0 | 2.19 | 17.76 | 1.8 | 13.10 |
| | eicosanoid | 20:0 | 0.65 | 0.21 | 0.6 | – |
| | docosanoic | 22:0 | 0.33 | – | 0.3 | – |
| Total | | | 8.62 | 48.04 | 7.26 | 36.45 |
| Monounsaturated | tetradecenoic | 14:1 | – | 0.24 | – | – |
| | hexadecenoic | 16:1 | 0.27 | 2.49 | 0.2 | 2.32 |
| | heptadecenoic | 17:1 | – | 0.49 | – | – |
| | oktadecenoic | 18:1 | 64.91 | 37.63 | 61.4 | 50.39 |
| | eicosanoid | 20:1 | 1.61 | 0.74 | 1.6 | 2 |
| | decosanoic | 22:1 | 0.68 | – | 0.3 | – |
| Total | | | 67.47 | 41.59 | 63.5 | 54.71 |
| Polyunsaturated | octadecadienoic | 18:2 | 16.46 | 4.96 | 19.4 | 5.30 |
| | octadecatrienoic | 18:3n3 | 5.15 | 0.49 | 9.3 | 1.15 |
| Total | | | 21.61 | 5.45 | 28.7 | 6.45 |
| Other | | | 2.30 | 2.46 | 0.4 | – |
| Total | | | 100 | 97.07 | 99.86 | 97.69 |

## 3. RESULTS AND DISCUSSION

Based on the analysis of physicochemical properties (Table 1) it has been established that the fats used in the research were partially biodegraded. This is shown by a high acid value: 2.6 mg $KOH \cdot g^{-1}$ in frying oil and 7,3 $mgKOH \cdot g^{-1}$ in animal fats. FO's high viscosity of 53.99 $mm^2 \cdot s^{-1}$ at 40 °C results from high mechanical pollution, also confirmed organoleptically. The analysis of raw materials showed an increased content of saturated acids in relation to fresh fats (Table 2). The increased content of saturated acids results from progressive degradation of the fats.

Results of the research confirming the presence of unreacted particles and free glycerol are given in Tables 2 and 3. Tests 1–4 were performed under the following conditions:

Test 1 – EH reaction at 35–40 °C,
Test 2 – EM reaction at 35–40 °C,
Test 3 – EH reaction at 60–65 °C,
Test 4 – EM reaction at 60–65 °C.

Table 3

Contents of mono-, di-, triglycerides and free glycerol in MEAL [%][a]

| Test No. | Triglycerides | | Diglycerides | | Monoglycerides | | Free glycerol | | Total | |
|---|---|---|---|---|---|---|---|---|---|---|
| | M | A | M | A | M | A | M | A | M | A |
| 1 | 0.02 | 0.02 | 0.06 | 0.06 | 0.24 | 0.24 | 0.26 | 0.23 | 0.58 | 0.55 |
| | 0.02 | | 0.06 | | 0.23 | | 0.23 | | 0.54 | |
| | 0.02 | | 0.06 | | 0.24 | | 0.21 | | 0.53 | |
| 2 | 0.02 | 0.02 | 0.09 | 0.10 | 0.31 | 0.34 | 0.12 | 0.11 | 0.54 | 0.57 |
| | 0.01 | | 0.11 | | 0.39 | | 0.14 | | 0.65 | |
| | 0.03 | | 0.11 | | 0.31 | | 0.08 | | 0.53 | |
| 3 | 0.02 | 0.02 | 0.06 | 0.05 | 0.21 | 0.22 | 0.18 | 0.20 | 0.47 | 0.48 |
| | 0.02 | | 0.05 | | 0.21 | | 0.19 | | 0.47 | |
| | 0.01 | | 0.05 | | 0.23 | | 0.22 | | 0.51 | |
| 4 | 0.03 | 0.04 | 0.09 | 0.14 | 0.31 | 0.45 | 0.02 | 0.13 | 0.45 | 0.76 |
| | 0.03 | | 0.12 | | 0.33 | | 0.12 | | 0.60 | |
| | 0.06 | | 0.20 | | 0.71 | | 0.25 | | 1.22 | |
| Standard EN14214 | | 0.20 | | 0.20 | | 0.80 | | 0.02 | | |

[a]M – measurement, A – average.

The presence of tri-, di- and monoglycerides in the methyl esters in question complied with the European standard EN 14214, regarding biodiesel quality. In all examined samples, the concentration of di- and triglycerides was below 0.2% and the concentration of monoglycerides was below 0.80%. The content of free glycerol was increased, several times higher than the limit value of 0.02%. This shows that the removal of post-reaction products is incomplete. Therefore, it is necessary to implement additional refining processes, such as rinsing with hot water, phosphoric acid or silica gel. A comparison of the refining methods mentioned above show that their effectiveness is similar, although Predojević [10] observed that the use of silica gel provides the smallest losses in biodiesel. It cannot be established based on Tables 3 and 4 alone, whether the environment of the reaction had any impact on pollution levels in methyl esters. A statistical analysis has been performed, taking a 95% confidence level, in order to describe the importance of the environment impact on the participation of unreacted particles and free glycerol. Independent variables with one degree of freedom are the following: temperature of the reactions and the equipment used for esterification reaction processes. Dependent variables are: contents of tri-, di-, monoglycerides and of free glycerol.

Table 4

Contents of mono-, di- and triglycerides and free glycerol in MEFO [%][a]

| Test No. | Triglyceride | | Diglyceride | | Monoglyceride | | Free glycerol | | Total | |
|---|---|---|---|---|---|---|---|---|---|---|
| | M | A | M | A | M | A | M | A | M | A |
| 1 | 0.11 | 0.12 | 0.11 | 0.08 | 0.16 | 0.16 | 0.09 | 0.05 | 0.47 | |
| | 0.17 | | 0.12 | | 0.16 | | 0.04 | | 0.49 | |
| | 0.09 | | 0.01 | | 0.15 | | 0.03 | | 0.28 | 0.41 |
| 2 | 0.28 | 0.12 | 0.18 | 0.11 | 0.16 | 0.14 | 0.11 | 0.08 | 0.73 | |
| | 0.08 | | 0.09 | | 0.12 | | 0.06 | | 0.35 | |
| | 0.01 | | 0.05 | | 0.13 | | 0.08 | | 0.27 | 0.45 |
| 3 | 0.00 | 0.00 | 0.11 | 0.12 | 0.24 | 0.22 | 0.08 | 0.08 | 0.35 | |
| | 0.00 | | 0.11 | | 0.23 | | 0.08 | | 0.42 | |
| | 0.00 | | 0.13 | | 0.19 | | 0.07 | | 0.39 | 0.39 |
| 4 | 0.03 | 0.02 | 0.11 | 0.10 | 0.21 | 0.21 | 0.09 | 0.06 | 0.44 | |
| | 0.02 | | 0.10 | | 0.22 | | 0.07 | | 0.41 | |
| | 0.00 | | 0.08 | | 0.19 | | 0.02 | | 0.29 | 0.38 |
| Standard EN14214 | | 0.20 | | 0.20 | | 0.80 | | 0.02 | | |

[a]M –measurement, A – average.

Table 5

Multifactorial analysis of variance for the participation of glycerides and free glycerol in methyl esters of higher fatty acids from frying oil (MEFO) and animal lard (MEAL)

| Independent variables | MEFO | | MEAL | |
|---|---|---|---|---|
| | $F_{calc.}$ | Risk of making a mistake ($p$) | $F_{calc.}$ | Risk of making a mistake ($p$) |
| | Triglycerides | | | |
| A. Mixing system | 1.672 | 0.232 | 0.019 | 0.894 |
| B. Temperature | 3.425 | 0.101 | 7.268 | 0.027 |
| A:B | 2.551 | 0.149 | 0.037 | 0.851 |
| | Diglycerides | | | |
| A. Mixing system | 0.627 | 0.451 | 0.016 | 0.903 |
| B. Temperature | 14.157 | 0.006 | 0.251 | 0.630 |
| A:B | 1.412 | 0.269 | 0.769 | 0.406 |
| | Monoglycerides | | | |
| A. Mixing system | 0.492 | 0.503 | 2.381 | 0.161 |
| B. Temperature | 6.277 | 0.037 | 38.095 | 0.000 |
| A:B | 1.004 | 0.346 | 0.095 | 0.766 |
| | Free glycerol | | | |
| A. Mixing system | 0.078 | 0.787 | 0.999 | 0.347 |
| B. Temperature | 6.832 | 0.031 | 1.000 | 0.347 |
| A:B | 0.558 | 0.477 | 1.003 | 0.346 |

Based on the analysis of multifactorial variance, it has been established that only temperature influenced the content of glycerol particles. Neither the esterificator type nor factorial interactions between the two variables had any impact. Also, a correlation was observed between the dependent variables. The correlation for dependent variables has been calculated, including variable temperature, which had a major impact on the results. These results are shown in Table 6.

Table 6

Correlation matrix of dependent variables and temperature

| MEAL / MEFO | Temperature | Triglycerides | Diglycerides | Monoglycerides | Free glycerol |
|---|---|---|---|---|---|
| Temperature | | –0.69 | 0.17 | 0.89 | 0.30 |
| Triglycerides | 0.47 | | 0.45 | –0.46 | –0.24 |
| Diglycerides | 0.76 | 0.85 | | 0.28 | 0.08 |
| Monoglycerides | 0.63 | 0.88 | 0.96 | | 0.48 |
| Free glycerol | –0.66 | 0.07 | –0.11 | 0.07 | |

As a result of the statistical factorial analysis, it has been established that the participation of triglycerides in MEAL falls with the increasing temperature, whereas the participation of monoglycerides increases. In the case of MEFO, there is a positive correlation between temperature and the participation of glyceride particles as well as a strong positive intergroup correlation. This means that the higher the temperature, the higher the contents of glyceride particles. A negative correlation of free glycerol suggests that with the increasing temperature, the contents of free glycerol particles decreases.

## 4. CONCLUSION

Presence of unreacted fat particles in biodiesel obtained based on low-temperature esterification technology from waste fats is compliant with the European standard EN 14214 regarding biodiesel quality.

Increased content of free glycerol in all samples points at the necessity of implementing initial filtration of biodiesel in order to separate free glycerol particles.

As a result of a statistical analysis, a major impact of temperature on the content of the particles in question has been observed. A temperature increase results in decreased reaction efficiency by increase of the content of glyceride particles in methyl esters from frying oil and decrease of the content of free glycerol. In the case of methyl esters from animal lard, a partly inversed correlation exists. Increasing temperature of the reaction causes the concentrations of monoglycerides to increase and of triglycerides to decrease.

## SYMBOLS

AL – animal lard
FO – frying oil
ME - methyl esters of higher fatty acids
MEFO – methyl esters of higher fatty acids from frying oil
MEAL – methyl esters of higher fatty acids from animal lard
EH – hydraulically-mixing esterificator
EM – mechanically-mixing esterificator

## REFERENCES

[1] SZLACHTA Z., *Power fuels from rapeseed of diesel engines*, Wyd. Komunikacji i Łączności, Warszawa, 2002 (in Polish).
[2] BOCHEŃSKI C.I., *Biodiesel agricultural fuel*, Wyd. SGGW, Warszawa, 2003 (in Polish).
[3] GRZYBEK A., *Technologies transesterification of rapeseed oil*, [In:] PODKÓWKA W. (Ed.), *Biofuel Glycerin Feed from rapeseed*, Wyd. Uczelniane ATR, Bydgoszcz, 2004 (in Polish).
[4] FRĄCKOWIAK P., J. Res. Replicat. Agricultural Eng., 2002, 47, 67.
[5] ROSIAK E., *Good economic situation for rape*. *Rape new challenges*, Wyd. Biznes-Press, Warszawa, 2008 (in Polish).
[6] WALISIEWICZ-NIEDBALSKA W., PODKÓWKA W., *Fat acid methyl esters from cooking oil and animals*, [In:] PODKÓWKA W. (Ed.), *Biofuel Glycerin Feed from rapeseed*, Wyd. Uczelniane ATR, Bydgoszcz, 2004 (in Polish).
[7] SULEWSKI M., GACA J., BRZESKI S., *Effect of oil quality and synthesis conditions on performance and selected parameters of biodiesel*. II International Conference Energy Process Eco-Euro-Energy Bydgoszcz 2006, p. 365–373 (in Polish).
[8] WANG Y., OU S., LIU P., ZHANG Z., Energy Consvers. Manage., 2007, 48, 184.
[9] LEUNG D.Y.C., GOU Y., Fuel Process Technol., 2007, 87, 883.
[10] PREDOJEVIĆ Z.J., Fuel, 2008, 87, 3522.
[11] PHAN A.N., PHAN T.M., Fuel, 2008, 87, 3490.
[12] GAWĘCKI J., *Fats as ford components*, [In:] GAWĘCKI J. (Ed.), *The truth About Fats*, Danone Institute, Warszawa, 1997, p. 1–2 (in Polish).
[13] TASHTOUSH G.M., AL-WIDYAN M.I., AL-JARRAH M.M., Eng. Convers. Manage., 2004, 45, 2697.
[14] WYATT V.T., HESS M.A., DUNN R.O., FOGLIA T.A., HAAS M.J., MARMER W.N., Jaocs., 2005, 82 (8), 585.
[15] GOLIMOWSKI W., NOWAK A., Probl. Inż. Roln., 2008, 62 (4), 173.
[16] ANGGRAINI A. A., LÖHRLEIN H. P., KRAUSE R., *Possibilities and limits of the Re-Use cooking oils with animals fat content as motor and heating fuel*, [In:] *Biomass for Energy and Industry*, Proc. 10th European Conf. Technol. Exhib., Würzburg, Germany, June 1998, p. 572–574.
[17] SKOTT T., BioEnergy Research, 2007, 19, 6.
[18] STRENZIOK R., WICKBOLDT P., *Modification and optimization of a diesel engine for operation with RME*, [In:] *Biomass for Energy and Industry*, Proc. 10th European Conf. Technol. Exhib., Würzburg, Germany, June 1998, p. 634–638.
[19] GOLIMOWSKI W., NOWAK A., PAWLAK S., *Biofuels from vegetables and animals fat*, [In:] *Selected Aspects of Current Environmental Conditions and Future Techniques in Animal Production*, J.L. Jugowa (Ed.), IBMER, Warszawa, 2008 (in Polish).

[20] PIKUL J., *Characteristics and receiving animals fat*, [In:] *The Truth about Fats*, J. Gawęcki (Ed.), Instytut Danone, Warszawa, 1997, p. 27–42 (in Polish).
[21] MATYSHOK H., KIEŻEL L.J., HOJNIAK M., Chemik, 1999, 52 (1), 6.

Environment Protection Engineering

Vol. 37 2011 No. 4

BARBARA KUCHARCZYK*, WŁODZIMIERZ TYLUS*

# EFFECT OF PROMOTOR TYPE AND REDUCER ADDITION ON THE ACTIVITY OF PALLADIUM CATALYSTS IN OXIDATION OF METHANE IN MINE VENTILATION AIR

The aim of the study was to examine how the palladium precursors such as $Pd(NO_3)_2$ or $PdCl_2$ and the reducers added (hydrazine hydrate or EDTA) influence methane combustion activity of monolithic palladium catalysts. Palladium nitrate was found to be a better Pd precursor, and the catalysts obtained displayed a noticeably higher activity in methane oxidation. The addition of hydrazine hydrate to 1% $Pd/Al_2O_3$ catalyst increased its activity when $PdCl_2$ was used as the palladium precursor. With $Pd(NO_3)_2$ as the palladium precursor, the addition of reducers – hydrazine hydrate or EDTA – decreased the activity of the monolithic palladium catalysts tested.

## 1. INTRODUCTION

Palladium-based catalysts are characterized by a high methane combustion activity which is influenced by the Pd precursor, the method of catalyst preparation and pretreatment, as well as the reaction conditions applied [1–7]. Pd precursors most frequently used are $Pd(NO_3)_2$, $PdCl_2$ or $H_2PdCl_4$ [1–6], but use can also be made of palladium acetate, palladium propionate or other organic palladium salts dissolved in a variety of solvents [3, 4]. Catalysts obtained by dissolving those salts in carboxylic acids (acetic and propionic) exhibit very high activity [3]. The type of the precursor used influences the dispersion of Pd and the form in which it occurs on the surface of the $Pd/Al_2O_3$ catalyst [4]. When palladium acetate dissolved in toluene is used as a Pd precursor, the extent of Pd dispersion is higher than when use is made of $Pd(NO_3)_2$ or $H_2PdCl_4$. It was reported that Pd dispersion did not change after 24 h ageing of the $Pd/Al_2O_3$ catalyst at 650 °C [4]. Pd particles of the size smaller than 5 nm were

*Wrocław University of Technology, Institute of Inorganic Chemistry and Mineral Fertilizers, Wybrzeże Wyspiańskiego 27, 50-370 Wrocław, Poland; corresponding author B. Kucharczyk, e-mail: barbara.kucharczyk@pwr.wroc.pl

quickly oxidized to PdO which alone was present on the catalyst surface. When Pd particles were of a larger size than 15 nm, palladium occurred in a metallic form and was covered with a PdO layer [4]. The form of Pd occurrence during methane oxidation – $Pd^0$, PdO or $PdO_x$/Pd – is ambiguous [1–4]. Depending on the reaction conditions (partial pressure of oxygen, temperature, composition of reaction mixture), PdO may undergo reduction or re-oxidation. The hydrocarbons present in the gas may induce the reduction of PdO at temperatures substantially lower than the temperature of its thermal decomposition in air or inert gas [6].

Methane emission is an inherent part of hard coal mining. As the emitted volume is large, methane has to be removed from the pit shaft with ventilation air for safety reasons. As methane concentration in ventilation air is low, not exceeding 0.75%, it cannot be fully utilized and in most instances methane is released into the atmosphere. The annual volume of methane entering the atmosphere with ventilation air approaches 581million cubic meters [8]. Methane is a greenhouse gas [9] with an environmental impact 23 times as strong as that of carbon dioxide, and its presence in the atmosphere contributes to climatic changes and consequently to global warming.

Continual increase in the concentration of air-borne $CH_4$ necessitates its removal from mine ventilation air. The best method for its removing in coal mines is catalytic combustion. Palladium catalysts on monolithic supports show a high activity in this process. The supports that may be used in catalytic combustion are either ceramic monoliths fabricated from aluminium oxide, silica, cordierite or mullite, or metallic monoliths made from heat-resisting foil of a 0.04–0.05 mm thick. Each of them has to be washcoated, e.g. with $\gamma$-$Al_2O_3$ of a high specific surface area. The washcoat is added to increase the specific surface area of the metallic support and stabilize its surface so as to prevent crystallite growth (at high temperatures, the crystallites of active components undergo sintering, causing them to increase in size) [10]. The benefits of applying monolithic supports are manifold: low cost of the support, possibility of using a comparatively small amount of active layer, low flow resistance of gases at high flow velocities ($>10^5\ h^{-1}$), which enables application of high gas hourly space velocities (GHSV) without considerable pressure drop on the catalytic layer [10]. As compared to ceramic monoliths, the walls of the support in metallic monoliths provide the catalyst with a larger free cross-section. As a result, the same conversion can be obtained at the volume of metallic monoliths which is by 20–30% lower than the volume of ceramic monoliths [10]. This is of importance when methane has to be removed from the ventilation air in coal mines because in that particular case large volumes of air are to be combusted, where methane concentration does not exceed 0.75%.

The aim of this work was to investigate the effect of Pd precursors and reducing agents chosen on the activity of the monolithic Pd catalyst in methane oxidation. The study included investigations into the specific surface area of the washcoat, Pd dispersion and size of Pd crystallites, as well as XRD and SEM examinations of catalyst surfaces.

## 2. METHODS OF PREPARATION AND INVESTIGATION OF THE CATALYST

The supports for the catalysts were metal monoliths made of a 0.05 mm thick, $Al_2O_3$ washcoated heat-resisting FeCr20Al5 steel foil. They were shaped into cylinders with the height and diameter of 70 mm and 26 mm, respectively, possessing a honeycomb cross-section with 112 triangular channels/cm$^2$ support. The washcoated support was calcined at 400 °C in air for 3 h. To obtain the active layer, 1% or 1.5% Pd (with the addition of 0.15% $Al(OH)_3$ sol solution) was deposited onto the support by impregnation. Palladium nitrate with Pd concentration of 19.69% or palladium chloride with Pd concentration of 20.04% was used as the palladium precursor. The catalysts were calcined at 500 °C in air for 3 h. To increase Pd dispersion, additional catalysts were prepared, where the washcoated monolithic support was impregnated with the solutions of two reducing agents: hydrazine hydrate or ethylenediaminetetraacetic acid (EDTA). As for hydrazine hydrate, the washcoated support was subject to 12 h drying at 105 °C, followed by 10 min impregnation with hydrazine hydrate solution at 50 °C. EDTA was deposited by impregnation of the support with 0.1 M EDTA solution at 70 °C for 30 min, or for 5 min ($Pd(NO_3)_2$) and 12 min ($PdCl_2$). Then the supports were subject to drying at 105 °C for 3 h, followed by deposition of 1.5% Pd from palladium nitrate or 1% Pd from palladium chloride. The catalysts are characterized in Table 1.

Table 1

Preparation conditions, Pd dispersion, and average size of Pd crystallites

| Catalyst $Pd/Al_2O_3$ [%] | Pd precursor | Reducer added | Impregnation temperature and time | Pd dispersion [%] | Average size of Pd crystallites [nm] |
|---|---|---|---|---|---|
| 1.5 | $Pd(NO_3)_2$ | no reducer | – | 2.82 | 42 |
| 1.0 | $Pd(NO_3)_2$ | no reducer | – | 4.43 | 33 |
| 1.5 | $Pd(NO_3)_2$ | 0.1M EDTA | 70 °C, 5 min | – | – |
| 1.5 | $Pd(NO_3)_2$ | 0.1M EDTA | 70 °C, 30 min | 0.83 | 133 |
| 1.5 | $Pd(NO_3)_2$ | hydrazine hydrate | 50 °C, 10 min | 1.79 | 62 |
| 1.0 | $PdCl_2$ | no reducer | – | – | 61 |
| 1.0 | $PdCl_2$ | 0.1M EDTA | 70 °C, 12 min | – | – |
| 1.0 | $PdCl_2$ | hydrazine hydrate | 50 °C, 10 min | – | – |

Methane combustion efficiency was tested using a laboratory flow reactor placed in a heater with a programmed temperature increment (heating ramp 3 °C/min). Over the catalysts, 1% methane in air was oxidized at GHSV of 5800 h$^{-1}$. Methane concentration in the gas mixture was measured with a Nanosens DP-27 analyzer.

BET surface area ($S_{BET}$), average pore size and pore volume of the washcoat were determined by nitrogen sorption at the temperature of liquid nitrogen, using the ASAP 2010C apparatus (Micromeritics, USA). Active surface and dispersion of Pd were

determined with the same apparatus, based on measurements of hydrogen chemisorption at 100 °C over the pressure range of 120–250 mm Hg.

XRD measurements were carried out using a PANalytical X'Pert Pro diffractometer with a Cu radiation source $K_\alpha$ of the wavelength of $\lambda = 1.5418$ Å. Use was made of the Bragg–Brentano scattering geometry. Morphology of the samples was examined by the scanning electron microscopy (SEM) with a Nova NanoSEM 230 microscope (made by FEI). Sample composition was determined by the energy dispersive X-ray spectrometry (EDXS), using an EDAX Pegasus XM4 spectrometer (with an SDD Apollo 40 detector) at 20 keV.

## 3. RESULTS AND DISCUSSION

Monolithic supports were covered with an $Al_2O_3$-based washcoat of the specific surface area ($S_{BET}$) of 335.1 $m^2/g$, total pore volume of 0.42 $cm^3/g$, and pore diameter of 4.98 nm. Pd dispersion in the monolithic catalysts was poor (Table 1). In the case of the 1.5% $Pd/Al_2O_3$ catalyst, impregnation of the washcoated support with EDTA or hydrazine hydrate solutions caused a decrease in Pd dispersion and consequently Pd crystallite growth. After 30 min of impregnation with EDTA, Pd dispersion dropped from 2.82% to 0.83%, and after 10 min of impregnation with hydrazine hydrate to 1.79%.

Impregnation of the support of the 1.5% $Pd/Al_2O_3$ catalyst with hydrazine hydrate solution at 50 °C for 10 min noticeably changed the appearance of the catalyst surface (Figs. 1 and 2). Although the surface of 1.5% $Pd/Al_2O_3$ with no reducer (Fig. 1) exhibits cracks, no single crystallites are detected even at 10 000× magnification. This indicates the presence of very fine Pd crystallites.

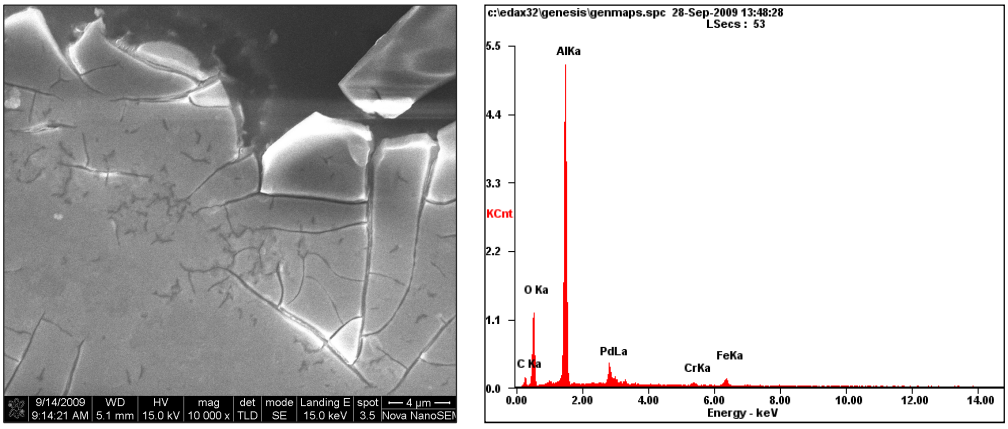


Fig. 1. SEM image (left) and results of X-ray microanalysis (right) of the surface of the 1.5% $Pd/Al_2O_3$ catalyst with no reducers; Pd precursor: $Pd(NO_3)_2$, magnification: 10 000×

After impregnation with hydrazine hydrate solution, the catalyst surface was covered with clusters of white crystallites. EDXS examinations have shown that Pd concentration in these crystallites is more than twice as high as in the grey fields on the catalyst surface (Fig. 2). White crystallites contain 6.05 at. % of Pd, 40.16 at. % of Al and 53.79 at. % of O, whereas in the dark fields of the surface 2.6 at. % of Pd, 45.9 at. % of Al and 51.5 at. % of O are found.

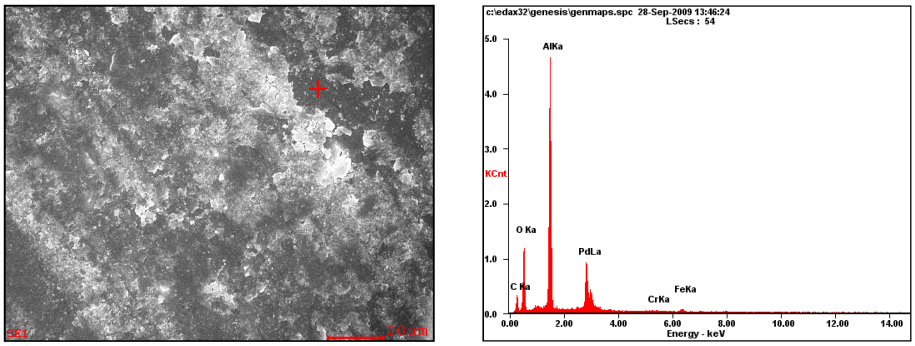


Fig. 2. SEM images and results of X-ray microanalyses of the surface of 1.5% $Pd/Al_2O_3$ catalyst impregnated with hydrazine hydrate solution at 50 °C for 10 min. Pd precursor: $Pd(NO_3)_2$

The XRD spectra of the 1.5% $Pd/Al_2O_3$ catalysts with no reducer addition and after 5 min impregnation with EDTA solution (Pd precursor: $Pd(NO_3)_2$), as well as the XRD spectra of the 1% $Pd/Al_2O_3$ catalyst (Pd precursor: $PdCl_2$), exhibit PdO peaks at $2\Theta$ of 34° and peaks of heat-resisting FeCr20Al5 steel.

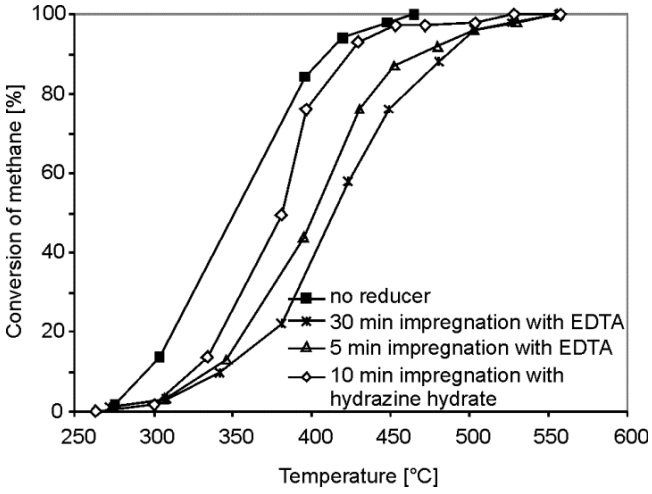


Fig. 3. Methane combustion activity of 1.5% $Pd/Al_2O_3$ catalysts with no reducer added, and after impregnation with EDTA and hydrazine hydrate

With $Pd(NO_3)_2$ as palladium precursor and in the absence of reducers, methane combustion efficiency increased when the Pd content increased from 1% to 1.5%. Over these catalysts, 100% conversion was achieved at 465 °C (1.5% of Pd) and 96% conversion at 509 °C (1% of Pd). Figure 3 shows temperature dependence of methane conversion over the 1.5% $Pd/Al_2O_3$ catalyst with $Pd(NO_3)_2$ as palladium precursor under the influence of EDTA or hydrazine hydrate addition. The activity of the catalyst was the highest when no reducing agent was added. Pd deposition onto the washcoated support which was impregnated with 0.1 M EDTA solution for 5 min caused a substantial decrease in the catalyst activity despite the insignificant decrease in the size of PdO crystallites from 42 nm to 33 nm (XRD). Methane combustion efficiency decreased upon increasing the time of support impregnation. When the washcoated support was impregnated with hydrazine hydrate solution for 10 min, the decrease in the catalyst activity was lower than when EDTA solution was used.

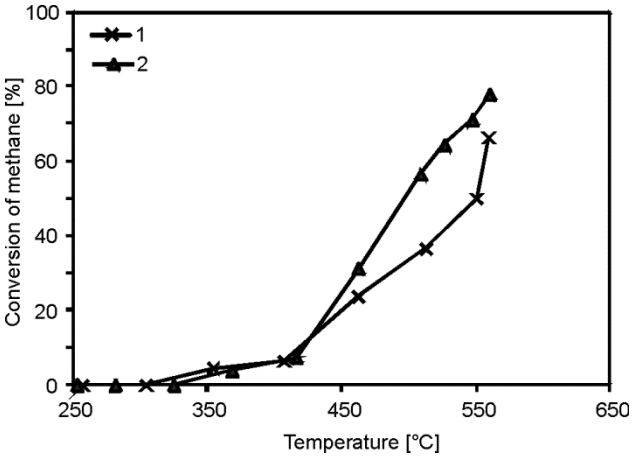


Fig. 4. Methane combustion activity of 1% $Pd/Al_2O_3$ catalysts prepared by various methods: 1 – Pd deposited without 0.15% $Al(OH)_3$ sol, 2 – Pd deposited using $Al(OH)_3$ sol; palladium precursor: $PdCl_2$

When $PdCl_2$ was used as palladium precursor, methane combustion efficiency increased with the Pd content of the catalyst from 1% to 1.5%. Figure 4 shows the effect of the preparation method used on the activity of the monolithic 1% $Pd/Al_2O_3$ catalyst. Palladium was deposited onto the surface of the washcoat prepared from $Al_2O_3$ powder in mixture with aluminium hydroxide sol (0.15% $Al(OH)_3$) or without it. When use was made of the $PdCl_2$ precursor, the 1% $Pd/Al_2O_3$ catalyst where Pd was deposited together with the 0.15% $Al(OH)_3$ sol displayed a higher activity. In spite of this, its activity is noticeably lower as compared to the catalyst prepared with $Pd(NO_3)_2$ as the palladium precursor. This may be due to the poorer Pd dispersion and to the pres-

ence of larger Pd crystallites (Table 1) but also due to the poisoning effect of the chlorine persisting in the catalyst after calcination.

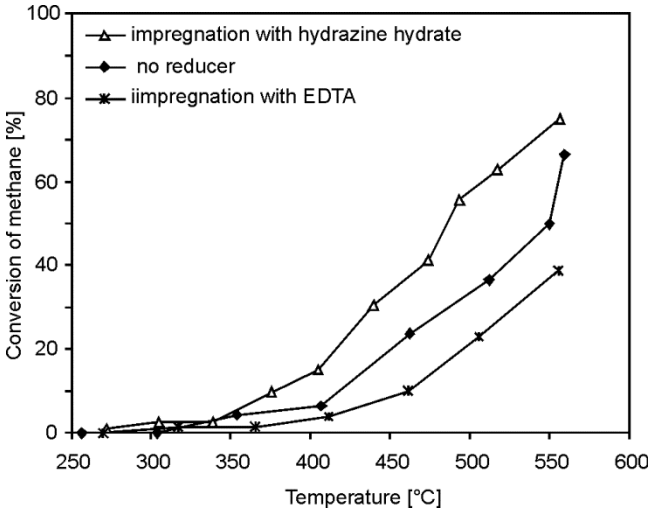


Fig. 5. Effect of the reducing agents (EDTA and hydrazine hydrate) on the methane combustion activity of the 1% $Pd/Al_2O_3$ catalyst; palladium precursor: $PdCl_2$, palladium deposited without $Al(OH)_3$ sol

With $PdCl_2$ as the palladium precursor and Pd deposition with no $Al(OH)_3$ sol, impregnation of the washcoated support with hydrazine hydrate solution improves the activity of the catalyst (compared to the catalyst with no reducer added). When the same catalyst is impregnated with 0.1 M EDTA solution, its activity decreases markedly (Fig. 5).

## 4. CONCLUSIONS

The catalysts show a noticeably higher methane combustion activity with palladium nitrate than with palladium chloride as the Pd precursor. Regardless of the Pd precursor applied, their activity increases with the increase in Pd content from 1% to 1.5%.

The activity of the catalysts depends on the preparation method used. With $PdCl_2$ as Pd precursor, the 1% $Pd/Al_2O_3$ catalyst where Pd was deposited together with the 1.5% $Al(OH)_3$ sol exhibited a higher methane combustion activity.

The addition of solution of hydrazine hydrate improves the activity of the 1% $Pd/Al_2O_3$ catalyst when use is made of $PdCl_2$ as the Pd precursor. With $Pd(NO_3)_2$ as the Pd precursor, methane combustion activity of the catalyst deteriorates.

The use of EDTA as a reducer decreases the activity of palladium-based catalysts irrespective of the Pd precursor applied.

ACKNOWLEDGEMENTS

The study was co-financed by the European Union from the European Regional Development Fund Project No. POIG.01.03.01-00-072/08 Program Innovative Economy 2007–2013.

REFERENCES

[1] SCHLAM M., SOUZA M.M.V.M., ALEGRE V.V., PEREIRA DA SILVA M.A., CESAR D.V., PEREZ C.A.C., Catal. Today, 2006, 118 (3–4), 392.
[2] GELIN P., PRIMET M., Appl. Catal. B, 2002, 39 (1), 1.
[3] KINNUNEN N.M., SUVANTO M., MORENO M.A., SAVIMAKI A., KINNUNEN T.J.J, PAKKANEN T.A., Appl. Catal. A, 2009, 370 (1–2), 78.
[4] ROTH D., GELIN P., KADDOURI A., GARBOWSKI E., PRIMET M., TENA E., Catal. Today 2006, 112 (1–4), 134.
[5] CIUPARU D., LYUBOVSKY M. R., ALTMAN E., PFEFFERIE L.D., DATYE A., Catal. Rev., 2002, 44 (4), 593.
[6] RYOO M.W., CHUNG S.G., KIM J.H., SONG Y.S., SEO G., Catal. Today, 2003, 83 (1–4), 131.
[7] MUSIALIK-PIOTROWSKA A., Ochr. Środ., 2011, 33 (1), 19.
[8] *Annual Report on Status of Basic Natural and technical Hazards in the Hard Coal Mining Industry*, GIG, Katowice 1986–2007 (in Polish).
[9] KUJAWSKI O., Environ. Prot. Eng., 2009, 3, 27.
[10] NIJHUIS T.A., BEERS A.E.W., VERGUNST T., HOEK I., KAPTEIJN F., MOULIJN J.A., Catal. Rev. 2001, 43 (4), 345.

Environment Protection Engineering

Vol. 37 2011 No. 4

ANDRZEJ BIELSKI*

# MODELLING OF MASS TRANSPORT IN WATERCOURSES CONSIDERING MASS TRANSFER BETWEEN PHASES IN UNSTEADY STATES. PART II. MASS TRANSPORT DURING ABSORPTION AND ADSORPTION PROCESSES

Equations describing the rate of adsorption and absorption processes and those based on Whitman's model have been analyzed. In the case of unstable states, the mass flux penetrating to the layer of the river sediment and calculated by means of these equations differs from the mass flux calculated from the mass diffusion equation. In order to minimize the discrepancies between the flux determined by Whitman's model and a real flux, the correction factor has been introduced into the concentration gradient equation originated from Whitman's model. This correction factor can be expressed as a time dependence of the product of a certain parameter and the concentration derivative at the phase boundary (solid phase side). The corrected equation for the concentration gradient has been used to derive another equation, describing a general rate of the absorption and adsorption processes at the linear interfacial equilibrium and the chemical reactions occurring in the liquid and solid phases; the chemical reactions follow the first order monomolecular mechanism in unstable states with reference to the liquid phase. Knowing the general rate of the earlier mentioned processes it is possible to construct an advective-dispersion model of mass transport in a river including these particular processes. Such a model contains a term defined as a correction factor referring to the time dependence of the concentration derivative with respect to time. The described model may be also used for simulation of the transport of pollutants undergoing adsorption and absorption in the layer river sediment; the processes occur with a finite and infinitely large rate through the equilibrium states.

## 1. MASS TRANSPORT IN ABSORPTION AND ADSORPTION PROCESSES

Mass exchange between phases when there is no discontinuity of concentration at the phase boundary has been discussed in our previous paper [1]. In the case of absorption and adsorption, concentrations associated with separate phases may take dif-

*Cracow University of Technology, Department of Environmental Engineering, ul. Warszawska 24, 31-155 Cracow, Poland, e-mail: abielski@riad.usk.pk.edu.pl

ferent values next to the phase boundary. It is assumed that close to the phase boundary, the equilibrium between these concentrations is reached almost immediately [2]. In a general case, the relationships between these concentrations are described with nonlinear functions and only for sufficiently low concentrations it is possible to use a linear function (Henry's law for the absorption equilibrium or for an adsorption isotherm).

In the case of absorption or adsorption, the analysis of mass transport through a phase boundary may be carried out in a similar way as it was presented previously [1]. However, in such a case it would be necessary to solve the mass transport equation in unsteady states (Eq, (1), [1])) for each phase separately to determine the concentration distribution in a liquid phase and either in adsorption or absorption phases. Such approach to the analysis of mass transport through a phase boundary would result in some major complications in calculations. Therefore, film Whitman's model is used [2–5] to describe the mass transfer rate through a phase boundary.

Numerous other models of mass transfer exist, such as the Higbie penetration model, Danckwerst surface renewal model, Dobbins, Toor and Marchello model, Kisziniewski model, King model [2, 4]. Neither of them provides any possibilities to consider periodic or aperiodic concentration changes at the phase boundary though the models are little more complex than Whitman's model. Just from the perspective of the mass transfer through a phase boundary in rivers, Whitman's model seems to be the most appropriate.

For the specific case of absorption or adsorption without a chemical reaction, the model based on Whitman's model may be described as follows:

$$\frac{dc}{dt} = -\frac{K}{h}\left(c - c^*\right) \tag{1}$$

$$\frac{da}{dt} = \frac{K}{L_0}\left(c - c^*\right) \tag{2}$$

$$a = \Gamma c^* \tag{3}$$

Based on Fick's law (Eq. (23), [1]) [4] and Eq. (1) it may be stated that:

$$-\frac{K}{h}\left(c - c^*\right) = -\left(-\frac{D}{h}\frac{dc}{dy}\right) \tag{4}$$

After introducing Eq. (3) into Eq. (4) the concentration gradient is given by:

$$\frac{dc}{dy} = -\frac{K}{D}\left(c - \frac{a}{\Gamma}\right) \tag{5}$$

Equation (5) refers to the average concentration gradient in the close vicinity of a phase boundary (Fig. 1).

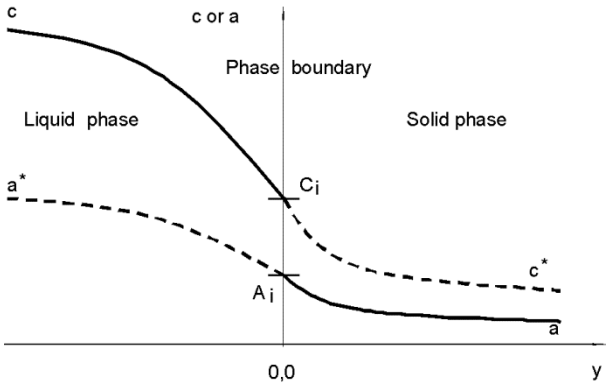


Fig. 1. Distribution of concentrations inside liquid and solid phases.
The dotted lines represent equilibrium concentrations

From Eqs. (2) and (3) it may be concluded that the degree of absorption or adsorption may be described as:

$$a = a\left(t = 0, x\right) + \int_0^t \frac{K}{L_0}\left(c - \frac{a}{\Gamma}\right) d\tau \tag{6}$$

Using Equation (5), Eq. (6) may be transformed into:

$$a = a\left(t = 0, x\right) - \frac{D}{L_0}\int_0^t \frac{dc}{dy} d\tau \tag{7}$$

Substitution of Eq. (7) into Eq. (5) yields to expression for the concentration gradient:

$$\frac{dc}{dy} = -\frac{K}{D}c - \frac{K}{\Gamma L_0}\int_0^t \frac{dc}{dy} d\tau + \frac{K}{D\Gamma} a\left(t = 0, x\right) \tag{8}$$

In Equations (1)–(3) and the following, the equilibrium concentration was denoted as $c^*$, the concentration at a phase boundary in a liquid phase was denoted as $C_i$ while the concentration in a liquid phase core was denoted as $c$ (Fig. 1). Equations (1) and (2) describe the mass transfer rate through a phase boundary. If concentration $c$ was equivalent to $C_i$, the coefficient $K$ would be defined as the penetration coefficient in a solid phase.

The first term of Eq. (8) refers to absorption or adsorption, while the second one to desorption processes. Let us use model (8) to analyze gradient changes for the concentration presented in Fig. 5 of [1].

Minimization of the product of a sum of squared deviations for both gradient and mass balance allowed one to determine the values of coefficients in Eq. (8). An equation for a concentration gradient has the following form:

$$\frac{dC}{dy} = -420.71C_i(t) - 1.4790\times10^{-4}\int_0^t \frac{dC}{dy}\,d\tau + 6.5773 \tag{9}$$

It was assumed that at the moment $t = 0$, the gradient $dC/dy = 0$ though such assumption does not necessarily have to be true. Therefore, a potential error influences the value of a constant – in this case it is 6.5773. A similar assumption may concern the following equations of the same type.

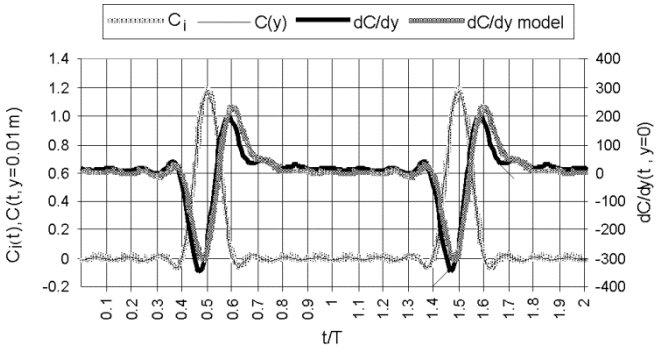


Fig. 2. Concentrations at the phase boundary and at the distance of $y = 1\times10^{-6}$ m in the solid phase, gradient of concentration at the phase boundary and gradient calculated using model Eq. (8); $T = 86\,400$ s, $C_{i,a} = 1$ g/m$^3$, $\Delta\tau = T/16$, $k_r = 1\times10^{-30}$ s$^{-1}$, $D = 1.7\times10^{-9}$ m$^2$/s. The average absolute error for a single gradient value = 27.96 g/m$^4$

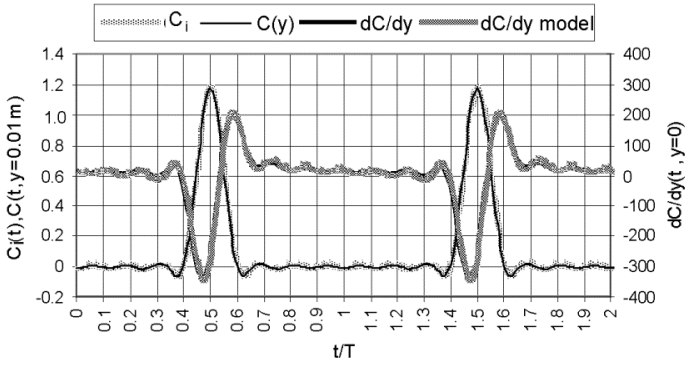


Fig. 3. Concentrations at a phase boundary, concentration at a distance of $y = 1\times10^{-6}$ m in a solid phase, gradient of concentration at a phase boundary and gradient calculated using model Eq. (10); $T = 86\,400$ s, $C_{i,a} = 1$ g/m$^3$, $\Delta\tau = T/16$, $k_r = 1\times10^{-30}$ s$^{-1}$, $D = 1.71.7\times10^{-9}$ m$^2$/s. The average absolute error for a single gradient value is 5.89 g/m$^4$

Model (8) shows substantial errors in calculations of the mass balance [6] (Fig. 3) and errors in calculations of the concentration gradient (Fig. 2) [6]. Its accuracy may still be improved by introducing a derivative of the concentration with respect to time, as it was proposed in previously (model (26) [1]). Then the model takes the form of:

$$\frac{dC}{dy} = a_1 C_i(t) + a_2 \left.\frac{dC_i}{dt}\right|_t + a_3 \int_0^t \frac{dC}{dy} d\tau + a_4 \tag{10}$$

In the above equation, a constant $a_4$ represents an initial value of absorption or adsorption – the value is zero in a particular case of an organic tracer introduced in an impulse mode. A term with the concentration gradient integral is responsible for desorption of the material back to a solid phase. The integral of a concentration gradient is proportional to the current value of absorption or adsorption. If the substance present in a solid phase is completely desorbed, the value of the integral is zero.

Minimization of the product of a sum of squared deviations for both gradient and mass balances allowed one to determine the values of the coefficients in Eq. (10) for the concentration curve presented in Fig. 5 of [1]. Now, the equation for the concentration gradient takes the following form:

$$\begin{aligned} \frac{dC}{dy} &= (-224.30) C_i(t) + (-92.478 \times 10^4) \left.\frac{dC_i}{dt}\right|_t \\ &+ (-4.0725 \times 10^{-5}) \int_0^t \frac{dC}{dy} d\tau + 15.209 \end{aligned} \tag{11}$$

Model (11) shows minor errors in calculation of the concentration gradient (Fig. 3) and a mass balance [6]. In Equation (11), the value of $a_4$ different from zero is related to a periodic occurrence of impulses. Therefore, the average amount of absorbed or adsorbed substance in a solid phase does not approach zero. It may be concluded that hardly any desorption process takes place, hence the concentration gradient should take a positive sign and such situation occurs since $a_4$ is positive.

Model (10) after its generalization may also be used as a tool for description of processes of absorption or adsorption accompanied with a chemical reaction in both liquid and solid phases.

If the reaction proceeds in solid phase with the rate ($-k_r a$), the concentration gradient has the following form:

$$\frac{dc}{dy} = -\frac{K}{D} c - \left( \frac{K}{\Gamma L_0} + k_r \right) \int_0^t \frac{dc}{dy} d\tau + \frac{K}{D\Gamma} a(t=0,x) - \frac{K k_r}{D} \int_0^t c \, d\tau \tag{12}$$

In such a situation, the concentration gradient is expressed using the relationship similar to Eq. (10) including also the concentration integral in function of time (under a momentary assumption that: $c \Leftrightarrow C_i$)

$$\frac{dC}{dy} = a_1 C_i(t) + a_2 \left.\frac{dC_i}{dt}\right|_t + a_3 \int_0^t \frac{dC}{dy} d\tau + a_4 + a_5 \int_0^t C_i d\tau \tag{13}$$

If the term including the concentration differential with respect to time is ignored in the above equation, the gradient and mass balance values are calculated with errors [6].

Based on Fick's law (Eq. (23), [1]) [4] and the concentration gradient (Eq. (12)) rates $r$ of absorption or adsorption accompanied with a chemical reaction with respect to a liquid phase may be calculated as:

$$\begin{aligned} r &= -\frac{dm}{dt}\frac{1}{V^*} = -\left(-D\frac{A^*}{V^*}\frac{dc}{dy}\right) = \frac{D}{h}\frac{dc}{dy} \\ &= -\frac{K}{h}c - \left(\frac{K}{\Gamma L_0} + k_r\right)\int_0^t \frac{D}{h}\frac{dc}{dy} d\tau + \frac{K}{h\Gamma} a(t=0,x) - \frac{Kk_r}{h}\int_0^t c\, d\tau \\ &= -\frac{K}{h}c - \left(\frac{K}{\Gamma L_0} + k_r\right)\int_0^t r\, d\tau + \frac{K}{h\Gamma} a(t=0,x) - \frac{Kk_r}{h}\int_0^t c\, d\tau \end{aligned} \tag{14}$$

Since the overall process rate in the liquid phase is:

$$r_{og} = r - k_c c \tag{15}$$

(rate of chemical reaction is $(-k_r c)$), based on Eq. (14), the following may be written:

$$\begin{aligned} r_{og} = &-\left(\frac{K}{h} + k_c\right)c - \left(\frac{K}{\Gamma L_0} + k_r\right)\int_0^t r_{og}\, d\tau + \frac{K}{h\Gamma} a(t=0,x) \\ &-\left[\frac{Kk_r}{h} + k_c\left(\frac{K}{\Gamma L_0} + k_r\right)\right]\int_0^t c\, d\tau \end{aligned} \tag{16}$$

Considering a differential of concentration with respect to time in the equation for an overall process rate in a liquid phase, Eq. (16) takes the form:

$$r_{og} = a_1' C_i + a_2' \left.\frac{dC_i}{dt}\right|_t + a_3 \int_0^t r_{og}\, d\tau + a_4' + a_5' \int_0^t C_i\, d\tau \tag{17}$$

under the assumption that $c \Leftrightarrow C_i$.

Parameter $a_2' = (D/h)a_2$ because after inserting the gradient equation, for example Eq. (13) to Eq. (14), the parameter $a_2$ will be multiplied through fraction $(D/h)$.

In the case of the concentration related to the core of a liquid phase, it may be written that:

$$r_{og} = a_1' c + a_2' \left.\frac{dc}{dt}\right|_t + a_3' \int_0^t r_{og}\, d\tau + a_4' + a_5' \int_0^t c\, d\tau \tag{18}$$

Equation (18) describes a general process rate of absorption and adsorption at a linear interphase equilibrium accompanied with chemical reactions taking place in both solid and liquid phases; the reactions follow a monomolecular first order reaction mechanism, at an unsteady state with respect to a liquid phase. Parameters $a_1'$, $a_4'$, $a_5'$ and probably $a_2'$ (uncertainty origins from both analysis of a mass transport equation that includes absorption or adsorption processes carried on through an equilibrium states and Eq. (16)) depend on the water level *h*.

Coefficients $a_1', a_2', a_3, a_4', a_5'$ are characteristic of a certain type of wave. By changing wave parameters, e.g. the period *T*, number of harmonics, impulse duration, etc., parameters of Eq. (18) change as well.

## 2. POLLUTANT TRANSPORT MODEL

Advection-diffusion transport of any substance in natural water courses may be accompanied with chemical and/or physical processes such as absorption and adsorption. The absorption and adsorption process rates are expressed as functions depending on concentrations of the analyzed substances within the phases participating in transport (e.g. liquid phase – water, solid phase related with water course sediment).

Substituting the overall rate (Eq. (18)) into a pollutant transport equation [7–14]:

$$\frac{\partial c}{\partial t} + V\frac{\partial c}{\partial x} = \frac{1}{A}\cdot\frac{\partial}{\partial x}\left(E_x A\frac{\partial c}{\partial x}\right) + r_{og} \tag{19}$$

we arrive at an equation where the concentration derivative with respect to time is multiplied by a coefficient higher than 1 ($1+|a_2'|$). Such a situation is similar to the one that occurs in the mass transport equation which takes into account processes of adsorption or absorption proceeding through the equilibrium states.

Using a classical approach of the mass transport model with other processes proceeding with no equilibrium, the set of equations would be expressed as follows (case with a linear isotherm):

$$\frac{\partial c}{\partial t} + V\frac{\partial c}{\partial x} = \frac{1}{A}\cdot\frac{\partial}{\partial x}\left(E_x A\frac{\partial c}{\partial x}\right) - \frac{K}{h}\left(c - c^*\right) - k_c c \tag{20}$$

$$\frac{da}{dt} = \frac{K}{L_0}\left(c - c^*\right) - k_r a \tag{21}$$

$$a = \Gamma c^* \tag{22}$$

The set of equations does not have any additional term assigned to the concentration differential with respect to time, therefore calculations based on from Eqs. (20)–(22) would not give an accurate results.

Introduction of a new term at a differential ∂c/∂t in Eq. (20) leads to a model that consists of three equations:

$$\left(1-\frac{D}{h}a_2\right)\frac{\partial c}{\partial t}+V\frac{\partial c}{\partial x}=\frac{1}{A}\cdot\frac{\partial}{\partial x}\left(E_x A\frac{\partial c}{\partial x}\right)-\frac{K}{h}\left(c-c^*\right)-k_c c \tag{23}$$

$$\frac{\partial a}{\partial t}=\frac{K}{L_0}\left(c-c^*\right)-\frac{D}{L_0}a_2\frac{\partial c}{\partial t}-k_r a \tag{24}$$

$$a=\Gamma c^* \tag{25}$$

Integrated with respect to time, Eq. (24) yields the dependence:

$$\begin{aligned}a\left(x,t\right)=&\int_0^t\left(\frac{K}{L_0}\left(c\left(x,\tau\right)-c^*\left(x,\tau\right)\right)-k_r a\left(x,\tau\right)\right)d\tau\\&-\frac{D}{L_0}a_2 c\left(x,t\right)+\frac{D}{L_0}a_2 c_0\left(x\right)+a_0\left(x\right)\end{aligned} \tag{26}$$

which may be easier to use in numerical applications.

To solve the set of the above equations, the following conditions have to be formulated:

1. Initial condition:

$$C(x,t=0)=C_0(x) \tag{27}$$

2. Boundary conditions related to:

a) concentration changes in the initial cross-section:

$$C(x=0,t)=C_p(t) \tag{28}$$

b) changes of the concentration gradient in the final cross-section (Neumann's condition [15–19]:

$$\left.\frac{\partial C}{\partial x}\right|_{x=L_{\mathrm{odc}},t}=0 \tag{29}$$

($L_{\mathrm{odc}}$ is the length of the water course segment)

3. Initial condition for adsorption or absorption:

$$a\left(x,t=0\right)=a_0\left(x\right) \tag{30}$$

It should be noted, however that if a thermodynamic equilibrium exists between the phases at the initial moment, Eq. (25) or a similar one resulting from the actual isotherm has to be true. In particular, for a pure solid phase:

$$a\left(x,t=0\right)=0 \tag{31}$$

though, if an interfacial equilibrium exists, concentrations in a liquid phase are also zero, at the initial moment.

## 3. THEORETICAL ANALYSIS OF THE MASS TRANSPORT MODEL INCLUDING ABSORPTION OR ADSORPTION RATES

The mass transport model, including absorption and/or adsorption, comprises three equations: advection and diffusion in a liquid phase (Eq. (23)), absorption and/or adsorption rate (Eq. (24)) and interfacial equilibrium equation (Eq. (25), in this case Henry's law). Equations (23) and (24) meet the conditions of the mass conservation law for the system [6].

If adsorption or absorption processes proceed through the equilibrium states, it may be shown that the model of mass transport fulfils the equations:

$$\left(1+\Gamma\frac{L_0}{h}\right)\frac{\partial c}{\partial t}+V\frac{\partial c}{\partial x}=\frac{1}{A}\frac{\partial}{\partial x}\left(AE_x\frac{\partial c}{\partial x}\right)+r+\frac{q_L}{A}\left(c_d-c\right) \tag{32}$$

whereas the rate of changes of adsorption or absorption level is [6]:

$$\frac{\partial a}{\partial t}=\frac{K}{L_0}\left(c-\frac{a}{\Gamma}\right)+\Gamma\frac{\partial c}{\partial t}\varepsilon \tag{33}$$

Comparing Equations (33) and (24), as well as considering Eq. (25), the following relationship is obtained:

$$-Da_2 \Leftrightarrow \Gamma L_0\varepsilon \tag{34}$$

A similarity of Eqs. (33) and (24) means that the set of Eqs. (23)–(25) may be used to simulate mass transport accompanied with adsorption/absorption processes proceeding at a finite rate through the equilibrium states. It may also be used in both cases simultaneously, when the sediment material consists of fractions that show different physicochemical affinity to a substance transported in the water phase.

## 4. IDENTIFICATION OF A MASS TRANSPORT MODEL ACCOMPANIED WITH ABSORPTION PROCESSES

The set of Eqs. (23)–(25) was used to describe propagation of copper sulfate in water. Water passed through a glass pipe partially filled with glass balls; the pipe length $L_{odc}$ was ca. 0.70 m, its diameter $d$ ca. 3 cm. In order to obtain very accurate results of measurements, the experiment was conducted in the laboratory. The pipe was slightly tilted up from its horizontal position and its upper end was equipped with an air release valve. This way the volume of a gas phase that built up over the water surface (air and water vapour) could be minimized. Water flowed over the entire cross-section of the pipe and only at the very end of the pipe both gas phase and free water level were present. Flow-through conductometric sensors were mounted at the both sides of the pipe to measure the conductivity in a real time. After calibration of sensors, it was possible to convert the measured conductivity into copper sulfate concentration. Along the lower end of a pipe wall glass balls were placed; the ball diameter was 3 mm, thickness of a ball layer ca. 1.13 cm.

A polyethylene capillary was introduced inside the layer of glass balls and close to the air release valve, at the upper end of the pipe. The capillary enabled one to draw a sample from the inside of the glass ball layer. The layer of the glass balls together with water immobilized inside the layer was considered a solid phase with mostly absorption properties. Adsorption of copper ions on glass is very low if compared with their absorption in water that filled the space between glass balls. Therefore, it was absorption that was considered a leading process in a layer of balls. It was assumed that water motion in the interspace between balls is negligible if compared with the main stream motion over the glass ball layer and is therefore not considered in the transport of copper sulfate. During the experiment, water of high purity (specific conductivity of about 1 μS/cm) was used as a liquid phase. Conductivity of pure water was used as a reference value to calculate the copper sulfate concentration. Conductivity measurements were performed including the temperature compensation coefficient of 0.02 °C$^{-1}$. Temperature of 25 °C was the reference temperature. All conductivity measurements were automatically converted to the values at the reference temperature. It was found that the relationship between specific conductivity $S$ [μS/cm], and the concentration $C$ [mol $CuSO_4 \cdot 5H_2O/m^3$] was as follows:

$$C = S^{1.0566}\left(3.7361\times10^{-3} + 5.4493\times10^{-6} S^{0.65704}\right) \tag{35}$$

(Note: The values of the specific conductivity $S$ in Eq. (35) are the readings of the conductometers for which the measuring constants were set in such a way as to make their readings identical. Hence, the results of Eq. (35) may slightly differ from the real values.)

### 4.1. EXPERIMENTAL RUNS

1 M copper sulfate solution was injected with a syringe to the water stream passing through the pipe connected to the exit electrode. Characteristic of an input impulse is presented in Fig. 4. In practice, the volume of a copper sulfate solution injected to the water did not change the flow volume of $Q$ = 3.48 cm$^3$/s. The volume of the pipe $V^*$ that extended over the layer of glass balls was estimated as ca. 228 cm$^3$. Based on this volume, the average hydraulic detention time in the system ($t_m$ = 228 cm$^3$ /3.48 cm$^3$/s = 65.59) as well as the average velocity $V$ = 0.70 m/65.59 s = $1.067\times10^{-2}$ m/s were calculated. It should be noted that, the velocity calculated this way is lower than the real mass advection velocity; the difference may be attributed to the boundary layer present next to glass balls. Therefore, the actual volume $V^*$ of the liquid core was smaller than 228 cm$^3$ and the estimated velocity $V$ was just an approximation of the real advection velocity.

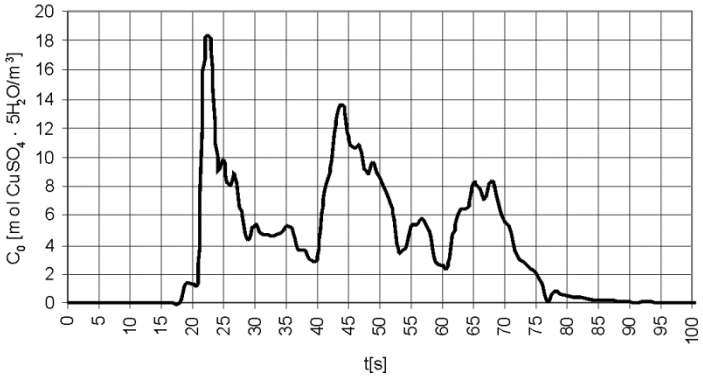


Fig. 4. Characteristic of the input impulse

Once the copper sulfate solution was introduced into the water stream, the conductivity measurements were performed every 1 s and every 2 s, at the inlet and outlet of the system, respectively. Measurements were recorded automatically with a computer.

### 4.2. ESTIMATION OF MODEL PARAMETERS

In simulation calculations the model was used that comprised Eqs. (23)–(25). Additionally, a complementary variable $S_{T6}$ and porosity of a balls layer $\varepsilon_0$ were introduced to the model. Finally, the model could be written as:

$$\left(1-\frac{D}{\dfrac{h}{S_{T6}}}a_2\right)\frac{\partial c}{\partial t}+VS_{T6}\frac{\partial c}{\partial x}=\frac{1}{A}\cdot\frac{\partial}{\partial x}\left(E_x A\frac{\partial c}{\partial x}\right)-\frac{K}{\dfrac{h}{S_{T6}}}\left(c-c^*\right)-k_c c \tag{36}$$

$$\frac{\partial a}{\partial t} = \frac{K}{\varepsilon_0 L_0}\left(c - c^*\right) - \frac{D}{\varepsilon_0 L_0} a_2 \frac{\partial c}{\partial t} - k_r a \tag{37}$$

$$a = \Gamma c^* \tag{38}$$

The constant $S_{T6}$ was introduced in order to compensate for the error caused by a rather rough determination of an advection velocity $V$. Since the velocity $V$ increased along with a decrease of the water depth $h$, the term $(h/S_{T6})$ in Eq. (36) appeared. Porosity $\varepsilon_0$ of the layer of glass balls in Eq. (37) resulted from the assumption that copper salts were absorbed mostly by water that filled void spaces between balls. Therefore, based on the mass balance, thickness of the layer of glass ball $L_0$ had to be multiplied by $\varepsilon_0$.

The values of some model parameters were assumed for the calculations: $h = 0.0109$ m, $V = 0.0107$ m/s, $A = 3.26\times10^{-4}$ m$^2$, $k_c = 0$, $\varepsilon_0 = 0.409$, $L_0 = 0.0113$ m, $k_r = 0$. The main goal of the experiment was to determine the values of the parameters or expressions: $E_x$, $Da_2$, $K$, $\Gamma$ and $S_{T6}$, based on the experimental results.

The parameter values of model (Eqs. (36)–(38)) were identified using measurements of copper sulfate concentration in water passing through the installation. Additionally, the measurements of the concentration of copper sulfate in a layer of glass balls were considered (absorption point in Table 1). The values of model parameters were determined by minimizing the sum of squared deviations between measured and calculated values. The function was minimized according to the simplex method of Nelder–Mead [20, 21].

Table 1

Results of estimation of the model parameters[a]

| Parameter or expression | One absorption point | One absorption point | Initial values | | No absorption point | Two absorption points |
|---|---|---|---|---|---|---|
| | | | No absorption point | No absorption point v2 | | |
| 1 | 2 | 3 | 4 | 5 | 6 | 7 |
| $E_x$ [$10^{-4}$ m$^2$/s] | 1.0236 | 0.61180 | 1.0829 | 5.2839 | 0.69805 | 0.42996 |
| $Da_2$ [$10^{-3}$ m] | –1.2966 | – | –0.64980 | –7.9260 | – | – |
| $K$ [$10^{-5}$ m/s] | 8.6887 | 22.870 | 6.8685 | 23.236 | 10.849 | 22.873 |
| $\Gamma$ | 1.0976 | 0.70157 | 1.0007 | 2.4553 | 0.68493 | 1.0156 |
| $S_{T6}$ | 1.3146 | 1.3874 | 1.2030 | 6.9646 | 1.2136 | 1.3676 |
| Average absolute error model fitting [mol $CuSO_4{\cdot}5H_2O/m^3$] | 0.002098 | 0.005491 | 0.004133 | 0.004407 | 0.006549 | 0.009507 |

[a]Coordinates of the experimental absorption point: $t = 92$ s, $c = 2.430$ mol $CuSO_4{\cdot}5H_2O/m^3$, coordinates of the theoretical absorption point $t = 180$ s, $c = 1.637$ mol $CuSO_4{\cdot}5H_2O/m^3$.

From the mathematical point of view, the model parameters may also be determined if concentration measurements in a layer of glass balls are not considered (Ta-

ble 1, columns 4 and 5). In such a case, tough approximation of the model parameters may by ambiguous due to a multiminimum character of the sum of squared deviations between calculated and measured concentrations. The results presented in column 2 of Table 1 served as a basis for the essential plots that were later compared to the plots referring to the columns 3, 4 and 6.

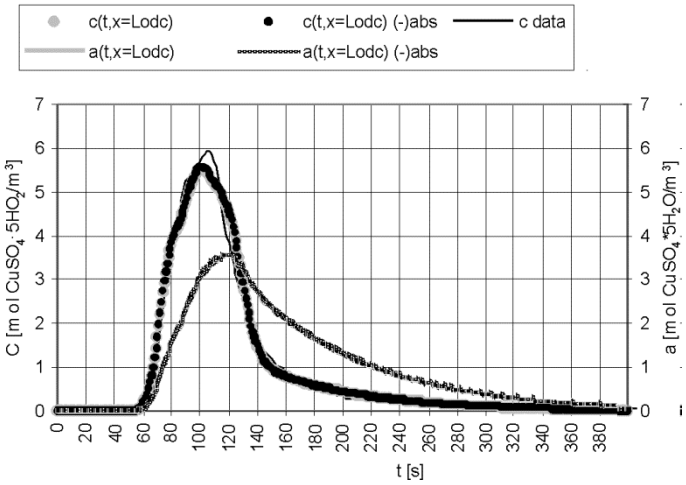


Fig. 5. Concentration *c* and absorption *a* curves obtained from the model (Eqs. (36)–(38)) for data with absorption (Table 1, column 2) and without absorption ((–)abs) (Table 1, column 4)

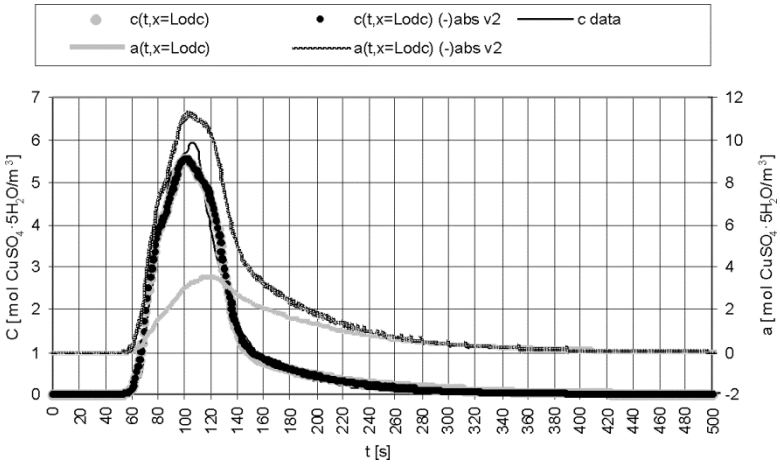


Fig. 6. Concentration *c* and absorption *a* curves obtained from the model Eqs. (36)–(38) for data with absorption (Table 1, column 2) and without absorption ((–)abs v2) (Table 1, column 5)

Model parameters that have been determined based on the data both including and neglecting absorption level may assume similar or significantly different values (Ta-

ble 1, columns: 2, 4 and 5). If the values are similar, the curves representing concentration $c$ and absorption level $a$ (Fig. 5) are also similar. Depending on the input values of model parameters, rather poor probability of the model parameters may be obtained after minimization of the sum of squared deviations (Table 1, column 5). A low value of the average absolute error of the model fitting, if compared with other errors, does not guarantee that the parameters values are accurate (Table 1, column 5). Curves of concentration $c$ are in this case also similar, but the absorption level assumes irrational values (Fig. 6; concentrations in the absorption layer cannot exceed in this case concentrations in the liquid phase). The value of the absorption coefficient $\Gamma$ is close to 1.0 in this experiment (for the system water in a liquid phase – water in a solid phase of glass balls). The value of 2.4553 (Table 1, column 5) cannot refer to this phase system, although such a value is entirely correct just from the mathematical point of view. Questionable value of the coefficient $\Gamma$ causes that the values of other parameters should also be considered as unlikely.

From the above discussion, it may be concluded that if the model (36)–(38) is to be used to analyze the quantity of substance in an absorption layer, it is necessary to obtain information on concentrations in this layer. Estimation of model parameters based on concentrations in just a mobile liquid phase may give wrong estimates. The results of actual measurements concerning liquid phase are usually used while modelling processes of pollutant transport in rivers, lakes, sea etc. Such approach may result in poor estimation of model parameters. It should be stressed that transport of any substance in any medium (natural or man-mad, e.g. pipe, wastewater drain, chemical reactor) is always accompanied with absorption and/or adsorption processes – to less or more extend. Absorption processes may also be analyzed with respect to dead zones in units that carry the flow. Therefore, if the theoretical model has to describe accurately the course of the real-life processes, it is recommended to use the specific measuring data that enable one to determine the model parameter values. It should be noted that in the case of natural water bodies: rivers, lakes, sea etc., the values of $Da_2$ and $\Gamma$ are not known. Evaluation of the values of the parameters using other methods would not be much reliable. Therefore, they have to be estimated simultaneously with the values of other model parameters, and as such require the specific data.

Determination of concentrations in an absorption layer is difficult since measurements in this layer cause turmoil that interfere with the absorption process. In the experiment, in order to determine the concentration $a$, the sample volume of ca. 0.1 cm$^3$ was taken from the layer core.

Assume that the product $Da_2$ serves only as a correction factor for Whitman's model to compensate for unsteady state conditions. Then, based on the estimated value $-1.2966\times10^{-3}$ m (Table 1, column 2), using equations published elsewhere (Eqs. (19), (22c) [1]) and assuming that the chemical process rate constant $k_r$ is 0 and the average wave period $T \approx 200$ s, it is possible to determine the value of the effective coefficient of turbulent diffusion from a liquid to solid phase. In this case

$D = E_z = 1.06 \times 10^{-7}$ m$^2$/s; the value is ca. 106 times higher than the molecular diffusion coefficient for copper sulfate.

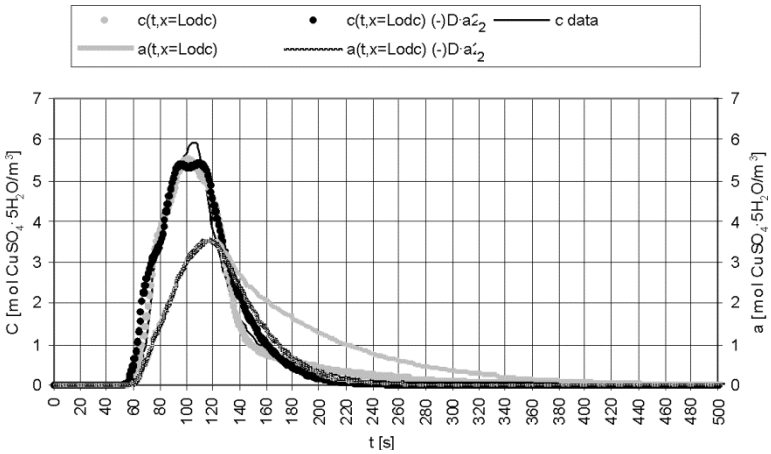


Fig. 7. Concentration $c$ and absorption $a$ curves obtained from the model (Eqs. (36)–(38)) (Table 1, column 2) and model (Eqs. (36)–(38)) without term $Da_2$ ((–)$Da_2$) (Table 1, column 3)

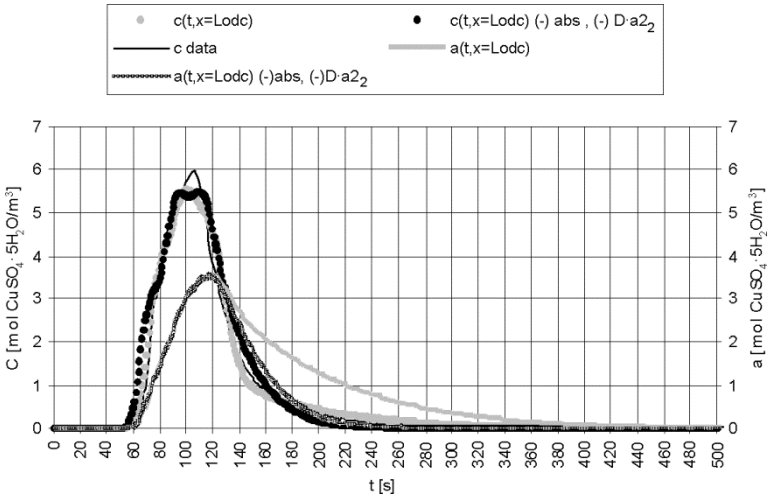


Fig. 8. Concentration $c$ and absorption $a$ curves using model (Eqs. (36)–(38)) for the data including absorption (Table 1, column 2) and model (Eqs. (36)–(38)) without term $Da_2$ ((-)$Da_2$) for the data without absorption ((–)abs) (Table 1, column 6)

Neglecting the term $Da_2$ in the model (Eqs. (36)–(38)) makes the model less accurate (the average absolute error of the model fit increases, Table 1, columns 3 and 6; Figs. 7 and 8). Absorption coefficients $\Gamma$ are lower than the theoretical one, which is close to one. Also other values of the model parameters differ, specially the ab-

sorption rate constant $K$. Major differences occur also between the values of model parameters presented in Table 1, columns 3 and 6, and the values of a complete model parameters with absorption (Table 1, column 2). Neglecting the term $Da_2$ in the model (Eqs. (36)–(38)) results in lower model accuracy in terms of concentration $c$ and absorption level $a$ (Figs. 7 and 8).

If two absorption points were considered in estimation of model parameters (Eqs. (36)–(38), neglecting term $Da_2$), the measured one and the one from the theoretical calculations using the complete model (Table 1, column 2), the absorption level $a$ would be improved (Fig. 9) but the average absolute error of the model fit would reach its maximum value (Table 1, column 7).

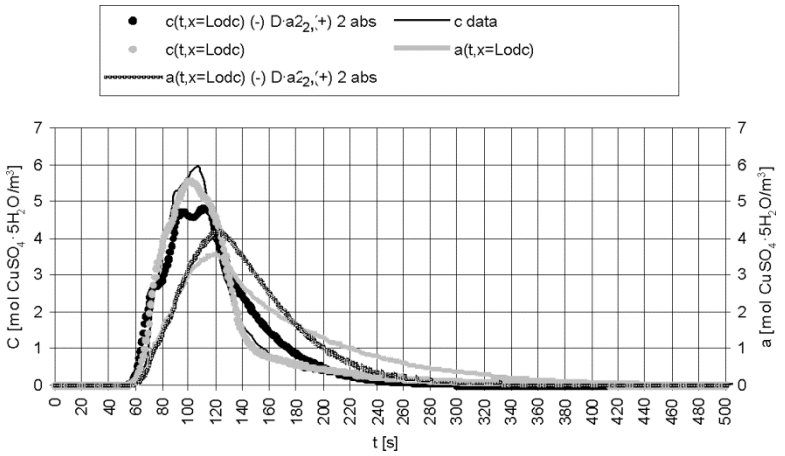


Fig. 9. Concentration $c$ and absorption $a$ curves obtained from model (Eqs. (36)–(38)) for the data including absorption (Table 1, column 2) and model (Eqs. (36)–(38)) without term $Da_2$ ((–)$Da_2$) for data considering two absorption points ((+)2 abs) from measurements and theoretical calculations (Table 1, column 7)

If the term $Da_2$ is neglected, fitting of the model (Eqs. (36)–(38)) becomes inadequate and its description of the real-life processes becomes less accurate. The same conclusion is true for the model of Eqs. (23)–(25). The described model has been also used for tracer transport modelling in the Colorado River, USA.

## 5. SUMMARY AND CONCLUSIONS

Application of Whitman's model for description of mass penetration due to absorption and adsorption mechanism in the solid phase enables one to determine the mass flux. The calculated flux values may differ from the real values depending on the character of concentration changes in time at the phase boundary. Analysis of dynamics of concentration changes within the solid phase, obtained due to integration of the

equation of diffusion in unsteady states, enables one to determine the real mass flux with respect to time. In order to decrease the discrepancies between the mass flux calculated from Whitman's model and the real mass flux, it is necessary to introduce the correction factor to the equation describing the concentration gradient close to the phase boundary in a solid phase. The correction factor may be expressed as the product of a certain parameter and the concentration derivative with respect to time, at a phase boundary. The parameter is equivalent to the coefficient $a_2$ (Eq. (22c), [1])) and therefore, it would be a function of: the concentration wave period, rate constant of chemical processes and the diffusion coefficient. The model comprises Eqs. (23)–(25) including the correction factor that incorporates the concentration derivative with respect to time. The model may be applied to simulate transport of pollutants which are subjected to adsorption or absorption processes in a river sediment layer. The processes proceed at a finite and an infinitely large rates through the equilibrium states. Therefore, the coefficient $a_2$ stands for the correction factor improving accuracy of Whitman's model and the parameter characterizing adsorption/absorption processes proceeding through the equilibrium states, simultaneously.

Model (23)–(25) was used to describe mass transport in a measuring apparatus; the experiments were conducted in a lab and in a full-scale model (river). The model accuracy improved when the term $Da_2$ was different from zero. Knowing the value of this term, one can estimate the effective coefficient of turbulent diffusion in the direction of the phase boundary, where the mass transport occurs.

## SYMBOLS

$(1/2)A_0$ – average concentration $C_i$, g/m$^3$
$A$ – surface area, m$^2$
$A^*$ – surface normal to diffusion direction, m$^2$
$A_n$, $B_n$ – coefficients of a trigonometric series, g/m$^3$
$C$, $c$ – concentration, g/m$^3$
$C^{\sim}$ – concentration in a phase core, g/m$^3$
$C^{\sim}_m$ – average concentration within a phase core, g/m$^3$
$C^{\sim}_{m,0}$ – average concentration in a phase core at an initial river cross-section, g/m$^3$
$C^{\sim}_{m,\mathrm{srd}}$ – average concentration in a phase core for a water course segment, g/m$^3$
$C^{\sim}_a$ – concentration amplitude in a phase core, g/m$^3$
$C^{\wedge}$ – Laplace transformation of a concentration function
$C_i$ – concentration at a phase boundary, g/m$^3$
$C_{i,m}$ – average concentration at a phase boundary, g/m$^3$
$C_{i,a}$ – concentration amplitude at a phase boundary, g/m$^3$
$C^{\wedge}_i$ – Laplace transformation of a concentration at a phase boundary, g/m$^3$
$D$ – diffusion coefficient, m$^2$/s
$E_x$ – longitudinal dispersion coefficient, m$^2$/s
$E_z$ – coefficient of vertical turbulent diffusion (perpendicular to a solid phase surface), m$^2$/s

$f$ – function
$G$ – transmittance
$g$ – acceleration of gravity
$h$ – water level or the average water level in a river, m
$i$ – drop of a water level in a water course, unless stated otherwise
$I$ – imaginary unit,
$k_r$ – process rate constant, 1/s
$k_w$ – coefficient of mass transfer at a liquid phase side, m/s; in the case of few different phases indexes: 1, 2, etc. are used; units may differ depending on the formula
$k_{z,\mathrm{og}}$ – overall equivalent rate constant for all processes occurring in liquid and solid phases, $s^{-1}$
$L$, $L_0$ – thickness of a solid phase layer, m
$L_{\mathrm{odc}}$ – length of water course segment, m
$M$ – transmittance module $|G|$
$m$ – mass, g
$r(C^{\sim})$ – process rate in the liquid phase core, g/(m$^3$·s)
$r_{\mathrm{og}}$ – total process rate, g/(m$^3$·s)
$R_h$ – hydraulic radius, m],
re(...) – real part of complex variables
im(...) – imaginary part of complex variables
$s$ – complex variable
$t$ – time, s
$t_{01}$, $t_{02}$ – time of appearing and disappearing of a concentration impulse in a initial river cross-section, s
$t_{k1}$, $t_{k2}$ – time of appearing and disappearing of a concentration impulse in a final river cross-section, s
$T$ – period of a function, s
$V$ – velocity, m/s
$V_{\mathrm{srd}}$ – average velocity, m/s
$V^*$ – liquid phase volume, m$^3$
$x$ – linear coordinate (longitudinal for a river), m
y – linear coordinate, m

GREEK SYMBOLS

$\alpha_M$, $\gamma_M$ – complementary parameters
$\Delta t$ – time difference or time shift, s
$\Delta t_1$, $\Delta t_2$ – time shifts, s
$\Delta t_0$, $\Delta t_k$ – time differences, s
$\Delta\tau$ – impulse time, s
$\varphi$ – argument of transmittance $G$, rad
$\omega$ – angular velocity, rad/s
$\omega_0$ – angular velocity for the main harmonic, rad/s
$\Omega_1$, $\Omega_2$ – integration constants

SELECTED SUBSCRIPTS

$i$ – concentration at a phase boundary
$a$ – amplitude, unless the list of variables states otherwise
$m$ – average value, unless the list of variables states otherwise

SELECTED SUPERSCRIPTS

~ – phase core (in the case of concentration)
^ – Laplace transformation

REFERENCES

[1] BIELSKI A., Environ. Prot. Eng., 2011, 37 (2), 35.
[2] KEMBŁOWSKI Z., MICHAŁOWSKI ST., STRUMIŁŁO C., ZARZYCKI R., *Theoretical Basis of Chemical and Process Engineering*, WNT, Warsaw, 1985 (in Polish).
[3] SZARAWARA J., SKRZYPEK J., *Basis of Chemical Reactors Engineering*, WNT, Warsaw, 1980 (in Polish).
[4] POHORECKI R., WROŃSKI S., *Kinetics* and *Thermodynamics of Chemical Engineering Processes*, WNT, Warsaw, 1977 (in Polish).
[5] ZARZYCKI R., CHACUK A., STARZAK M., A*bsorption* and *Absorbers*, WNT, Warsaw, 1987 (in Polish).
[6] BIELSKI A., *Selected Aspects of Mass Transfer Rate Determination between Phases in the Water-course. Part III. Modification of Whitman's Model for Concentration Changing in Time*, Technical Bulletin, Cracow University of Technology, 2006, No. 2.
[7] BRUNNER G.W., *HEC-RAS, River Analysis System, Hydraulic Reference Manual*, Version 3.1, November 2002 (US Army Corps of Engineers, Hydraulic Engineering Center, http://www.hec.usace.army.mil
[8] BOWIE G.L., MILLS W.B., PORCELLA D.B., *Rates, Constants* and *Kinetics Formulations in Surface Water Quality Modeling*, Environmental Research Laboratory Office of Research and Development U.S. Environmental Protection Agency, Athens, Georgia, June 1985 (EPA/600/3-85/040), http://www.epa.gov//ordntrnt/ORD/WebPubs/surfaceH2O/surface.html
[9] FRANZ D.D, MELCHING C.S., *Full Equations (FEQ) Model for the Solution of the Full, Dynamic Equations of Motion for One-Dimensional Unsteady Flow in Open Channels and through Control Structures*, U.S. Geological Survey, Water-Resources Investigations Report, California, 1997, (http://water.usgs.gov/software/code/surface_water/feq/doc/feq.pdf).
[10] Ukrainian Center of Environmental and Water Projects, web page address: http://www.ucewp.kiev.ua, files address: http://www.ucewp.kiev.ua/publ/nazwa, name = { p1.pdf, p2.pdf, p3.pdf, …, p23.pdf }
[11] PUZYREWSKI R., SAWICKI J., *Fluid Mechanic and Hydraulics*, PWN, Warsaw, 1987 (in Polish).
[12] LYNESS J.F., MYERS W.R.C., WARK J.B., J. Chart. Inst. Water Environ. Manage., 1997, 11 (5), 335.
[13] HAIMES Y.Y., *Hierarchical Analyses of Water Resources Systems*, McGraw-Hill, New York, 1977.
[14] CUNGE J.A., HOLLY F.M., VERWEY A., *Practical Aspects of Computational River Hydraulics*, Pitman Publ. Ltd., London, 1980.
[15] BIAŁAS S., OLAJOSSY A., *Differential Methods of Solving Differential Equations. Part I, II*, Technical University of Mining and Metallurgy, Cracow, 1984.
[16] SZYMKIEWICZ R., *Mathematical Modelling of Flows in Rivers* and *Channels*, PWN, Warsaw, 2000 (in Polish).
[17] WESSELING P., *Principles of Computational Fluid Dynamics*, Springer, Berlin, 2001.
[18] FLETCHER C.A.J., *Computational Techniques for Fluid Dynamics*, Vol. 1, 2, Springer, Berlin, 2000.
[19] SAWICKI J.M., *Pollutant Migration*, Gdańsk Techn. Univ. Publ,, 2003 (in Polish).
[20] SIENIUTYCZ S., O*ptimization in Process Engineering*, WNT, Warsaw, 1978 (in Polish).
[21] KRĘGLEWSKI T., ROGOWSKI T., RUSZCZYŃSKI A., SZYMANOWSKI J., *Methods of Optimization in FORTRAN*, PWN, Warsaw, 1984 (in Polish).

Environment Protection Engineering

Vol. 37 2011 No. 4

MOHAMED ALWAELI*

# AN ECONOMIC ANALYSIS OF JOINED COSTS AND BENEFICIAL EFFECTS OF WASTE RECYCLING

Much research has been done throughout the world to determine the economic and ecological profitability of waste utilization as a substitution for raw materials. Unfortunately, Poland has no sufficient solutions in this field. The deficiency of solutions impedes the work of groups of specialists in various fields involved with the rational planning of recycling. This research seeks to offer a simple unified framework to study the key economic features of the use of waste as substitute for nonrenewable resources in production in Poland and other countries. The purpose of this paper is to develop a model to obtain some key insights about the cost-effectiveness and define certain parameters which determine the effectiveness of production plants dedicated for processing waste into useful products. A plant's productive possibilities can be described by the production function which is determined empirically. In this model, the emphasis is put on plant functioning and is dependent on the amount of work destined for the production in fixed units, technical maintenance costs of the work fixture in fixed units (e.g. machines', cars' operating costs etc.), and the amount of modified waste. In order to calculate these costs, we need to consider the issue of precise measuring the overhead costs in order to maximize profitability of this kind of measures allocation so that the profit will be the highest. The task of measuring overhead (costs) comes down to finding the maximum of the production function. This research presents the mathematical model and provides some key insights about the profitability of the plants dedicated for processing waste into secondary materials. In this research, we also determined the maximum of the profit function and assess when the recycling plant will bring the profit and when it is the highest.

## 1. INTRODUCTION

We live in a socially interconnected world as well as in one displaying environmental interdependence. In most cases, human desires to use the Earth's available resources, including environmental resources, exceed the capacity of these resources to satisfy human wants completely [1]. From an economic viewpoint, developing

*Silesian University of Technology, Faculty of Energy and Environmental Engineering, ul. Konarskiego 18, 44-100 Gliwice, Poland, e-mail: mohamed.alwaeli@polsl.pl

countries such as Poland are heavily dependent on living resources and natural environments. Furthermore, developed countries benefit substantially from the conservation of their own resources through recycling/reuse.

The analysis of waste utilization as substitute natural resources has largely evolved as separate branches in economic literature. A notable exception is *On Natural Resources Substitution*" by Andre and Creda, presenting a simple dynamic model to gain some key insights about the substitution of renewable resources for non-renewable resources, and the consequences for sustainability [2]. Ready and Ready presented a dynamic model according to which the price of landfill disposal increases from the time a new landfill is opened until it is filled, then decreases slightly as a new landfill is opened, and then begins increasing once again, due to the problem of land scarcity [3]. Therefore, it is economical to start recycling some of the waste before the price of landfill disposal reaches that of recycling, in order to reduce the costs of landfill over time. In his pioneering work, Vivian [4] studied the costs and benefits of the current practice of dumping the construction waste into landfills and extracting new natural materials for new concrete production, as well as the proposed concrete recycling method to recycle the construction waste as aggregate for new concrete production. With the advent of the cost on the current practice, it is found that the concrete recycling method can result in huge savings.

The benefits gained from the concrete recycling method can balance the cost expended for the current practice. Therefore, recycling concrete waste for new production is a cost-effective method that also helps to protect the environment as well as to achieve construction sustainability.

Towards the end of the 20th century, and at the beginning of the 21st century, the problem of using waste as a substitute for primary materials has become one of the basic issues of environmental protection and waste management in the world. Much research on recycling has been done by such authors as Rhyner [5], Sharma et al., [6], di Vita [7, 8], Fletcher and Mackay [9], Hsu and Kuo [10] Nakamura [11, 12], Berglund [13], Haque et al. [14] and Alwaeli [15, 16]. The authors analysed various microeconomic models in which the economic profitability from waste recycling and certain ways of reducing the current value and future costs connected with waste management were considered.

Over the last few decades, consumption behaviour in Poland has changed dramatically in accordance with rapid economic growth. Waste disposal caused serious problems. Altogether more than 1.74 milliard tons of waste have been landfilled in Poland, and this amount increases approximately by 133 million tons every year [17]. Landfilling is still the main disposal method in Poland, although other methods are used on a negligible scale. Recycling is the most effective method for solving this problem because it not only reduces amount of waste, but also mitigates the depletion of natural resources resulting from economic development.

## 2. THE MODEL

The cost-effectiveness of waste recycling depends on a variety of inherent expenses. These costs include the expenses borne by the waste supplier, namely the cost of obtaining waste, transporting it to the segregation plants, and finally, the cost of the actual waste segregation. By contrast, recycling plants which use waste as raw materials bear the costs of waste processing as well as their clearance. In addition, we need to take into consideration those costs which are associated with amortization, equipment maintenance, waste storage, and labour. This work emphasizes the economic profitability of the plants dedicated for processing waste into secondary materials. The economic cost-effectiveness of the plant dedicated for processing waste into secondary materials can be defined as a production function. From economic experience [2, 7, 18] it seems that the production function has the form:

$$f(x_1, x_2, x_3, x_4) = a x_1^{\alpha_1} x_2^{\alpha_2} x_3^{\alpha_3} x_4^{\alpha_4} \tag{1}$$

In which coefficients $a$, $\alpha_1$, $\alpha_2$, $\alpha_3$, $\alpha_4$, are empirically matched and fulfil the following conditions:

$$\alpha > 0, \quad \alpha_2 > 0, \quad \alpha_3 > 0, \quad \alpha_4 > 0, \quad \alpha_1 + \alpha_2 + \alpha_3 + \alpha_4 < 1$$

The production function depends on the amount of work destined for the production in fixed units ($x_1$), the technological maintenance costs of the work fixture in fixed units ($x_2$), the amount of the modified raw material ($x_3$), and the amortization costs ($x_4$), etc.

Let us denote unit costs of particular elements of the production by $q_1$, $q_2$, $q_4$, $q_4$,. This means that the work unit costs $q_1$ ZLP, technological maintenance unit of the work fixture costs $q_2$ ZLP, etc. The unit of the product has the price of $\gamma$ZLP.

Having available $x_1$, $x_2$, $x_3$, $x_4$, the production plant will produce $f(x_1, x_2, x_3, x_4)$ of the product units in a specific time unit (e.g. one month).

Owing to the fact that we have $K$ means destined for the production in a given time, we get the condition that the sum of the input designated for the plant exploitation will not exceed $K$ reduced by the permanent costs $K_1$, (maintenance of both administration and plant). The aforementioned costs must be borne despite the volume of the production.

$$q_1 x_1 + q_2 x_2 + q_3 x_3 + q_4 x_4 \leq K - K_1 \tag{2}$$

The left side of the inequality stands for the relative sum of the plant, whereas the right side signifies the amount of measures available.

We need to consider the issue of measuring overhead costs in order to ensure the highest possible profit. The profit from the production is expressed by the following formula:

$$\Phi(x_1, x_2, x_3, x_4) = \gamma f(x_1, x_2, x_3, x_4) - (q_1 x_1 + q_2 x_2 + q_3 x_3 + q_4 x_4) \tag{3}$$

Because of the fact that the function increases with regard to each variable, the whole capital which we have at our disposal, must be divided. The following conclusion can be drawn:

$$x_1 > 0, \qquad x_2 > 0, \qquad x_3 > 0, \qquad x_4 > 0, \qquad x_1 + x_2 + x_3 + x_4 = K - K_1 \tag{4}$$

The task of measuring overhead costs comes down to finding the maximum of the function (3) taking into account the aforementioned conditions (4). The mathematical solution to the issue of optimization will be discussed later.

Assuming that $(\bar{x}_1, \bar{x}_2, \bar{x}_3, \bar{x}_4)$ is the solution to the problem, the profit from the plant operating in a specific time will be:

$$\Phi\left(\bar{x}_1, \bar{x}_2, \bar{x}_3, \bar{x}_4\right) = \gamma f\left(\bar{x}_1, \bar{x}_2, \bar{x}_3, \bar{x}_4\right) - (K - K_1)$$

However, the profit must fulfil certain economic conditions.

The value of the plant amounts to $\Pi$ ZLP, the interest on the financial market in a fixed time unit comes to $p$%, total depreciation of the working place amounts to $q$%. It may be concluded that the profit from the plant exploitation must be higher. Eventually, it will come to:

$$\Phi(\bar{x}_1, \bar{x}_2, \bar{x}_3, \bar{x}_4) - \Pi \cdot \frac{p}{100} \cdot \frac{q}{100} > 0 \tag{5}$$

The profit must be positive in order for the plant to have economic profitability.

The profit issue of optimization will be solved based on the Kuhn–Tucker (K–T) methods. From the K–T condition, if the system of equations

$$\frac{\partial L}{\partial x_i} = 0, \qquad i = 1, 2, ..., n$$

$$\frac{\partial L}{\partial \lambda} = 0$$

has a positive solution

$$x_i > 0, \qquad i = 1, 2, ..., n, \qquad \lambda > 0$$

in which

$$L(x, \lambda) = \gamma f(x) - \lambda\left(q_1 x_1 + q_2 x_2 + ... + q_n x_n - K\right)$$

is the Lagrange function, and the function for $f(x)$ is a concave one which means that the solution of the system of Eqs. (5) is the solution to the problem of the maximization of the profit function

$$\Phi(x) = \gamma f(x) - K$$

Nevertheless, there is the condition

$$q_1 x_1 + q_2 x_2 + ... + q_n x_n = K$$

Hence, we have the system of equations to be solved

$$\frac{\partial L}{\partial x_i} = \gamma \frac{\partial f}{\partial x_i} - \lambda q_i = 0, \qquad i = 1, 2, ..., n$$

$$\frac{\partial L}{\partial x} = q_1 x_1 + q_2 x_2 + ... + q_n x_n - K = 0$$

If the solution of this system is positive, it is a point in which the profit function reaches a maximum,

The profit function obtained from the production amounts to:

$$Z(x) = \gamma f(x) - K \tag{6}$$

where $\gamma$ is the unit cost of the produced product, $K$ – the amount of money destined for the production in a specific time (e.g. one month).

The function $f(x)$ is the productive function depending on the means of production and is expressed as

$$f(x) = a x_1^{\alpha_1} x_2^{\alpha_2} ... x_n^{\alpha_n} \tag{7}$$

where:

$$x = (x_1, ..., x_n) \in R_+^n$$

$$\alpha_i > 0, \qquad i = 1, 2, ..., n, \qquad \sum_{i=1}^{n} \alpha_i = a < 1$$

The function (7) is the concave one.

We determine the maximum of the function $Z(x)$ having the given condition

$$q_1 x_1 + q_2 x_2 + ... + q_n x_n = K, \qquad x_i > 0, \qquad i = 1, 2, ..., n \tag{8}$$

in which ($q_1$, $q_2$, …, $q_n$) is the vector of the unit prices of the means of production $x \in R_+^n$.

The Lagrange function

$$L(x, \lambda) = \gamma f(x) - \lambda(q_1 x_1 + q_2 x_2 + ... + q_n x_n - K), \qquad x \in R_+$$

and the Kuhn–Tucker function should be applied

$$\left\{\begin{array}{l}\dfrac{\partial L}{\partial x_i}=\gamma\dfrac{\partial f}{\partial x_i}-\lambda q_i=0, \qquad i=1,2,...,n \\ \dfrac{\partial L}{\partial \lambda}=q_1x_1+q_2x_2+\cdots+q_nx_n-K=0\end{array}\right\} \tag{9}$$

If the system has only one solution and $L(x,\lambda)$ is the concave function, the solution is the maximum of the function given by Eq. (1). However, the condition in Eq. (3) must be fulfilled.

We determine the solution of the system depending on the parameter γ. Because of the fact that

$$\frac{\partial f}{\partial x_i}=ax_1^{\alpha_1}...(\alpha_i x_i^{\alpha_i-1})...x_n^{\alpha_n}=\frac{\alpha_i}{x_i}f(x)$$

the system of Eqs. (9) is represented by:

$$\gamma\frac{\alpha_i}{x_i}f(x)-\lambda q_i=0, \qquad i=1,2,...,n$$

For $i\neq j$ we have

$$\gamma\frac{\alpha_i}{x_i}f(x)=\lambda q_i \tag{10a}$$

$$\gamma\frac{\alpha_j}{x_j}f(x)=\lambda q_j \tag{10b}$$

Dividing Eq. (10a) by (10b), we obtain

$$\frac{\dfrac{\alpha_i}{x_i}}{\dfrac{\alpha_j}{x_j}}=\frac{q_i}{q_j}, \qquad \frac{\alpha_i x_j}{\alpha_j x_i}=\frac{q_i}{q_j}, \qquad \frac{\dfrac{x_j}{\alpha_j}}{\dfrac{q_j}{q_i}}=\frac{\dfrac{x_i}{\alpha_i}}{\dfrac{q_i}{q_i}}$$

Hence, the vectors

$$(x_1,x_2,...,x_n) \qquad \text{and} \qquad x\left(\frac{\alpha_1}{q_1},\frac{\alpha_2}{q_2},...,\frac{\alpha_n}{q_n}\right)$$

have proportional coordinates; in consequence, we obtain

$$x_i=t\frac{\alpha_i}{q_i}, \qquad i=1,2,...,n$$

where $t$ is a parameter.

After introducing the obtained values into Eq. (8) we get

$$q_1 t\frac{\alpha_1}{q_1} + q_2 t\frac{\alpha_2}{q_2} + ... + q_n t\frac{\alpha_n}{q_n} - K = 0$$

The conclusion is that

$$t(\alpha_1 + \alpha_2 + ... + \alpha_n) = K$$

Eventually,

$$t = \frac{K}{\alpha}$$

Consequently, we get the solution of the systems Eqs. (9) and (5)

$$\overline{x}_i = \frac{K}{\alpha}\cdot\frac{\alpha_i}{q_i}, \qquad i = 1, 2, ..., n$$

which is the solution of the optimum task.

The maximum profit, if we take into consideration investing $K$ capital, amounts to:

$$\tilde{Z}(K) = Z(\overline{x}_1, \overline{x}_2, ..., \overline{x}_n) = \gamma a(\frac{K}{\alpha}\frac{\alpha_1}{q_1})^{\alpha_1}\cdot(\frac{K}{\alpha}\frac{\alpha_2}{q_2})^{\alpha_2}\cdot ...\cdot(\frac{K}{\alpha}\frac{\alpha_n}{q_n})^{\alpha_n} - K$$

$$= \gamma a(\frac{K}{\alpha})^{\alpha_1+\alpha_2+...+\alpha_n}(\frac{\alpha_1}{q_1})^{\alpha_1}(\frac{\alpha_2}{q_2})^{\alpha_2}...(\frac{\alpha_n}{q_n})^{\alpha_n} - K = \gamma(\frac{K}{\alpha})^{\alpha} f(\frac{\alpha_1}{q_1}, \frac{\alpha_2}{q_2}, ...\frac{\alpha_n}{q_n}) - K$$

Marking the constant

$$\gamma f\left(\frac{\alpha_1}{q_1}, \frac{\alpha_2}{q_2}, ..., \frac{\alpha_n}{q_n}\right) = R,$$

we get

$$\tilde{Z}(K) = \left(\frac{K}{\alpha}\right)^{\alpha} R - K$$

Now, we need to study how much money we have to invest in the production in order to achieve the maximuml profit. For this purpose, the variability of function $\tilde{Z}(K)$ must be studied

$$\tilde{Z}'(K) = \frac{R}{\alpha^{\alpha}}\alpha K^{\alpha-1} - 1 = 0$$

$$R\alpha^{\alpha-1} = K^{1-\alpha}$$

$$\tilde{K} = \alpha R^{1/(1-\alpha)}$$

$$\tilde{Z}(\tilde{K}) = (R^{1/(1-\alpha)})^{\alpha} R - \alpha R^{1/(1-\alpha)} = R^{1/(1-\alpha)} - \alpha R^{1/(1-\alpha)} = (1-\alpha) R^{1/(1-\alpha)}$$

Based on the fact that $Z(K) = 0$ for $K = 0$ and $K = R^{1/(1-\alpha)}/\alpha^{1/(1-\alpha)}$, the course of the function $Z(K)$ is as shown in Fig. 1.

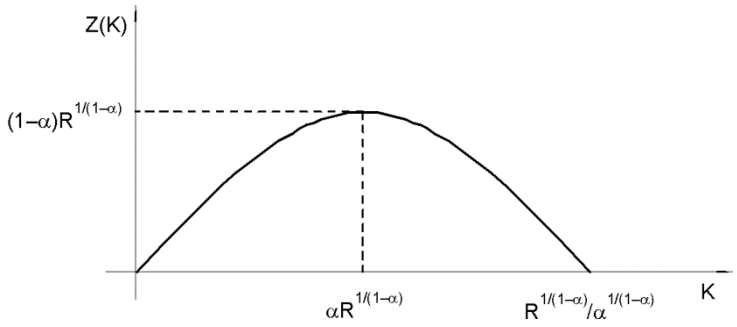


Fig. 1. Profit dependence on the invested capital

The unconditional extreme of the function (6), i.e. without the condition (8), is seen in the point

$$\overline{x}_i = R^{1/(1-\alpha)} \frac{\alpha_i}{q_i}, \qquad i = 1, 2, ..., n$$

For $K > \alpha R^{1/(1-\alpha)}$, it is uneconomic to invest $K$ funds due to the fact that the profit from the production will be smaller than for the unconditional extreme.

## 3. DISCUSSION

It is a challenge to reduce the increasing flow of waste. The development of an efficient waste recycling approach will help us to explore new opportunities for urban and environmental protection. Despite the fact that properties of the primary materials have been lost, the waste still carries both the value of subjective human work as well as the energy used for their production. This waste constitutes a potential source of secondary materials and fuels. Recycling is the most effective method for solving these problems because the recycling process not only reduces amount of waste, but also mitigates the depletion of natural resources resulting from economic development. Additionally, recycling reduces the cost of transportation and, relying on the analysis of the use of waste as a substitute in the production held by LCA, shortens, in some cases, the production process.

Owing to the fact that we have $K$ meaning destined for the production in a given time, we get the condition that the sum of the input designated for the plant exploitation will not exceed $K$ reduced by the permanent costs $K_1$, that is, the maintenance of both the administration and the plants.

Because of the fact that the production function increases with regard to each variable, the whole capital, which we have at our disposal, must be divided. We considered the issue of measuring and dividing overhead costs, in order that the highest profit can be achieved.

The purpose of this research is to present the mathematical model and to provide some key insights about the profitability of the plants dedicated for processing waste into secondary materials. The profit function obtained from the production amounts to $Z(x) = \gamma f(x) - K$ in which $\gamma$ is the unit cost of the produced product, $K$ is the quantity of money destined for the production in a specific time (e.g. one month) and $f(x)$ is the production function.

In this research, we also determined the maximum of the profit function. Based on Eq. (6), the maximum profit, implicate that if we take into consideration investing $K$ capital, amounts to:

$$\tilde{Z}(K) = \left(\frac{K}{\alpha}\right)^{\alpha} R - K = K\left(\frac{R}{\alpha}\left(\frac{\alpha}{K}\right)^{1-\alpha} - 1\right)$$

This means that the profit is proportional to the sum of invested capital $K$ multiplied by the factor $\left(\frac{R}{\alpha}\left(\frac{\alpha}{K}\right)^{1-\alpha} - 1\right)$ which is decreasing upon increasing $K$. Thus in order to have the maximum profit, we have to invest $K = R^{1/(1-\alpha)}/\alpha^{1/(1-\alpha)}$.

Based on Fig. 1, the recycling plant will bring the profit for $0 < K < \alpha R^{1/(1-\alpha)}$; nevertheless, the profit is the highest for $K = (\alpha R_2)^{1/(1-\alpha}$. While for $K > \alpha R^{1/(1-\alpha)}$ it is uneconomic to invest $K$ fund due to the fact that the profit from the production will be smaller than for the unconditional extreme.

Much research has been done throughout the world to determine the economic and ecological profitability of utilization of secondary materials (waste) as a substitution for raw materials. Unfortunately, Poland does not have sufficient solutions in this field. The deficiency of solutions impedes the work of groups of specialists in various fields involved with the rational planning of recycling. These are the results of our mathematical model of economic profitability of secondary materials (waste) utilization as the substitute for primary materials. Currently, no empirical analyses have been carried out on this issue. This research seeks to offer a simple unified framework to study the key economic features of the use of waste as substitute for nonrenewable resources in production in Poland and other countries.

## APPENDIX A

As a first attempt to evaluate the empirical performance of the model of the previous section, we will consider example in which the production function is as follows:

$$f(x_1, x_2) = x_1^{0,25} x_2^{0,25}$$

The profit function amounts to

$$Z(x_1, x_2) = P x_1^{0,25} x_2^{0,25} - q_1 x_1 - q_2 x_2$$

where: $P$ is the unit price of the produced product, $q_1$, $q_2$ – unit prices of raw materials.

We need to determine the unconditional extreme of the function. We have

$$\frac{\alpha_1}{q_1} = \frac{1}{4q_1}, \qquad \frac{\alpha_2}{q_2} = \frac{1}{4q_2}, \qquad f\left(\frac{1}{4q_1}, \frac{1}{4q_2}\right) = \left(\frac{1}{4q_1}\right)^{0,25} \left(\frac{1}{4q_2}\right)^{0,25} = \frac{1}{2(q_1 q)^{0,25}}$$

$$R = \frac{P}{2(q_1 q_2)^{0.25}}$$

$$\overline{x}_1 = \left(\frac{P}{2(q_1 q_2)^{0,25}}\right)^2 \frac{1}{4q_1} = \frac{P^2}{16 q_1 (q_1 q_2)^{0,5}}, \qquad \overline{x}_2 = \left(\frac{P}{2(q_1 q_2)^{0,25}}\right)^2 \frac{1}{4q_2} = \frac{P^2}{16 q_2 (q_1 q_2)^{0,5}}$$

$$f(\overline{x}_1, \overline{x}_2) = \frac{P}{4\sqrt{q_1 q_2}}$$

$$Z(\overline{x}, \overline{y}) = \frac{P^2}{4\sqrt{q_1 q_2}} - \frac{P^2}{8\sqrt{q_1 q_2}} = \frac{P^2}{8\sqrt{q_1 q_2}}$$

We can conclude that if we invest the means of production $\overline{x}_1, \overline{x}_2$, we will obtain the production $f(\overline{x}_1, \overline{x}_2)$ whose profit amounts to $Z(\overline{x}, \overline{y})$.

## APPENDIX B

Now we have to consider one more example in which the production function is as follows:

$$f(x) = \alpha_1 \ln x_1 + \alpha_2 \ln x_2 + \ldots + \alpha_n \ln x_n$$

where

$$x = (x_1, \ldots, x_n) \in R_+^n, \qquad \alpha_i > 0, \qquad i = 1, 2, \ldots, n$$

The function $f(x)$ is concave for $x \in R_+^n$.

The profit function

$$Z(x) = Pf(x) - K$$

where $P$ is the price of the produced product, $K$ the total sum of means destined for the production, i.e.

$$q_1 x_1 + q_2 x_2 + ... + q_n x_n = K$$

where $q_i$ is the unit price of the used raw material.

We maximize the Lagrange function

$$L(x, \lambda) = \gamma f(x) - K - \lambda(q_1 x_1 + q_2 x_2 + ... + q_n x_n - K)$$

We solve the system of equations

$$\frac{\partial L}{\partial x_i} = P\frac{\alpha_i}{x_i} - \lambda q_i = 0, \qquad i = 1, 2, ..., n$$

$$\frac{\partial L}{\partial x} = q_1 x_1 + q_2 x_2 + ... + q_n x_n - K = 0$$

we have

$$\frac{P\alpha_i}{x_i} = \lambda q_i, \qquad i = 1, 2, ..., n$$

For $i \neq j$ we have

$$\frac{P\alpha_i}{x_i} = \lambda q_i, \qquad \frac{P\alpha_j}{x_j} = \lambda q_j$$

Dividing the equations by their members, we obtain

$$\frac{\alpha_i}{x_i}\frac{\alpha_j}{x_j} = \frac{q_i}{q_j}$$

Hence we get

$$\frac{\frac{x_j}{\alpha_j}}{q_j} = \frac{\frac{x_i}{\alpha_i}}{q_i}.$$

Therefore, the vectors

$(x_1, x_2, ..., x_n)$ and $x\left(\frac{\alpha_1}{q_1}, \frac{\alpha_2}{q_2}, ..., \frac{\alpha_n}{q_n}\right)$, are parallel.

In that case there exists a constant such that

$$x_i = t_i \frac{\alpha_i}{q_i}, \qquad i = 1, 2, ..., n$$

Substituting it into Eq. (8), we have

$$t\alpha_1 + t\alpha_2 + ... + t\alpha_n = K$$

Stating that

$$\alpha_1 + \alpha_2 + ... + \alpha_n = a$$

we obtain

$$ta = K, \qquad t = \frac{K}{a}$$

consequently

$$\overline{x}_i = \frac{K}{a}\frac{\alpha_i}{q_i}, \qquad i = 1, 2, ..., n$$

is the solution to the problem of maximization. We have

$$f(\overline{x}) = \alpha_1 \ln \frac{K}{a}\frac{\alpha_1}{q_1} + \alpha_2 \ln \frac{K}{a}\frac{\alpha_2}{q_2} + ... + \alpha_n \ln \frac{K}{a}\frac{\alpha_n}{q_n}$$

$$= (\alpha_1 + \alpha_2 + ... + \alpha_n)\frac{K}{a} + \alpha_1 \ln \frac{\alpha_1}{q_1} + \alpha_2 \ln \frac{\alpha_2}{q_2} + ... + \alpha_n \ln \frac{\alpha_n}{q_n} = a \ln \frac{K}{a} + f(\overline{x})$$

Therefore the maximum profit from the production process is

$$Z(\overline{x}) = P(a \ln \frac{K}{a} + f(\overline{x})) - K$$

Stating that $Pf(\overline{x}) = R$ we have

$$Z(\overline{x}) = Pa \ln \frac{K}{a} - K - R$$

We investigate which means have to be involved so that the profit is maximized. We have

$$\frac{dZ(\overline{x})}{dK} = \frac{Pa}{K} - 1 = 0$$

thus $K = Pa$.

Therefore, the maximum profit amounts to

$$\bar{Z} = Pa \ln P - Pa - R \qquad \text{for} \qquad \bar{x}_i = \frac{P\alpha_i}{q_i}, \qquad i = 1, 2, ..., n$$

REFERENCES

[1] TISDELL C.A., *Economics of Environmental Conservation*, 2nd Ed., Edward Elgar, Cheltenam., UK, 2005.
[2] ANDRE F.J., CREDA E., Resour. Policy, 2006, 30 (4), 233.
[3] READY M., READY R., J. Environ. Econ. Manage., 1995, 28 (3), 307.
[4] VIVIAN W.Y.T., Resour. Conserv. Recycl., 2008, 52 (2), 821.
[5] RHYNER CH.R., Resour. Conserv. Recycl., 1998, 24 (3-4), 349.
[6] SHARMA V.K., BEUKERING V.P., BARNALI N., Resour. Conserv. Recycl., 1997, 21 (1), 55.
[7] DI VITA G., Resour. Policy, 2006, 31 (3), 172.
[8] DI VITA G., Ecol. Econ., 2007, 63 (1), 138.
[9] FLETCHER B.L., MACKAY M.E., Resour. Conserv. Recycl., 1996, 17 (2), 141.
[10] HSU E., KUO C.M., Waste Manage., 2005, 25 (1), 53.
[11] NAKAMURA S., Ecol. Econom., 1999, 28 (1), 1333.
[12] NAKAMURA S., KONDO Y., Ecol. Econom., 2006, 57 (3), 494.
[13] BERGLUND C., Ecol. Econom., 2006, 56 (4), 560.
[14] HAQUE A., MUJTABA I.M., BELL J.N.B., Waste Manage., 2000, 20 (8), 625.
[15] ALWAELI M., Mineral Energy Economy, 2008, 24 (4/1), 19.
[16] ALWAELI M., Environ. Prot. Eng., 2011, 1, 51.
[17] *Statistical Yearbook*, GUS, Poland, 2008.
[18] SHARMA V.K., BEUKERING P.V., NAG B., Resour. Conserv. Recycl., 2007, 21 (1), 57.

Environment Protection Engineering

Vol. 37 2011 No. 4

ANDRZEJ KOTOWSKI*, HENRYK SZEWCZYK**, WOJCIECH CIEŻAK*

# ENTRANCE LOSS COEFFICIENTS IN PIPE HYDRAULIC SYSTEMS

The entrance loss coefficients have been investigated for four, most frequently occurring geometric shapes of inlets placed on the reservoir bottom. The minor (entrance, inlet) losses coefficients determined in the paper, having not been investigated experimentally so far, may be used, for example, to correctly dimension throttling pipes. Throttling pipelines are commonly used in sewage systems for limiting the volume flow rate of sewage channelled to sewage treatment plants from storage reservoirs, storm overflows or rainwater separators during torrential rainfall.

## 1. INTRODUCTION

The possibility to find correct values of entrance resistance coefficients of pipes in hydraulic systems given in available manuals, handbooks or standards and similar materials is only illusory. This is no surprise, since the coefficients are determined by specific shapes of a given minor loss and, in general, depend on the Reynolds number (*Re*). However, in practice, the Reynolds number is so high that the *K* coefficient can be constant. The paper presents the results of investigation of four specific shapes of pipe inlets typical of hydraulic (particularly sewage) systems, which however, have not been hydraulically investigated so far.

The sewage flow from a number of sewage facilities (storage reservoirs, storm overflows, separators) occurring during torrential rainfall must be limited prior to its introduction to the sewage treatment plant. To this end various types of flow regulators are used. However, most often this is realized by means of a pipeline working under pressure called a throttling pipe [1, 2]. The throttling pipe is an example of liquid flow regulator which makes it possible to empty a reservoir completely because it

*Institute of Environmental Protection Engineering, Wrocław University of Technology, pl. Grunwaldzki 9, 50-370 Wrocław, Poland, e-mail addresses: andrzej.kotowski@pwr.wroc.pl (corresponding author), wojciech.ciezak@pwr.wroc.pl

**Institute of Thermal Engineering and Fluid Mechanics, Wrocław University of Technology, Wybrzeże Wyspiańskiego 27, 50-370 Wrocław, Poland, e-mail: henryk.szewczyk@pwr.wroc.pl

is placed on its bottom level. Minor losses on the inlet and outlet of a throttling pipe – apart from linear losses – influence the selection of the length and diameter of the pipe which should ensure the assumed distribution of volume flow rates on a storm overflow [3–5], or in a light liquid separator with inner by-pass channels [6].

The calculation of dimensions (diameter and length) of a throttling pipe is based on the phenomenon of liquid flow between two open reservoirs and connected by means of a pipeline operating under elevated pressure. Its correct dimensioning requires the knowledge of the linear ($f$) and minor ($K$) loss coefficients because they appear in the Darcy–Weisbach formula which is used to calculate energy losses in closed conduits. Therefore, the energy loss head $\Delta h_{l,d}$ occurring in liquid flow with the mean velocity $u$ through the pipeline of the diameter $d$ and length $l$ amounts to

$$\Delta h_{l,d} = \left( f\frac{l}{d} + K + \alpha \right)\frac{u^2}{2g} \tag{1}$$

These are the entrance resistance of the coefficient $K$ and outlet resistance of the coefficient $\alpha$. It should be noted that the entire kinetic energy is lost on the outlet of the throttling pipe [6], thus, the outlet loss head is $\alpha u^2/2g$ ($\alpha$ is the kinetic energy correction factor).

As can be seen from Eq. (1), the knowledge of correct values of coefficients $f$, $K$ and $\alpha$ is essential in the procedure of dimensioning of the throttling pipe. Thus, the friction factor $f$, which depends on relative roughness $k/d$ (where $k$ is a mean wall roughness head) and the Reynolds number and hence $f = f(k/d, Re)$, is assumed according to known formulae or from nomograms [8]. In the case of plastic sewage pipes of the wall smoothness comparable to glass the friction factor can be then calculated from the Blasius formula [7–11]:

$$f = \frac{0.3164}{\sqrt[4]{Re}} \wedge Re = \frac{ud}{\nu} = \frac{4q_V}{\pi d\nu} \tag{2}$$

where: $\nu$ is the kinematic viscosity (it was calculated using the formula making it dependent on the water temperature) and $q_V$ is volume rate of flow.

As already mentioned, the entire kinetic energy is lost on the outlet of the throttling pipe, therefore the outlet loss head is $\alpha u^2/2g$. However, in many textbooks and publications [7, 10, 12] the outlet loss coefficient ($\alpha$) is assumed equal to 1. It is nearly consistent with reality but only for a high turbulent flow. Whereas, Szewczyk [13] gave the following explicit dependence for the kinetic energy correction factor valid in the wide range of $Re \in [2.8\times10^3, 36\times10^6[$, for the flow in smooth hydraulic pipes

$$\alpha = 1 + 0.101\left(\frac{10}{\ln Re}\right)^6 - 0.107\left(\frac{10}{\ln Re}\right)^4 + 0.113\left(\frac{10}{\ln Re}\right)^2 \tag{3}$$

In order to illustrate the course of the dependence $\alpha(Re)$, a number of values of $\alpha$ calculated from Eq. (3) were given, that is: $\alpha(\{5, 10, 10^2, 10^3\}\times 10^3) = \{1.22, 1.15, 1.07, 1.04\}$.

The selection of values for the inlet loss coefficient $K$ encounters a number of difficulties, since literature data differ by as much as 100%. Typically, the Borda–Carnot formula was employed here [7, 10, 14, 15] and for the outflow from a large reservoir to the throttling pipe $K$ is obtained as equal 0.5. According to the model testing on lateral overfalls with throttled outflow carried out by Kallwass [16, 17], values of the outlet loss coefficient amount to: $K = 0.25$, for the round-edged inlet, or $K = 0.35$ for the sharp-edged inlet. However, Imhoff and Imhoff [18] and the TGL standard [19] recommend to assume $K = 0.40$, if edges are technically sharp, but according to the DVWK-ATV-A 111 guidelines [1] give $K = 0.45$.

The reservoir wall containing the throttling pipe can be flat and perpendicular to the pipe axis, but it may also contain bevels – guides (usually at the angle of $\pi/4$ rad), and finally, the reservoir bottom may contain invert channels (typically of the depth of $d/2$). Furthermore, the influence of the height and width of a liquid jet in front of a pipe inlet have not been investigated.

## 2. THE IDEA OF ENTRANCE LOSSES MEASUREMENT, INVESTIGATION PROGRAM AND TESTING STATION

Figure 1 shows an idealized, axially symmetrical case of laminar and turbulent liquid flows through a straight pipe of the length more than $l_e$ and diameter $d$ connecting two quasi infinite liquid areas (areas of recirculation behind the pipe inlet were omitted for simplification).

The average flow velocity in the pipe amounts to $u$, whereas the shape of velocity distribution is formed at the entrance length $l_e$ obtaining an unchangeable shape, characteristic of laminar or turbulent flow, only behind this length. Therefore, on the length $l_e$ the energy grade line (EGL) drop is descending to become steady behind the entrance length. As can be seen, the minor loss is spread on the entire entrance length $l_e$, which in laminar flow amounts to approximately $0.06Red$ and $l_e \approx 40d$[*] in a turbulent flow. For practical reasons, energetic losses in the conduit are shown in the form of a simple sum of two components: minor losses and friction losses changing real curves EGL and HGL (the hydraulic grade line) into their apparent courses, which were marked with dotted lines in Fig. 1. As it can be seen in the figure, $K$ cannot be well determined based on differential pressure $p_0 - p_i$ measurements in front of the inlet and in the section $]0, l_e[$, especially, when the value of $K$ being measured is as

[*]Some authors give different values, e.g. according to Schlichting [20] $l_e \in [25, 40]d$ (in a turbulent flow).

small as in the investigated case. A method similar to the one, forced by many authors, can be used to determinethe minor losses coefficient of fittings offering a high resistance, e.g. a flow regulating valve. Then, two measurement sections are located close in front of and behind a fitting being investigated and their velocity heads are assumed identical, whereas friction losses are typically omitted. Such assumptions are not acceptable in the investigated case, where $K$ is ca. 0.5 and $f$ is ca. 0.02, and if the measurement is performed in a typical distance of $5d$ behind the inlet*, then friction losses constitute 0.2 of minor losses. It should be emphasized that the subject of the investigations was a flow far more complex than the one shown in Fig. 1. Namely, there is no axial symmetry of flow and recirculation areas are present, which were not accounted for in the figure.

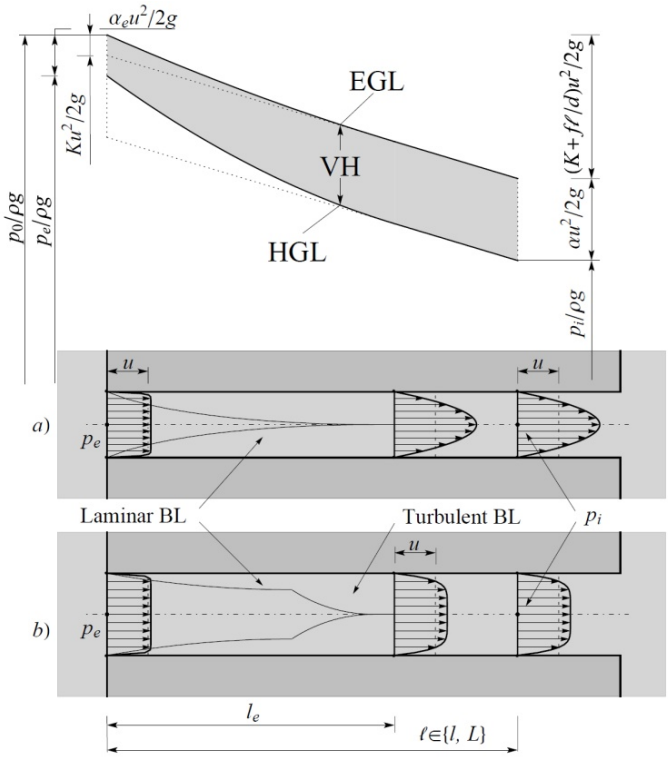


Fig. 1. Laminar (a) and turbulent (b) flows in the entrance of the tube, EGL – the energy grad line, VH – the velocity head, HGL – the hydraulic grade line, BL – the boundary layer, $\alpha$ – the kinetic energy correction factor ($\alpha_e \approx 1$), $l_e$ – the entrance length, $p_k$ ($k \in \{i = 1, 2; 0, e\}$) – the liquid pressure

* Notice that additionally the measurement section may be located beyond a recirculation zone and in the section $]0, l_e[$ the kinetic energy correction factor $\alpha$ is unknown [21].

A similar explanation of the shape of the phenomenon velocity of distribution formation and interpretation of inlet losses are given by White [10] and Szewczyk [13].

The investigations aimed at determining the influence of geometrical shapes most frequently used in engineering practice forming reservoir sections adhering to the inlet of the pipe on its inlet resistance. The investigations covered:

- measurements related to the identification and calibration of model elements, which include: the inner diameter of polypropylene pipes used to produce the throttling pipe, the hydraulic characteristic of a triangular measuring overfall and physicochemical properties of circulating water used for the investigations,
- measurements related to the implementation of the fundamental paper objective, that is: determination of the piezometric pressure heads in hydrometric sections, measurements of water volume flow rates (by means of the overfall) for varying depths of reservoir filling and for different shapes of its inlet section adhering to the throttling pipe and variable heights ($z_0$) and widths ($b$) of the water jets, and finally, measurements of water temperature.

The inner diameter of polypropylene pipeline being investigated was determined by measuring the volume of water filling a pipe section of the known length, obtaining $d$ = (71.0±0.1) mm. The hydraulic characteristic of the triangular measuring overfall (of the angle of π/2 rad) were determined by the volumetric method, establishing its flow coefficient at $\mu$ = 0.600. The physicochemical properties of water used in the investigations were verified at the beginning, in the middle and at the end of investigations, while the composition of circulating water during the test proved to be stable.

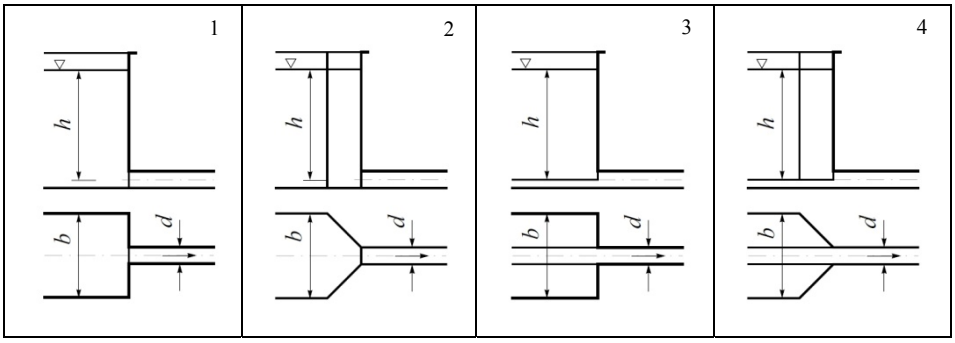


Fig. 2. The shapes of pipe inlets (1–4): vertical cross-sections and horizontal projections ($b/d \in \{1.25, 2.5, 5, 10\}$, $h/d \in \{2.5, 5, 10, 19\}$)

The testing program covered four basic options of geometrical shapes of reservoirs in the section adhering to pipe inlets that is (Fig. 2):

1) a flat wall perpendicular to the throttling pipe axis with sharp-edged inlet, without an invert channel on the reservoir bottom;

2) an inlet to the pipe in the form of guides produced from vertical, flat walls convergent at the angle of $\pi/4$ rad in the throttling pipe direction (sharp-edged), without an invert channel on the reservoir bottom;

3) a flat wall perpendicular to the pipe axis with a sharp-edged inlet and invert channel of the depth of $d/2$ in the reservoir bottom;

4) an inlet to the pipe in the form of guides produced from vertical, flat walls convergent at the angle of $\pi/4$ rad in the pipe direction (sharp-edged) and with an invert channel of the depth of $d/2$ in the reservoir bottom.

Figure 2 shows investigated geometrical shapes for pipe inlets. Each of them includes four suboptions of the reservoir width ($b$) on the outflow to the pipe, that is: $b/d \in \{1.25, 2.5, 5, 10\}$. Whereas, each suboption included four measurement runs of the relative height of reservoir filling: $h/d \in \{2.5, 5, 10, 19\}$. Each run contained at least 10 measurements of the volume flow rates and simultaneous reading out of piezometric pressure heads ($z_i$) and water temperature. The diagram of the testing station used to carry out model tests in question is shown in Fig. 3.

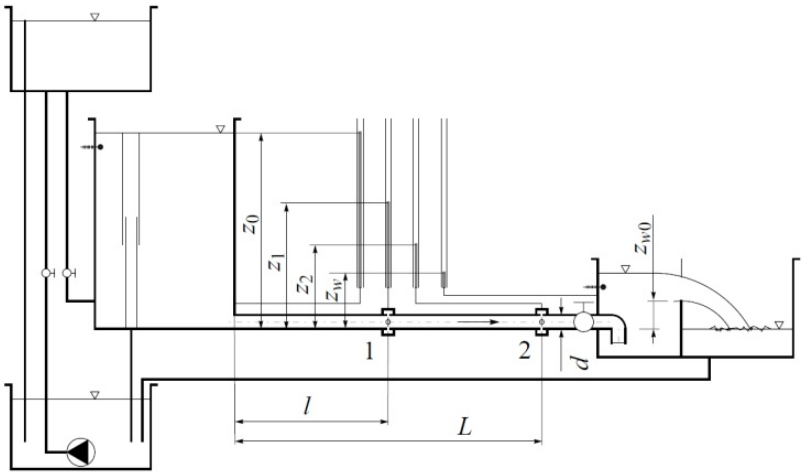


Fig. 3. The testing station (description in the text)

The testing section was produced from connection bell pipes of the mounting lengths of 1.0 m. Two hydrometric sections were placed on the testing pipeline: the first was located in the distance of $l = 60d$, while the other in the distance of $L = 110d$ behind the pipeline inlet. Thus, the turbulent flow was fully developed in the hydrometric sections, which occurs when water flows the distance of approximately $40d$, counting from the pipe inlet. The straight section of the testing pipeline behind the second hydrometric section was of the length of ca. $20d$, which was followed by a ball valve, and then, by the reservoir with a measuring overfall (triangular).

The adjustment of the valve, as well as of other valves shown in Fig. 3, made it possible to set required parameters ($h/d$, $q_V$). The remaining values of quantities necessary to determine the loss coefficients ($f$, $K$) and Reynolds number ($Re$) were read out from piezometers ($z_i$, $i \in \{0, 1, 2, w\}$), and water temperature was measured in two locations shown in Fig. 3. Water was supplied to the piezometers by means of circuit pressure delivery chambers to which pressure signal was provided through 4 piezometric holes ($\phi$3 mm), drilled precisely and symmetrically in the pipe circumference. The obtained volume flow rates were in the range ]1.45, 10.3[ dm$^3$/s, while the water flow velocities were in the range ]0.37, 2.6[ m/s, the temperatures of water were in the range ]7.0, 13.1[ °C thus, the flow was always turbulent, since $Re \in$ ]19, 155[$\times 10^3$.

## 3. RESULTS OF INVESTIGATIONS

### 3.1. THE OUTPUT EQUATIONS FOR FRICTION FACTOR AND MINOR LOSS COEFFICIENT

By writing generalized Bernoulli's equation in relation to the comparative level located on the inlet chamber bottom, set for the first section lying on the water surface in the chamber and for the second cross-section of the water jet flowing through the pipe, the following two equations can be yielded in the form of

$$z_0 = z_i + \alpha\left(\frac{4q_V}{\pi d^2}\right)^2 \frac{1}{2g} + f\frac{\Lambda}{d}\left(\frac{4q_V}{\pi d^2}\right)^2 \frac{1}{2g} + K\left(\frac{4q_V}{\pi d^2}\right)^2 \frac{1}{2g}, \qquad \{i, \Lambda\} \in \{\{1, l\}, \{2, L\}\} \tag{4}$$

which gives the following dependences with regards to $f$ and $K$

$$f = \frac{\pi^2 g d^5 \left(\frac{z_1}{L-l} - \frac{z_2}{L-l}\right)}{8q_V^2} \tag{5}$$

$$K = \frac{\pi^2 g d^4 \left(z_0 - \frac{z_1}{1-\frac{l}{L}} + \frac{z_2}{\frac{L}{l}-1}\right)}{8q_V^2} - \alpha \tag{6}$$

The fact that the flow in Sections 1 and 2 is fully developed was accounted for, thus $\alpha$ is identical there. It follows from Eqs. (5) and (6) that owing to the applied compensatory measurement method the influence of the minor losses on the measured value of the friction factor and the influence of the friction losses on the measured value of the minor loss coefficient can be eliminated. It can be seen from Eq. (6) that

a sufficiently accurate knowledge of the kinetic energy correction factor is very important in the measurement procedure of the coefficient $K$. It should be remembered that the minor loss coefficient has the numerical value of the order of 0.5 in relation to $\alpha > 1.04$, and thus, the assumption of $\alpha = 1$ involves the error of the order of 10% measurement results of the factor $K$.

In the experiment, it can be acknowledged that the pipe is hydraulically smooth, because the empirically obtained dependence of $f(Re)$ diverges insignificantly from the Blasius curve (2). This is illustrated in Fig. 4, which shows the results of the determination of the friction factor $f$ based on thet measurements using Eq. (5). The volume flow rate $q_V$, as in Eqs. (5) and (6), was determined based on equation specifying the liquid flow through the measuring triangular overfall (Fig. 3)

$$q_V = \frac{8}{15}\mu\sqrt{2g(z_w - z_{w0})^5} \tag{7}$$

In Equation (7), $\mu = 0.60$ was taken as the value obtained as a result of the overfall calibration on the testing station presented in the Fig. 3.

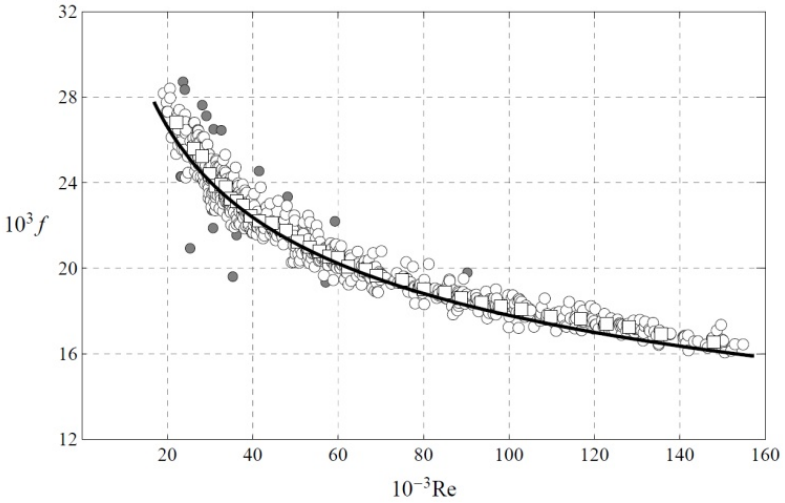


Fig. 4. The dependence $f(Re)$ obtained empirically by the authors (the solid line is the Blasius curve)

In Figure 4, the results of all measurements (the total of 719) are given. They are marked with circles, therewith, the grey circles indicate results recognized as inaccurate – divergent by more than 5% from the mean value (there were 18). The square centers visible in Fig. 4 contain coordinates of mean values of $Re$ and $f$ calculated in 35 subsets of measurement results, which the entire usable set of measurement results was divided into (701 points). The averaging of results makes sense, since there is

a relatively large dispersion of results, which have normal distribution in the subsets. The subsets contained 20 results each (only the last one contained 21 results).

The solid line in Fig. 4 is the Blasius curve and, as can be seen, it lies close to the path set out by the squares. Therefore, the pipe being investigated was deemed hydraulically smooth and the Eq. (3) was employed to determine the kinetic energy correction factor.

### 3.2. RESULTS OF MEASUREMENT OF THE ENTRANCE LOSS COEFFICIENT *K*

The results of measurements conducted for each determined sub-option $b/d \in \{1.25, 2.5, 5, 10\}$ and all measurement runs $h/d \in \{2.5, 5, 10, 19\}$, in each geometric option of the reservoir (that is, for each of four pipe inlet shapes – Figure 2) were properly prepared prior to their marking on the diagrams. Namely, raw results (719) were sorted, while results whose values deviated by more than ±3×(Standard Deviation) from the mean value for a given set were rejected as incredible (41).

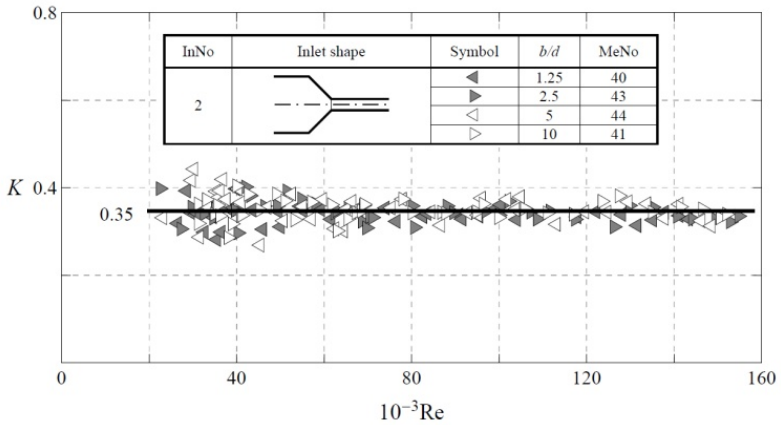


Fig. 5. Results of measurement of the entrance loss coefficient *K* (an example for the pipe inlet No. 2) for $h/d \in \{2.5, 5, 10, 19\}$ and each $b/d \in \{1.25, 2.5, 5, 10\}$ (InNo is the pipe inlet number, while MeNo denotes the number of measurement results)

Thus, results for four measurement runs (*h*/*d*) were presented for the inlet option No. 2, in Fig. 5. Each suboption (for specified *b*/*d*) was marked with a different square subsequent to the rejection of incredible values. The horizontal line is located at the height of the mean value from all 4 measurement runs (the total of MeNo = 168 results). All measurement runs were marked in Fig. 5 by means of layers (a layer of symbols denote a single run). Analyzing the distribution of symbols on the diagram plane, the dependence of *K* on *Re* [14, 15, 22] and the relation of *K* with values *b*/*d*

and $h/d$ could not be found. All symbols are mixed and do not form separate paths, which would mark out 4 different curves. Furthermore, many symbols are not visible, since previous layers were covered with subsequent layers of symbols belonging to subsequent measurement runs. The mean value of the set produced from the sum of measured values of $K$ in all four measurement runs were taken credible in the situation.

The set of $K$ values assigned in such manner to a single pipe inlet shape and sorted by ascending Reynolds numbers was presented in Fig. 6. The figure shows a considerable dispersion of results of single measurements around the mean value of the entire 168-element set. However, the confidence interval is relatively narrow ±0.01 in relation to the mean 0.35. This can be explained by the fact that the value set is numerous and has normal distribution. Thus, the uncertainty of the $K$ value, and thus the confidence interval were calculated based on the mean square error of the arithmetic mean with the probability of 95%.

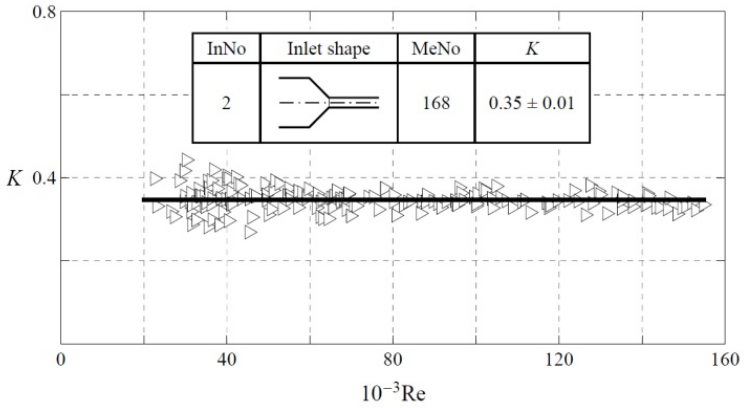


Fig. 6. Complete results of measurements of the coefficient $K$ for the pipe inlet No. 2

Subsequent results of measurements assigned to other investigated inlet shapes (Nos. 1, 3 and 4 cf. Fig. 2) are given in Table 1.

It follows from the cumulative juxtaposition of the results of investigation (Table 1) that the invert channel (on the reservoir bottom) and the guides (vertical flat converging toward the pipe) have the influence on the value of the entrance loss coefficient $K$, that is:

- the presence of guides decreases the value of $K$ by 16–19%,
- the presence of invert channel increases the value of $K$ by 22–24%,
- the lowest value of $K = 0.35$ exists when the guides are located in the tank without invert channel on its bottom,

• the highest value of $K = 0.55$ exists when the tank has not a guides but the invert channel is located on its bottom.

Table 1

The cumulative juxtaposition of results of measurement of the entrance loss coefficient $K$ of all investigated pipe inlets

| InNo | Inlet shape | $K$ | MeNo | $10^{-3}Re$ |
|---|---|---|---|---|
| 1 | 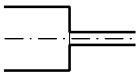 | 0.43 ± 0.01 | 176 | ]20, 155[ |
| 2 | 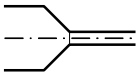 | 0.35 ± 0.01 | 168 | ]22, 155[ |
| 3 | 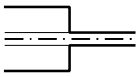 | 0.55 ± 0.01 | 164 | ]20, 135[ |
| 4 | 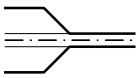 | 0.46 ± 0.01 | 170 | ]19, 135[ |

It was found that an invert channel of the depth $d/2$, located on the tank bottom, increases the values of the coefficient $K$, whereas guides, produced from vertical, flat walls converging at the angle $\pi/4$ rad towards the pipe, decrease the values of $K$ in relation to inlets without such elements. This can be explained by the fact that a liquid inlet to the pipe with an invert channel is hindered with respect to an inlet without an invert channel. Namely, the bottom half of a pipe flow section is only supplied by liquid from an invert channel, while the top half draws liquid from a quasi quarter-space. This results in an increase of the energetic loss in the pipe inlet. Whereas, the guides ease the pipe inlet, thus reducing recirculation areas constituting the source of relation to a inlet without and invert channel, where the space from which liquid flows to a energetic losses. Hence, losses in a supply system containing guides are lower in comparison to a system without guides.

## 4. CONCLUSIONS

The subject matter literature does not provide the influence of a geometrical shape of a reservoir section adhering directly to a pipe on its entrance loss, which the pipe is placed on the reservoir bottom. The paper presents results of investigation of the entrance losses coefficients for four, most frequently used in practice, geometrical sec-

tions of pipe inlets: a sharp-edged inlet from a wall perpendicular to the pipe axis, an inlet with guides produced from two vertical wall deviated from the pipe axis at the angle of $\pi/4$ rad, therewith, both cases may include (or not) invert channels of the depth of $d/2$. Sufficiently accurate results were obtainrd owing to the application of the measurement compensatory method (the influence of the friction losses on the measured value of the minor loss coefficient was eliminated) and the consideration of the kinetic-energy correction factor.

It was found that the invert channel of the depth of $d/2$ located on the reservoir bottom produces the increase of the value of the coefficient $K$ by 22–24%, whereas the guides built from flat, vertical walls divergent at the angle of $\pi/4$ rad towards the throttling pipe decrease the value of $K$ by 16–19% with respect to the inlets without such elements. The values of the minor loss coefficients, that were measured empirically, can be applied in the process of dimensioning of many hydraulic systems.

ACKNOWLEDGEMENTS

All calculations, figures and tables were carried out by means of *Mathematica* 8 by S. Wolfram, where own algorithms were prepared and ready-made calculation packets were applied.

SYMBOLS

$b$ – width of a reservoir
$d$ – diameter (inner) of the pipe
$f$ – Darcy's friction factor
$g$ – acceleration due to gravity
$h$ – reservoir filling
$\Delta h_{ld}$ – energy loss head (pipeline of the diameter $d$ and length $l$)
$k$ – pipeline roughness (mean height of wall roughness)
$K$ – minor loss coefficient
$L$ $l$ – length of a pipeline section
$Re$ – Reynolds number
$q_V$ – volume flow rate
$u$ – liquid average velocity
$z_i$ – piezometric pressure head in the $i$th hydrometric section
$\Delta z$ – pressure loss head
$\alpha$ – kinetic energy correction factor
$\mu$ – discharge coefficient

REFERENCES

[1] DVWK-ATV-A 111, *Guidelines for the Hydraulic Dimensioning of Drainage Systems*, Gfa, Hennef, 1994 (in German).
[2] HAGER W.H., *Wastewater Hydraulics. Theory and Practice*, Springer, Berlin, 1994 (in German).

[3] DEL GIUDICE G., HAGER W.H., J. Irrig. Drain Eng. ASCE, 1999, 125 (5), 298.
[4] KOTOWSKI A., Gas-Wasserfach, 2001, 142 (12), 843.
[5] KOTOWSKI A., SZEWCZYK H., Chem. Proc. Eng., 2008, 29 (4), 1037.
[6] KOTOWSKI A., WOJTOWICZ P., Environ. Prot. Eng., 2007, 33 (4), 41.
[7] JEŻOWIECKA-KABSCH K., SZEWCZYK H., Fluid Mechanics, Ofic. Wyd. PWr., Wrocław, 2001 (in Polish).
[8] SWAMEE P.K., SWAMEE N., J. Hydraul. Res. IAHR, 2007, 45 (6), 841.
[9] KOTOWSKI A., WÓJTOWICZ P., Environ. Prot. Eng., 2004, 30 (3), 71.
[10] WHITE F.M., *Fluid Mechanics*, McGraw-Hill, New York, 2009.
[11] AFZAL N., SEENA A., BUSHRA A., J. Hydraul. Eng. ASCE, 2007, 133 (9), 1080.
[12] IDELCHIK I. E., *Handbook of Hydraulic Resistance*, 3rd Ed., CRC Press, Boca Raton, 1994.
[13] SZEWCZYK H., Chem. Proc. Eng., 2008, 29 (4), 979.
[14] STRZELECKA K., JEŻOWIECKA-KABSCH K., Ochr. Środ., 2010, 32 (1), 33.
[15] WĘDRYCHOWICZ W., JEŻOWIECKA-KABSCH K., GRYGORIEV A., STRZELECKA K. , Ochr. Środ., 2006, 28 (3), 51.
[16] KALLWASS G.J., *Hydraulic Calculation of Stormwater Overflows*, Diss., Tech. Hochschule, Karlsruhe, 1964 (in German).
[17] KALLWASS G.J., Gas-Wasserfach, 1968, 109 (6), 150.
[18] IMHOFF K., IMHOFF K. R., *Handbook of Urban Drainage*, R. Oldenbourg Verlag, München, 1993 (in German).
[19] TGL No. 42375, *Stormwater Overflows*, Berlin, 1984 (in German).
[20] SCHLICHTING H., *Boundary Layer Theory*, McGraw-Hill, New York, 1987.
[21] SZEWCZYK H., Chem. Proc. Eng., 2008, 29 (1), 271.
[22] STRZELECKA K., JEŻOWIECKA-KABSCH K., Ochr. Środ., 2008, 30 (2), 29.

Environment Protection Engineering

Vol. 37 2011 No. 4

EWELINA STASZEWSKA*, MAŁGORZATA PAWŁOWSKA*

# CHARACTERISTICS OF EMISSIONS FROM MUNICIPAL WASTE LANDFILLS

Biogas is formed by the methanogenic anaerobic bacteria which decompose organic substances. Processes occurring during fermentation of methane involve conversion of organic compounds with various oxidation levels to gaseous final products, mainly methane and carbon dioxide. The process of biogas formation involves the following stages: hydrolysis, acidogenesis, acetogenesis and methanogenesis. The composition and quantity of biogas depend mainly on the chemical composition of organic compounds being fermented, maintenance of fermentation conditions and substrate residence time in the reactor. Biogas generated in the fermentation process is utilised mainly for generation of power and heat.

## 1. INTRODUCTION

In accordance with the Intergovernmental Panel of Climate Change (IPCC) one of the most important threats to wellbeing of human civilization is climate warming due to anthropogenic emission of greenhouse gases. A mitigation measure which has to be taken requires multidimensional approach based on sustainable development concept [1, 2].

Sustainable development is a pattern of resource use that aims to meet human needs while preserving the environment so that these needs can be met not only in the present, but also for generations to come. The term was used by the Brundtland Commission who defined sustainable development as the one that *meets the needs of the present without compromising the ability of future generations to meet their own needs* [3]. To ensure the survival of human civilisation, it is necessary to introduce considerable changes in almost all its aspects: resource management [4], world economy [4–6], pattern of manufacturing of goods [7, 8] and lifestyle [9, 10].

*Lublin University of Technology, Faculty of Environmental Engineering, ul. Nadbystrzycka 40B, 20-618 Lublin, Poland, corresponding author E. Staszewska, e-mail: e.staszewska@wis.pol.lublin.pl

One of particular problems is climate change which is an inevitable and urgent global challenge with long-term implications for the sustainable development of all countries. Warming of climactic system is expected to impact the availability of basic necessities like freshwater, food security, and energy. The links between climate change and sustainable development are strong. While climate change has no boundaries, poor and developing countries, particularly those low developed, will be among those most adversely affected and least able to cope with the anticipated shocks to their social, economic and natural systems. The Earth's average surface temperature has increased by 0.76 °C since 1850. The IPCC projects that, without further action to reduce greenhouse gas emissions, the global average surface temperature is likely to rise by a further 1.8–4.0 °C this century. Even the lower end of this range would take the temperature increase since pre-industrial times above 2 °C, the threshold beyond which irreversible and possibly catastrophic changes become far more likely.

Human activities that contribute to climate change include in particular the burning of fossil fuels, agriculture and land-use changes like deforestation. These cause emissions of carbon dioxide ($CO_2$), the main gas responsible for climate change, as well as of other greenhouse gases (GHG). These gases remain in the atmosphere for many decades and trap heat from the sun in the same way as the glass of a greenhouse. To bring climate change to a halt, global greenhouse gas emissions must be reduced significantly. Therefore, there is urgent need to decrease emission of greenhouse gases to mitigate climate warming. The most important is reduction of $CO_2$ emission from energy sector.

The only alternatives to fossil fuels, presently accounting for over 80% of global primary energy, are nuclear energy and various forms of renewable energy. Nuclear energy today provides less that 6% of world energy, and official forecasts do not see its share increasing much in coming decades, mainly because of its high costs and political problems. Other alternatives such as lowering atmospheric $CO_2$ emissions by carbon capture and storage from fossil fuel use, or capturing $CO_2$ directly from the atmosphere would either have limited global impact or entail heavy energy costs, if implemented at the needed scale [11]. Like geoengineering, these approaches do not address fossil fuel depletion. Many researchers thus argue that removable energy will have to replace fossil fuels as the dominant global energy source in the coming decades.

However, carbon dioxide is not the only trace gas which is responsible for in climate change. Methane is another one which some have estimated to be over a third as much as that of carbon dioxide. Gas from natural sources, cows and other ruminants, and natural sources where natural decomposition by fermentation produces methane, all contribute to the blanketing which is the cause of the greenhouse effect. However, human activity is also responsible for a lot of methane gas production and Municipal Solid Waste Landfills (MSWL) have in turn been recognized to be a source of greenhouse gases which is contributing to the atmospheric build-up.

However, the magnitude of the landfill gas contribution to the greenhouse effect have been uncertain, and the subject of some debate. But, as time goes on, the evidence

becomes stronger, and the fact of climate change is now accepted by the vast majority of scientists working in this field. Thus, it appears that landfill gases make an important net contribution to the greenhouse phenomenon. Therefore better understanding of landfill gases formation may help to decrease their emissions from landfill sites.

Table 1

Composition of gases released from waste landfills (after [18–20])

| Main components | | | |
|---|---|---|---|
| Component | Typical value [vol. %]) | Component | Typical value [vol. %] |
| Methane | 45–60 | Ammonia | 0.1–1 |
| Carbon dioxide | 40–60 | NMOCs | 0.01–0.6 |
| Nitrogen | 2–5 | Sulphides | 0–1 |
| Oxygen | 0.1–1 | Hydrogen | 0–0.2 |
| Trace components | | | |
| Component | Concentration range [mg/m$^3$] | Component | Concentration range [mg/m$^3$] |
| Alkanes | | Alkenes | |
| Propane | < 0.1–1.0 | Butadiene | < 0.1–20 |
| Butanes | < 0.1–90 | Butenes | < 0.1–90 |
| Pentanes | 1.8–105 | Pentadienes | < 0.1–0.4 |
| Cycloalkanes | | Cycloalkenes | |
| Cyclopentane | < 0.2–6.7 | Limonene | 2.1–240 |
| Cyclohexane | < 0.5–103 | Other terpenes | 14.3–311 |
| Methylcyclopentane | < 0.1–79 | Methene | <0.1–29 |
| Halogenated compounds | | Aromatic hydrocarbons | |
| Chloromethane | < 0.1–1 | Benzene | 0.4–114 |
| Chlorofluoromethane | < 0.1–10 | Styrene | < 0.1–7 |
| Dichloromethane | < 0.1–190 | Xylenes | 34–470 |
| Chloroform | < 0.1–0.8 | | |
| Chlorobenzene | < 0.1–2.1 | | |
| Esters | | Organosulphur compounds | |
| Ethyl acetate | < 0.1–64 | Carbonyl sulphide | < 0.1–1 |
| Methyl butanoate | < 0.1–15 | Carbon disulphide | < 0.1–2 |
| Ethyl propionate | < 0.1–136 | Methanethiol | < 0.1–87 |

A mixture of organic and inorganic wastes is disposed at a landfill with varying humidity and much heterogeneity. Approximately 75% of municipal waste is biodegradable organic material. Substances in waste have various decomposition rates. Food waste is most readily degraded. Garden waste forms a group with medium half-life (5 years). Paper, cardboard, wood and textile waste decomposes slowly (half-life of 15 years), while plastics and rubber are not degraded at all [12]. A number of factors affect the quantity of gases formed at landfills and their composition, such as

waste type and age, quantity and type of organic components, waste humidity and temperature. Landfill gases form in microbiological processes, as a result of evaporation or in chemical reactions [13].

The main components of landfill gases are methane and carbon dioxide. Methane makes up ca. 45–60 vol. %, while carbon dioxide 40–60 vol. %. Landfill gases also contain small amounts of nitrogen, oxygen, ammonia, sulphides, hydrogen, carbon monoxide and less than 1% of non-methane organic components (NMOC), also called non-methane hydrocarbons (NMHCs) (Table1). Some of them have strong, pungent odour, such as hydrogen sulphide. Non-methane organic components (NMOC), such as volatile organic compounds (VOC) and hazardous air pollutants (HAP), may react under the influence of sunlight and form smog. More then 200 NMOC have been identified [13-15]. Among the landfill gases, carcinogenic substances such as benzene chloride and vinyl chloride may be harmful to the life of the staff and residents of neighbouring areas, while chlorofluorocarbons (CFCs) or hydrochlorofluorocarbons (HCFCs) contribute to ozone layer depletion and climate change [15–17].

## 2. MECHANISM OF BIOGAS FORMATION

Anaerobic fermentation is widespread in nature, occurring for example in peat bogs, on sea bottom, in manure and at landfills. Organic matter is converted into biogas [21].

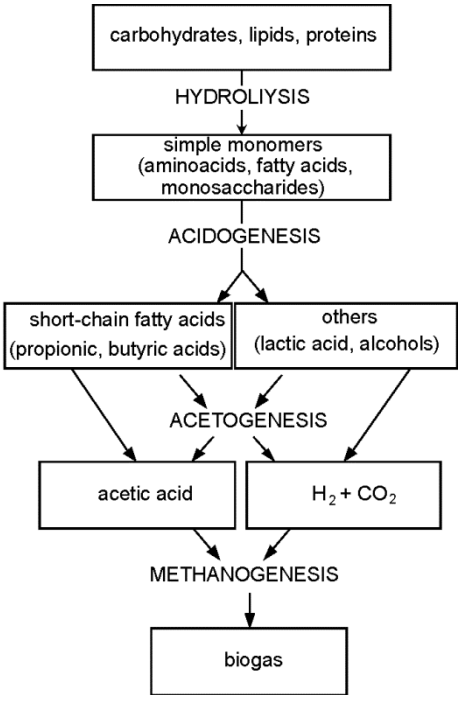


Fig. 1. Scheme of the process of biogas formation (after [22])

Furthermore, certain quantities of fermented biomass form and heat is emitted. The process of biogas formation (Fig. 1) involves such stages as hydrolysis, acidogenesis, acetogenesis and methanogenesis.

### 2.1. STAGE OF HYDROLYSIS

This stage involves the decomposition of insoluble organic compounds (carbohydrates, proteins, fats). Proteins hydrolyse to amino acids, polysaccharides (including cellulose) to simple sugars, and fats to polyhydroxyalcohols and fatty acids. The quantity of hardly degradable polymers such as cellulose, lignins, non-degradable fats, proteins and carbohydrates is considered the hydrolysis rate limiting step. In the anaerobic fermentation of solid waste as little as 50% of organic substances are decomposed. The rest of complex organic substances are not biodegraded due to the lack of specific depolymerisation enzymes resulting from the absence of specific organisms which secrete various extracellular enzymes [23, 24].

### 2.2. ACIDOGENIC STAGE (ACIDOGENESIS)

In this stage, facultative acidogenic bacteria convert chemical substances dissolved in water, including hydrolysis products, to short-chained organic acids ($C_1$–$C_6$) (formic, acetic, propionic, butyric, valeric acid), alcohols (methanol, ethanol), aldehydes and carbon dioxide and hydrogen.

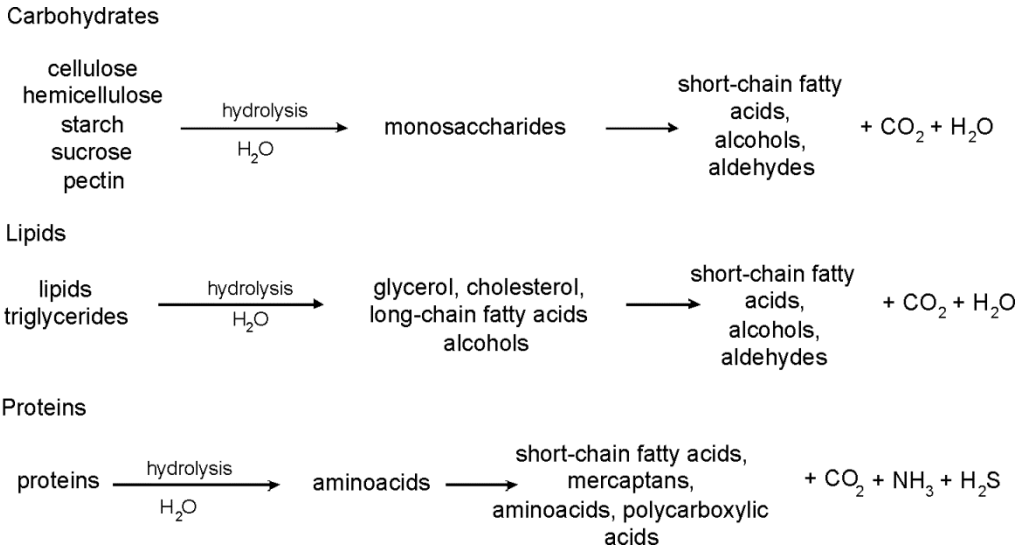


Fig. 2. Scheme of degradation of respective groups of compounds during acidogenesis (after [25])

Acidogenic bacteria include for example: *Clostridium*, *Bacteroides*, *Ruminococcus*, *Butyrylvibrio*, *Escherichia coli*, *Bacillus*, *Bifidobacterium*. Bacteria involved in acidic fermentation are obligate or facultative anaerobes. Considering the classification of substrates with respect to their structure, the degradation of respective groups of compounds has been shown in Fig. 2.

### 2.3. ACETOGENIC STAGE (ACETOGENESIS)

During acetogenesis, ethanol and volatile fatty acids ($C_3$–$C_6$) are converted by acetogenic bacteria to $CO_2$ and $H_2$. For example, the decomposition of propionic acid, butyric acid and ethanol to acetic acid may involve the following reactions:

$$CH_3CH_2COO^- + 3H_2O \rightarrow CH_3COO^- + H^+ + HCO_3^- + 3H_2$$

$$CH_3CH_2CH_2COO^- + 2H_2O \rightarrow 2CH_3COO^- + H^+ + 2H_2$$

$$CH_3CH_2OH + H_2O \rightarrow CH_3COO^- + H^+ + 2H_2$$

The reactions occur only if hydrogen is removed from the system and its partial pressure is maintained at a low level. Therefore, acetogenesis occurs only with the syntrophy* of acetogenic organisms with hydrogen-consuming methanogenic organisms. Hydrogen may be used in the formation of acetic acid from carbon dioxide and hydrogen:

$$2HCO_3^- + H^+ + 4H_2 \rightarrow CH_3COO^- + 4H_2$$

or at the methanogenesis stage. Acetogenesis determines biogas formation efficiency. Reactions of higher organic acids at this stage contribute to approximately. 25% of acetate and 11% of hydrogen generated during waste fermentation. The following genera of acetogenic bacteria are most widespread: *Syntrophobacter*, *Syntrophomona* [22, 23].

### 2.4. METHANOGENIC STAGE

Methanogenic organisms form the last element of the anaerobic food chain which, as discussed before, starts with polysaccharides (cellulose, starch), proteins and lipids and involves fermentation bacteria: 1) bacteria responsible for cellulose fermentation to succinate, propionate, butyrate, lactate, acetate, alcohols, $CO_2$ and $H_2$, 2) acetogenic bacteria responsible for the fermentation of the former to acetate, formate, $CO_2$ and $H_2$. These products, acetates and alcohols are substrates for methanogenic organisms. Methane forms from the following substrates:

*Syntrophy is the symbiosis of organisms, of which one generates hydrogen and the other consumes it.

- acetic acid (almost 70%)

$$CH_3COO^- + H_2O \rightarrow CH_4 + HCO_3^-$$

- $H_2$, $CO_2$ and formate

$$HCO_3^- + 4H_2 + H^+ \rightarrow CH_4 + 3H_2O$$

$$4HCOO^- + H^+ + H_2O \rightarrow CH_4 + 3\ HCO_3^-$$

- methanol, methylamine or dimethyl sulphide

$$4CH_3OH \rightarrow 3CH_4 + CO_2 + 2H_2O$$

$$4CH_3NH_2 + 4H^+ + 2H_2O \rightarrow 3CH_4 + CO_2 + 4NH_4^+$$

$$2(CH_3)_2NH + 2H^+ + 2H_2O \rightarrow 3CH_4 + CO_2 + 2NH_4^+$$

$$2(CH_3)_2S + 2H_2O \rightarrow 3CH_4 + CO_2 + 2H_2O$$

It was found based on stoichiometric relationships that almost 70% of methane forms in the reduction of acetates, even though a few bacterial species only are able to produce methane from acetates, while almost all known methanogenic bacteria can product methane from hydrogen and carbon dioxide [22, 23].

Biochemical transformations of $CO_2$ and $H_2$ to methane and acetate to methane and $CO_2$ occur with various enzymes and prosthetic groups, found so far in methanogenic organisms only. The probable pathways for methane formation from acetate and from hydrogen and carbon dioxide are shown in Fig. 3 [22, 26].

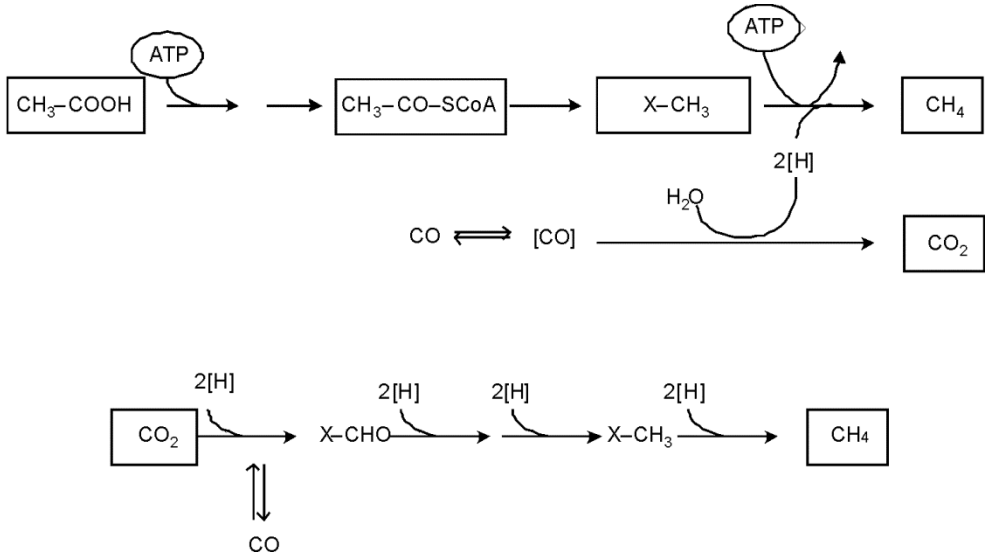


Fig. 3. Probable pathways for methane formation (based on [26])

## 3. CHARACTERISTICS OF MICROORGANISMS

Three groups of microorganisms contribute to biogas formation: acidogenic, acetogenic and methanogenic bacteria. The first two stages are dominated by both obligate anaerobes (*Bacillus*, *Pseudomonas*, *Clostridium*, *Bifidobacterium*) and facultative anaerobes (*Streptococcus*, *Enterobacterium*). Some acidogenic bacteria are obligate anaerobes (*Aerobacter*, *Alcaligenes*, *Clostridium*, *Escherichia*, *Lactobacillus*, *Micrococcus*, *Flavobacterium*). The growth rates of these bacteria are from 5 h in the presence of carbohydrates to 72 h during fat degradation. The optimum conditions for the growth of acidogenic microorganisms are pH of ca. 6 and temperature of ca. 30 °C. Products of the acidogenic stage (butyric and propionic acids and alcohols) are converted by acetogenic bacteria (*Syntrophomonas* and *Syntrophobacter* sp.). The acetates and hydrogen which form can be used by methanogenic bacteria. The latter may grow only if hydrogen is consumed by hydrogen producing organisms. The cooperation between hydrogen producing and hydrogen consuming bacteria is called interspecies hydrogen transfer. Hydrogen is also removed by homoacetogenic bacteria in the process of acetate formation from $CO_2$ and $H_2$. However, the process does not occur in typical fermentation conditions.

Table 2

Selected species of methanogenic bacteria (according to [23])

| Genus | Species |
|---|---|
| *Methanobacterium* | *M. bryantii*<br>*M. formicicum*<br>*M. thermoautotrophicum* |
| *Methanobrevibacter* | *M. arboriphilus*<br>*M. ruminantium*<br>*M. smithi* |
| *Methanococcus* | *M. vannielii*<br>*M. volta* |
| *Methanogenium* | *M. wariaci*<br>*M. marisnigri* |
| *Methanomicrobium* | *M. mobile* |
| *Methanospirillum* | *M. hungatei* |
| *Methanosarcina* | *M. barkeri* |
| *Methanotrix* | *M. soehngenii* |

Methanogenic bacteria are all *Archaeobacteriales*. They are obligate anaerobes with any air quantities being lethal. Approximately 40 strains of methanogenic bacteria have been isolated. They are divided into two groups: acetic acid consumers and $H_2/CO_2$ consumers. Methanogenic bacteria have a form of rods (*Methanobacterium*),

spirals (*Methanospirillum*) or coccidia (*Methanococcus*, *Methanosarcina*). Optimum temperature for methanogenesis is in a range of 35–45 °C and optimum pH is 7. Selected species of methanogenic bacteria are presented in Table 2 [23, 26].

Acidic fermentation products can also be consumed by other groups of microorganisms such as sulphate or nitrate reducing bacteria. The presence of the first group of bacteria leads to the presence of hydrogen sulphide in the biogas, while the other contributes to the presence of ammonia.

## 4. HYDROGEN SULPHIDE FORMATION

Due to the presence of hydrogen sulphide, landfill gases have a peculiar odour of rotten eggs. The unpleasant odour is perceptible even at very low concentrations. Some people with a very low odour perception level can detect sulphide at concentrations as low as 0.5 ppb). Hydrogen sulphide forms during anaerobic waste degradation from sulphur containing amino acids or due to reduction of inorganic sulphur containing compounds. Dissimilation sulphate reduction is a process in which bacteria use sulphates as electron acceptors in oxidation of organic matter. Bacteria of genera *Desulfovibrio* and *Desulfotomaculum* are classified as sulphate reducing bacteria (SRB).

Hydrogen sulphide is usually the first sulphur product of bacterial degradation of sulphur containing organic compounds. Part of the hydrogen sulphide formed passes to biogas; however, most is dissolved in twaters as $H_2S_{(aq)}$ or $HS^-$. These forms are in equilibrium with $H_2S_{(g)}$ [27].

## 5. AMMONIA FORMATION

Proteins are the chief source of ammonia nitrogen. The process of conversion of organic to inorganic nitrogen by heterotrophic bacteria is called ammonification. It is a two-stage process which involves hydrolysis of enzymatic protein to amino acids by aerobic and anaerobic microorganisms, followed by deamination and fatty acid fermentation leading to the formation of carbon dioxide, ammonia nitrogen and volatile fatty acids. During deamination (Fig. 4) amino groups are released and the form ammonia or ammonium ions.

Ammonia is not a greenhouse gas and, therefore, it is not so harmful to the environment as methane. However, exposure to the gas may lead to certain adverse health effects. Ammonia has pungent odour and may be irritant to the respiratory system. In addition, ammonia may dissolve in the skin protective layer and form ammonium hydroxide, a corrosive substance which causes skin irritation [28].

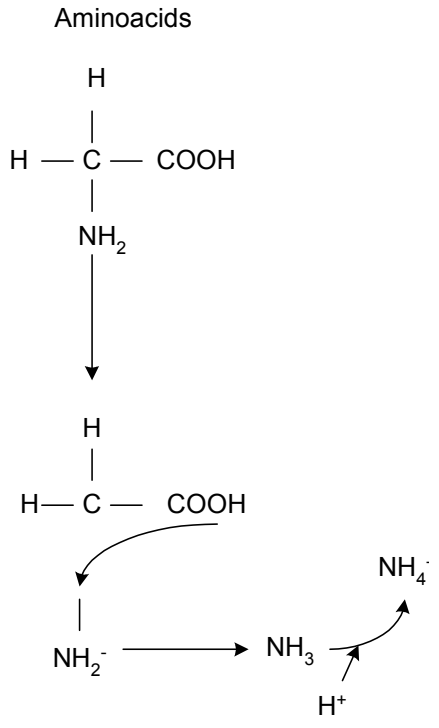


Fig. 4. Deamination process [28]

## 6. SUMMARY

The quantity of landfill gases depends on the properties of waste (composition and age) and multiple environmental factors (oxygen content, humidity, temperature). Higher content of organic waste at a landfill leads to the increased generation of gases, such as carbon dioxide, methane, nitrogen or hydrogen sulphide, by bacteria responsible for degradation, while higher content of chemical waste contributes to the formation of NMOCs due to evaporation or chemical reactions.

More gases are released from waste stored for less than 10 years as a result of bacterial degradation, evaporation and chemical reactions than from that stored for more than 10 years. The highest emission of gases from landfills occurs 5–7 years after the start of storage.

Bacteria can produce methane only in anaerobic conditions. The higher the oxygen content, the longer waste is decomposed by aerobic bacteria at the first stage. If waste is loosely packed, better oxygen accessibility is ensured and, consequently, aerobic bacteria live longer and produce carbon dioxide and water for a longer period. If waste is compacted, anaerobic bacteria which produce methane grow more rapidly, to be later replaced by aerobic bacteria.

More than 40% humidity (based on wet waste matter) contributes to more rapid gas release from landfills. This is caused by the favourable effect of humidity on bacterial growth and transport of nutrients throughout the landfill.

High temperature increases bacterial activity which, in effect, leads to higher emissions of gases from landfills. Lower temperatures reduce bacterial activity. Due to the heat emitted during bacterial degradation processes, landfill temperatures are 25–45 °C. It was found that the quantity of NMOCs being released doubles with each 8 °C temperature increase [29, 30].

## REFERENCES


[1] UDO V., PAWŁOWSKI A., Probl. Ekorozw., 2011, 6 (1), 33.
[2] VENKATESH G., Probl. Ekorozw., 2010, 5 (2), 29.
[3] CIACH R., KARPYN H., PIĄTKOWSKA M., Environ Prot. Eng, 2006,32(1), 5.
[4] HOEDL E., Probl. Ekorozw., 2011, 6 (1), 11.
[5] KRONENBERG J., IIDA N., Probl. Ekorozw., 2011, 6 (1), 67.
[6] HUETING R., PROBL. EKOROZW., 2011, 6 (1), 31.
[7] PAWŁOWSKI L., Probl. Ekorozw., 2011, 6 (1), 59.
[8] DASGUPTA P., TANEJA N., Probl. Ekorozw., 2011, 6 (1), 65.
[9] KRAS E., Probl. Ekorozw., 2011, 6 (1), 11.
[10] PIĄTEK Z., Probl. Ekorozw., 2011, 6 (1), 83.
[11] KUJAWSKI O., Environ. Prot. Eng., 2009, 35(3), 27.
[12] LEWICKI R., *Monitoring of Landfill Ga*s, OBREM, Łódź, 1991.
[13] EPA, U.S. Environmental Protection Agency, *Frequently Asked Questions About Landfill Gas and How It Affects Public Health, Safety, and the Environment*, 2008.
[14] ABUSHAMMALA M.F.M., BASRI N.E.A., KADHUM A.A.H., Eur. J. Sci. Res., 2009, 30 (3), 427.
[15] SCHEUTZ C., BOGNER J., CHANTON J.P., BLAKE D., MORCET M., ARAN, C., KJELDSEN, P., Waste Manage., 2008, 28 (10), 1982.
[16] MOLINA M., ROWLAND F.S., Nature, 1974, 249 (5460), 810.
[17] NIKIEMA J., BIBEAU L., LAVOIE J., BRZEZINSKI R., VIGNEUX J., HEITZ, M., Chem. Eng. J., 2005, 113 (2–3), 111.
[18] EPA, U.S. Environmental Protection Agency, *Compilation of Air Pollutant Emissions Factors, AP-42*, *Vol. 1. Stationary Point and Area Sources*, *Sect. 2.4. Municipal Solid Waste Landfill*s, 5th Ed., 1995.
[19] TCHOBANOGLOUS G., THEISEN H., VIGIL S., *Integrated Solid Waste Management, Engineering Principles and Management Issues*, McGraw-Hill, New York, 1993.
[20] WILLIAMS P.T., *Waste Treatment and Disposal*, Wiley, Chichester, 2005.
[21] SZENTGYÖRGYI E., NEMESTÓTHY N., BÉLAFI-BAKÓ K., Environ Prot. Eng., 2010, 36 (4), 117.
[22] GŁODEK E., KALINOWSKI W., JANECKA L., WERSZLER A., GARUS, T., KOŚCIANOWSKI J., *Acquisition and use of agricultural biogas energy*, Paperwork under the project No. Z/2.16/II/2.6/16/06, Opole Centre for Transfer of Innovation in the field of Building Materials and Renewable Energy, 2007.
[23] JĘDRCZAK A., *Biological Treatment of Waste*, PWN, Warsaw, 2007 (in Polish).
[24] BHATTACHARYYA J.K., KUMAR S., DEVOTTA S., Waste Manage., 2008, 28 (1), 164.
[25] JANOSZ-RAJCZYK M., *The Selected Unit Processes in Environmental Engineering*, Wyd. Politechniki Częstochowskiej, Częstochowa, 2004.

[26] SCHLEGEL H.G., *General Microbiology*, PWN, Warsaw, 2003 (in Polish).
[27] ERSES A.S., ONAY T.T., J. Hazardous Mater., 2002, B99, 159.
[28] BERGE N.D., REINHART D.R., Crit. Rev. Environ. Sci. Techn., 2005, 35 (4), 365.
[29] CRAWFORD J.F., SMITH P.G., *Landfill Technology*, Butterworths, London, 1985.
[30] EPA, U.S. Environmental Protection Agency, *Solid waste disposal facility criteria. Technical manua*, EPA 530-R-93-017, 1993.

Environment Protection Engineering

Vol. 37 2011 No. 4

JADWIGA KRÓLIKOWSKA*

# DAMAGE EVALUATION OF A TOWN'S SEWAGE SYSTEM IN SOUTHERN POLAND BY THE PRELIMINARY HAZARD ANALYSIS METHOD

In the paper, the technical risk has been evaluated for the sewage network of a city in Southern Poland. The basis for calculations were field studies concerning operation of the said network, with the focus on technical data (network type, length, materials, size) and the failure rate information (type and duration of failure, unwanted event frequency). A two-dimensional matrix for failure risk in the pipelines was prepared with consideration to the type of pipeline and the material, as well as a risk map for pipeline malfunction. Obviously, the number of factors may be extended. In order to perform such analyses and add new factors, an appropriate database is needed, while in the case of sewage systems there is still little data collected. The evaluated risk of failure for the studied network was discovered to be in the tolerated and controlled-risk groups. The matrices and technical risk maps can prove to be useful in the process of optimizing the operation of the sewage network, e.g. in planning and executing repair works.

## 1. INTRODUCTION

Sewerage systems can pose a potential danger to the natural environment, the system's users and their immediate surroundings. Analysis of these systems should include evaluation both of the system's functional reliability as well as its safety. Increasing breakdowns, often with catastrophic consequences and external operating conditions impose such an approach in the evaluation and management of these systems.

The evaluation of functional reliability usually boils down to the question of the failure frequency and the removal of the failure's cause. Reliability generates system safety, but does not directly define its value. Expanding studies into functional reliability by incorporating research into the impact of failures on the environment and surroundings, including the community leads us to safety [1, 2]. Thus, safety, viewed

*Tadeusz Kościuszko Cracow University of Technology, Institute of Water Supply and Environmental Protection, ul. Warszawska 24, 31-155 Cracow, Poland, e-mail: j.kapcia@upcpoczta.pl

from an engineering perspective, i.e. technological safety, replaces reliability. Safety (reliability of safety) on a macro scale, in the scope of a sewerage system, can be defined by analogy to water supply systems [3–6] as a state of sewage management which allows collecting, removal and treatment of both current and forecast volumes of domestic (communal) sewage and rainwater, keeping to the requirements of sanitary regulations, environmental protection and public order. The following are directly connected to safety:

- undesirable events,
- dangers,
- losses.

Undesirable events are associated with the unreliability of the system's safety, posing threats to the assets which translates into losses due to its negative consequences. These losses may be financial, human, ecological or emotional. Assuming that failures within gravitational sewerage systems are difficult to detect, the losses borne by the natural environment (ecological losses) may be significant and therefore should not be excluded from the safety analysis. Undesirable events generally relate to individual components of a sewerage system, i.e. to pipes, pumps, manholes, etc. but they can also affect entire subsystems, e.g. sewage drainage or sewage treatment subsystems. Superimposing multiple failures, the so-called domino effect, may result in total system failure. Risk is often used to determine the level of safety. It is intuitively seen as opposing safety and defines the probability of a threat with its associated losses.

Failures in sewerage systems cannot be entirely eliminated. These systems are extensive, comprising many separate parts grouped to form subsystems and systems. There is a dependence between the devices and structures embracing the system which is a result of their capability to process the sewage by volume and quality over time and distance, qualified by health, environmental and economic issues. During their operation, sewerage systems are exposed to a number of adverse factors, most of which are random, practically impossible to control in a planned manner, but assessable statistically. Therefore, it is impossible to precisely predict, and more so, fully eliminate their detrimental effects. The risk of their appearance is a normal phenomenon, and in the field of safety there is no "safe condition".

However, awareness of this risk and its management allows us to significantly reduce the frequency of undesirable events, and limit their undesirable consequences, which is an important activity in improving safety and as a safety management tool.

## 2. RISK EVALUATION

Risk evaluation (assigning a probability value to a risk) is a stage in the risk management process preceded by gathering information on threats relating to the given

system. The available information forms the basis for estimating the risk (Fig. 1). According to the above definition, risk is a function of:

- variables characterising the probability of losses occurring (measure of unreliability),
- variables characterising the magnitude of the loss (measure of threat).

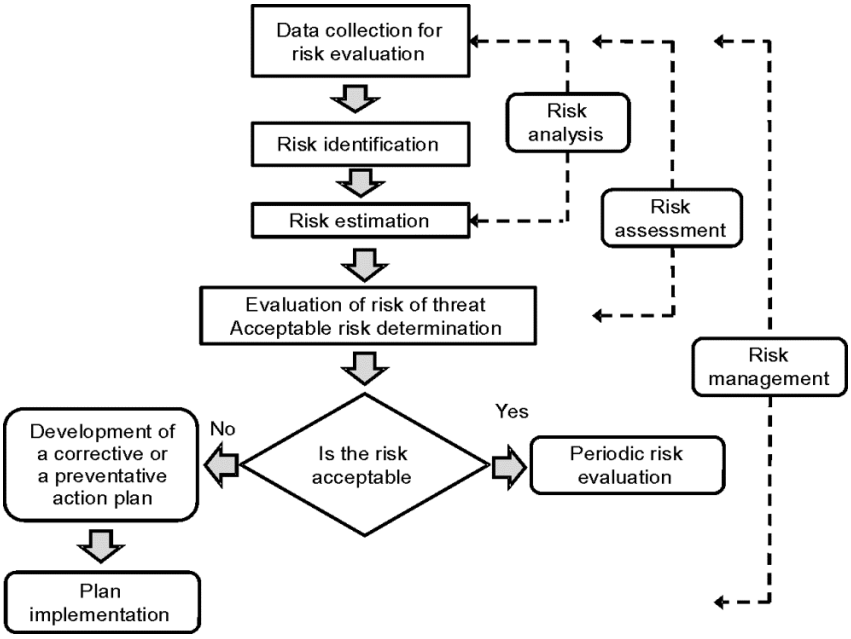


Fig. 1. Algorithm for a risk modelling (management) process

The relationship between the measure of risk, and the measures of failure and threat can be written as follows:

$$\begin{pmatrix}\text{measure}\\ \text{of risk}\end{pmatrix}=\begin{pmatrix}\text{measure}\\ \text{of failure}\end{pmatrix}\cdot\begin{pmatrix}\text{measure}\\ \text{of threat}\end{pmatrix} \tag{1}$$

The measure (level) of failure is usually expressed by the probability (or intensity) of an undesired event happening, while the level of threat is expressed in terms of the expected losses, i.e. consequences of the event. Thus

$$\text{Risk} = P(Z)\cdot S(Z) \tag{2}$$

where: $P(Z)$ is the probability of undesired event $Z$ happening, $S(Z)$ – the consequences (losses) due to the undesired event Z.

Equation (2) implies that the risk can be reduced by minimizing the probability of an undesired event happening and/or limiting the consequences of the undesired event, i.e. minimizing the threat. Risk evaluation should be performed independently for each

of the identified threats. Risk analysis can be performed either by means of a quantitative method, or a qualitative method using matrices, graphs and calculations.

Quantitative methods allow more rational evaluation and promote better safety than qualitative methods. They are, however, more difficult to use and require a larger amount of initial data. To perform a quantitative risk analysis, it is essential to use the appropriate model – a probability risk model, which should include:

- model of threats, enabling determination of the probability of threat occurring,
- reliability model, enabling determination of the correct probability of the undesired event including the probability of the initial hazardous events,
- relations between these models [1]

Qualitative methods are approximate methods of risk analysis. Qualitative risk evaluation is usually a subjective estimate, based on best practices and experience. These estimates result in lists of threats together with the related risk ranked. In qualitative methods each risk and its potential consequences are presented descriptively. The preliminary hazard analysis (PHA) method is an example of a qualitative method of risk evaluation which will be discussed later in this paper. This method can be successfully applied as an initial risk assessment during the preparation of a detailed risk evaluation. It was used to estimate and evaluate the risk of damage to the sewerage network in the city of Cracow.

## 3. GENERAL INFORMATION ON THE REASONS AND CONSEQUENCES OF FAILURES OF THE SEWERAGE SYSTEM

The current discussion concerns a gravitational sewerage network, whose characteristic feature is inability to identify system outage during operation whilst the state of awaiting repair is usually discrete, since network inspections are carried out at set frequencies [7]. This is why an indicator of its condition based on accepted breakdowns (unreliability) within a sewerage system is not always accurate. Situations exist in which a given network is highly reliable but its condition is essentially poor.

A failure can be defined as a set of conditions and causes for its occurrence, forces destructive to the subsystem components and soil subsidence towards the sewer, as well as post failure consequences [8]. Factors affecting the natural aging process of the sewer and the likelihood of damage to the sewerage network include the following:

- factors related to the sewer construction technology (e.g. inappropriate and consolidated soil surrounding the sewer),
- potential hydraulic overload of the sewer (e.g. flood, unplanned development),
- global power shortage,
- uncontrolled inflow of harmful substances into the sewer network,
- rheological phenomena in the ground (e.g. mining subsidence, earth tremors),
- erosive impact of the groundwater environment,

- reactive substances present in the sewage or formed during its flow (e.g. sulfate corrosion),
- sewer abrasion,
- external factors (road traffic),
- acts of vandalism and terrorism.

The most frequent phenomena occurring within the gravitational sewerage system are unsealed sewers and the infiltration of groundwater containing soil particles into the sewer [9, 10]. Voids then form which may cause the ground directly above the sewer to collapse. Infiltration of groundwater with soil particles into the sewer may even lead to a catastrophic failure. The scale of these phenomena is determined by the size of the unsealed area, type of ground, as well as the particle size distribution curve and concentration in the area of the sewer's orientation. If the problem occurs, smaller particles are washed away as long as a filter composed of bigger particles exists above the unsealed area. In the case of sewer backflow or during the sewer's operation under pressure, the filter becomes damaged. This process eventually leads to subsidence directly above the sewer. As a result, this leads to the ground at the surface collapsing in addition to the foundations located directly above the sewer. In the case of rigid surfaces (e.g. roads) on unconsolidated ground, voids form locally directly under the road surface. When these voids reach large dimensions, the ground then settles or cracks, followed by the collapse of the road surface.

On consolidated ground voids appear above the areas where the fragments are missing in the upper part of the sewer structure. These voids can reach large dimensions with heights attaining several meters. Voids are predominantly found above concrete sewers built during the 1950s and 1960s as the quality of the concrete in these sewers is very poor. Studies undertaken by researchers at Kielce University of Technology [11] have shown that the concrete classification was often below B10.

The greatest and most frequent problems in the operation of gravitational sewage systems are blockages or silting and sliming (obstructions in the sewers, lateral sewers and manholes). Sewers require unblocking. More commonly it is the lateral sewers which become blocked due to improper usage. Silting and sliming in addition to sedimentation in sewers occurs in sections where the rate of flow is insufficient to transport the suspended particles (is not self-cleansing). The silting of suspended particles in sewers increases the resistance to flow, causing foulness in the sewer. Under such conditions, the normal rate of flow may be reduced by as much as 70%. Foulness in sewers may also be caused by an uneven gradient and by specific sewage composition (e.g. sewage from a dairy containing a lot of fats). Root penetration is also a frequent phenomenon. Sewage, due to a higher temperature and high mineral contents are a perfect feeding medium for tree roots and therefore, after infiltrating the sewer they expand rapidly, and in time block the sewer stopping the flow.

A significant percentage of sewer damage consists of cracking, deformations, cave-ins, dislocation of pipes at joints, cradles (counterslopes), as well as corrosion

and abrasion caused by a number of reasons including ground subsidence, external and internal loading, careless construction work, or the abovementioned root infiltration. Corrosion, on the other hand, is caused by reactive substances found in sewage, or ones formed via chemical or biological reactions in the sewer during sewage flow. Sulfate corrosion is most common due to the release of hydrogen sulfide under anaerobic conditions during the decomposition of pollutants in sewage at relatively high temperatures and slow sewage flow. It has been noted recently that this problem affects both old and relatively new sewer sections alike.

Table 1 presents the failure frequency of sewerage networks in Poland based on long-term surveys carried out by various authors [12].

Table 1

General failure frequency based on population size [12]

| Population size | Below 10 000 | From 10 000 to 20 000 | From 20 000 to 50 000 | From 50 000 to 100 000 | From 100 000 to 200 000 | More than 200 000 | Total |
|---|---|---|---|---|---|---|---|
| Mean value of all failures [No./(km·year)] | 0.51 | 2.11 | 3.53 | 2.29 | 3.26 | 2.00 | 2.6 |
| Median of all failures [No./(km·year)] | 0.37 | 1.42 | 2.14 | 2.14 | 3.10 | 0.82 | 1.56 |
| Number of water companies analysed | 11 | 21 | 40 | 40 | 14 | 9 | 135 |

The presented damages and failures, taking into account their consequences, can be of two types. The former, visible on the surface, usually in the form of flooded structures, roads collapsing, equipment failure (e.g. pumps), no inflow into sewage treatment works (vacuum systems) are removed as they occur. The other, invisible on the surface, often remain undetected for long periods of time. It is these failures that pose a greater threat to the environment and may cause sewer catastrophes. They cause contaminations in groundwater and subterranean water due to sewage leaking from damaged sewers. This process is uncontrolled and may be long lasting. They may also cause water infiltration into the sewers, lowering the groundwater level, and thereby may increase the cost of sewage treatment. Losses caused by undesired events may be viewed on three levels: technical, economic, and socio-environmental which may include:

- environmental pollution,
- lowering of the standard of living,
- infrastructure flooding,
- flooding of the terrain,

- ill health caused by diseases linked to environmental pollution,
- compensation payments,
- environmental charges.

In gravitational sewerage systems, damage detection is very small, due to the general lack of continuous monitoring of these networks. Usually these damages affect the natural environment and are difficult to assess. When considering reliability, the following need to be taken into account: the main collectors, intercepting sewers, critical network components, e.g. pumping stations, holding tanks with associated anti-siphonage pipes which generate significant consequences.

## 4. PROCEDURE OF RISK EVALUATION IN THE PRELIMINARY HAZARD ANALYSIS

The PHA technique does not take into account a numerical value for the probability of a risk occurring but enables specification of only its severity and sets the acceptable risk level, usually by means of a risk matrix (mathematical interpretation of risk). The risk matrix is an excellent and convenient tool for illustrating ranking risk. The ranking of risk is in itself an important part of its analysis [1, 2, 13]. The risk matrix is a risk map divided into 9, 16, 25 or more cells, depending on the accepted scale of risk evaluation. It links the probability of an undesired risk occurring (e.g. sewer damage) with its consequence level (severity) according to Eq. (2). Frequency values ($W_1$) are assigned to individual probability categories for undesired events, while categories for the consequences of these events are described using a weighted numeric scale for the consequences ($W_2$) [14].

$$r = W_1 W_2 \tag{3}$$

Thus, each risk is assigned to coordinates in the matrix (combinations of accepted probability levels for undesired events and the consequences of these events). The division of the risk map into cells is related more to the risk indicators expressed in points (value ranges) than numbers (continuous scales). Risk evaluation can be performed on a grading scale of three or more. The matrix can be constructed as required, usually in the form of a chart or table. The scales refer equally to the severity of the consequences in failure scenarios (undesired events) as well as to the probability (frequency) of their occurrence, allocating them to an appropriate category, based on expert opinions. By assigning a probability to each defined event, an ordered list of threats is created. Categories (levels) are presented as a qualitative description – one could say, imprecise. The number of categories is selected independently for each analysis and matched to the potential size of the consequences. The probability for failure scenarios (random events) is described by categories, e.g. unlikely, quite likely, likely, etc., and consequences are described as, e.g. negligible, marginal, serious or

catastrophic, alternatively, small medium and large. Table 2 presents a sample risk matrix of failures (undesired events) relating to a given threat.

Table 2

Numeric values for a risk occurring in a given failure scenario – two parameter risk matrix (developed by the author)

| Event occurrence | The effects of consequences | | |
|---|---|---|---|
| | Small $W_2 = 1$ | Medium $W_2 = 2$ | Large $W_2 = 3$ |
| Not very likely, $W_1 = 1$ | 1 | 2 | 3 |
| Quite likely, $W_1 = 2$ | 2 | 4 | 6 |
| Most likely, $W_1 = 3$ | 3 | 6 | 9 |

The evaluated risk should be allocated to the accepted risk category. This is known as evaluating the risk of the likelihood of an undesired event occurring. If the risk severity lies outside the acceptable range, preventive and prompt actions must be defined, in particular actions such as the preparation of the means allowing reduction of the risk of the event potentially occurring. As a general rule, small losses occur relatively frequently whilst big losses do occasionally.

## 5. RISK EVALUATION FOR A GIVEN TYPE OF DAMAGE IN THE ANALYSED SEWERAGE NETWORK

The sewerage network under examination consists of two separate subnetworks, each with its own separate sewage treatment works. Both networks are gravitational. However, in areas where the gravitational draining of the sewage into the central network is impossible for height reasons, local sewerage networks exist with their own sewage treatment works. In central parts of the city, the sewerage network is a combined system, whilst on the outskirts it is a separate system where foul sewage is drained into the central system and storm water into the local watercourses. The main sewer collectors, despite having been constructed in the early 20th century, still possess spare capacity and are capable of operating efficiently without the need for implementing significant changes. This allows new urban areas which are in the immediate neighbourhood of existing sewers to be connected to the central sewerage network. The total length of the network (lateral sewers including the external network) is 1780 kilometres, built from concrete, stone, reinforced concrete, cast iron, PVC, steel and PE.

In the period of the network's operation, sometimes over a century, the operating conditions changed, the amount of sewage increased, the load bearing capacity of the sewers decreased as their condition deteriorated, and the dynamic load increased due to road traffic. There followed a gradual deterioration of the pipelines, the flow conditions changed mainly due to silting and badly laid sewers, potential conditions were

created for the formation of hydrogen sulfide and sulfate corrosion. Figure 2 shows the number of failures over a 10 year period.

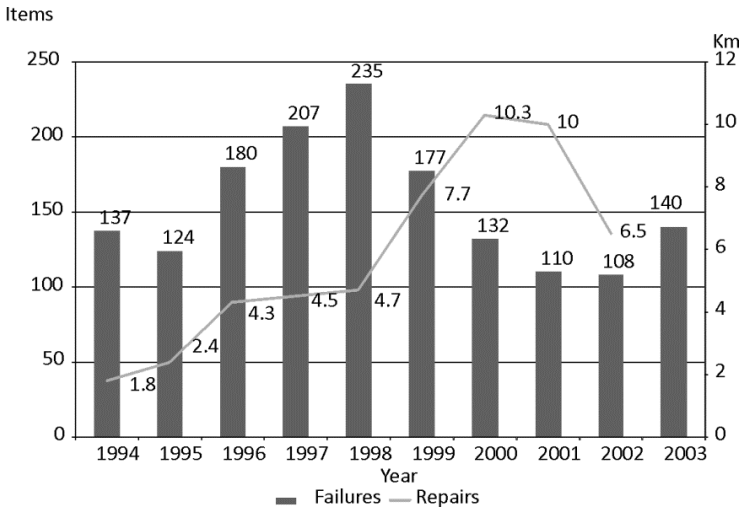


Fig. 2. Failures and repairs in the sewerage system of a town in Southern Poland [15]

A failure was defined as an event where some (or all) of the sewage failed to reach the sewage treatment works, seeped into the ground or was transported directly to the receiver. Such events include loss of network seals, cave-ins, deformation, cracks in the sewer, manhole damage and others. Since 2003 the average failure count has remained steady at around 150. This is possible due to gradual renovation and replacement of damaged sewers – annually around 10 km of pipeline undergo a general overhaul. If possible, work is undertaken using trenchless technologies. In recent years, thanks to the availability of modern technologies, new sewers are being constructed in a similar manner. A risk evaluation for a given type of damage in the analyzed sewerage system was performed based on detailed data on those failures which occurred in 2003 (Fig. 3).

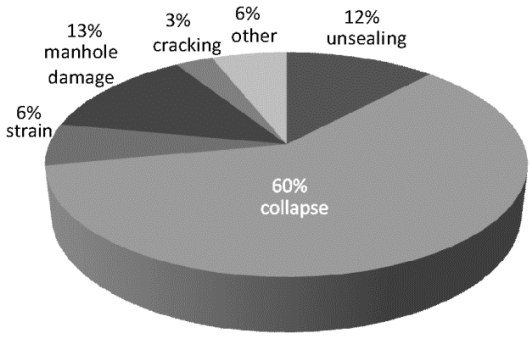


Fig. 3. Failure types by percentage on the analysed sewerage network in 2003 [15]

The sewer unit failure rate indicator $\lambda$ [$a^{-1}\cdot km^{-1}$] was adopted as a criterion for the probability of sewer damage. The choice of this criterion made the evaluation of the risk of damage to the sewer not too difficult, although the availability of data on the number of failures in sewerage systems is worse than for example, in water supply systems. This is due to the fact that damage to a sewer is detected long after its occurrence, the detection often being incidental.

The adoption of a probability category (estimated probability level) is no longer unequivocal. The size of the network, the number of repair crew and technical backup play decisive roles. After analysing an analogous indicator for a water supply system, the characteristic sum of the individual estimated probability levels (probability categories) of the failure scenarios was related to an assumed, limiting failure rate value of $\lambda = 0.03$ [$a^{-1}\cdot km^{-1}$]. It is a limiting value for properly functioning sewerage network.

On a grading scale, the following three probability categories were adopted:

- low (not likely); $\lambda \leq 0.03$ $a^{-1}\cdot km^{-1}$, $W_1 = 1$,
- moderate (quite probable); $0.03 < \lambda \leq 0.3$ $a^{-1}\cdot km^{-1}$, $W_1 = 2$,
- high (probable); $\lambda > 0.3$ $a^{-1}\cdot km^{-1}$, $W_1 = 3$

The value of the total system sewer unit failure rate indicator was $\lambda = 0.102436$ $a^{-1}\cdot km^{-1}$ (for the network length of 1367 km and 140 failures). The values of the individual sewer unit failure rates (frequency) classified by type of event and the probability category of these damages are specified in Table 3.

Table 3

Summary of unit failure rates indicator, probability categories and categories of consequences of damage (by the author)

| Failure rate indicator [$a^{-1}\cdot km^{-1}$] | Probability category | Consequence category |
|---|---|---|
| 0.012292 | 1 | 1 |
| 0.061461 | 2 | 2 |
| 0.006146 | 1 | 1 |
| 0.013316 | 1 | 2 |
| 0.003073 | 1 | 2 |
| 0.006146 | 1 | 1 |

Each event carried a clearly defined consequence. Unsealing, sewer cracks, manhole damage contributed to a drop in the load bearing capacity of the sewer, they were followed by the ground subsiding around the sewer, manhole (damage caused by vehicles), polluting the groundwater. Problems were also noted, relating to the odour emanating from the damaged sewer. Sewer deformation, silted and slimy sewers, blocked manholes resulted in sewage flooding street properties.

Weighting the consequences of a given damage is very difficult. The size of the consequences for a given damage depends at least on the place where it occurred, the

effectiveness of the repair crews, access to the failure location, the time taken to detect the failure, the extent of the damage to the sewer (e.g. crack).

Individual evaluation levels of undesired events in a sewerage network are characterized according to a three category grading scale:

- low – failures in lateral and branch sewers which are simple to fix, and do not cause flow problems (deformation, insignificant unsealing, cracking), $W_2 = 1$,
- moderate – failures relating to collecting pipes and collectors (may cause disruption to road traffic, also incurs environmental costs, discharge sewers, combined sewers (collapsed sewers, infrastructure, sewer cracks, collapsed manholes) $W_2 = 2$,
- high – failures relating to the main and intercepting sewers, significantly affecting the road traffic, road damage, high environmental costs, combined sewers (significant sewer damage, disturbed ground, seepage of toxic substances into the sewer, e.g. ammonia) $W_2 = 3$. To evaluate risk, to a greater accuracy, 5 levels of risk were defined (Table 4).

Table 4

Categories and numeric values assigned to risk (by the author)

| Risk likelihood | Value | Category of accepted risk |
|---|---|---|
| Very small | 1 | tolerated |
| Small | 2 | |
| Moderate | 3 and 4 | controlled |
| Large | 6 | unacceptable |
| Very large | 9 | |

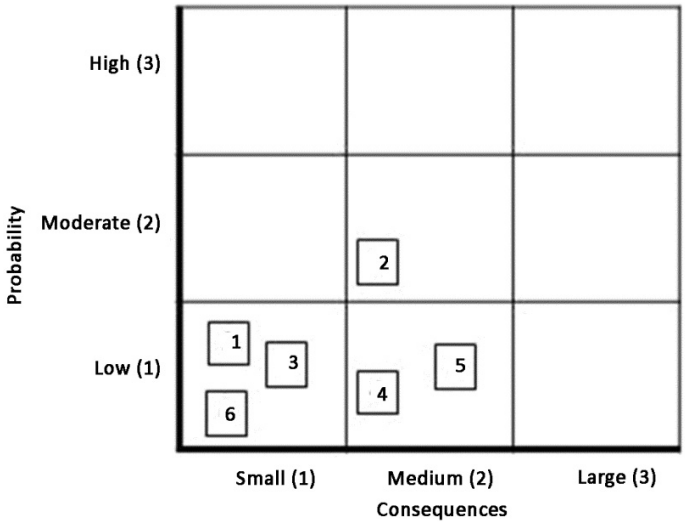


Fig. 4. Risk damage map of the analysed sewage system (by the author)

The likelihood of failure in the analysed sewerage network taking into account the type of failure is presented in the form of a risk map in Fig. 4.

## 6. SUMMARY

The evaluated risk of damage of the analysed sewerage system, using the PHA method, discussed in this paper, is a point for further discussion. This assessment was preceded by a characteristic of the evaluation of reliability and safety of the discussed system as necessary actions to evaluate risk and required information on the causes and consequences of sewerage system failures. After describing the PHA technique by means of the risk matrix, the risk of certain types of damage (unsealing of sewers, collapsed sewers, sewer deformation, manhole damage, sewer cracks and others) was assessed using the unit failure rate indicator, on the basis of proposed probability category values and consequence categories. These results cannot be compared with any previously published ones due to lack of such data relating to sewerage systems.

## REFERENCES

[1] BIEDUGNIS S., SMOLARKIEWICZ M., *Safety and Reliability of Water Supply Systems*, Wyd, Przem. WEMA Sp. z o.o., Warsaw, 2004 (in Polish).
[2] WOLANIN J., *A Citizen Security Outline.* Wyd. DANMAR, Warsaw, 2005 (in Polish).
[3] RAK J., *Chosen Aspects of Reliability and Safety in Water Supply.* Ofic. Wyd. Politechniki Rzeszowskiej, Rzeszów, 2008 (in Polish).
[4] RAK J., Environ. Prot. Eng., 2009, 35 (2), 23.
[5] TCHÓRZEWSKA-CIEŚLAK B., Environ. Prot. Eng., 2009, 35 (2), 29.
[6] OPYRCHAŁ L., FIEDLER K., JANKOWSKI W., MAZURCZYK A., *A Damming Structure Analysis by Means of the 'Tree of Events' Method, as Exemplified by the Klimkówka Dam.* Proc. 14th Conf. Science and Technology, Computer Methods in Structural Design and Analysis of Hydrotechnical Constructions, Korbielów, 2002, p. 147–159 (in Polish).
[7] KRÓLIKOWSKA J., KRÓLIKOWSKI A., *Rising the Reliability Level of Sewage Draining Subsystems' Operation in the Light of Working Experience.* Proc. 5th Polish Conf. Science and Technology, Present Issues in Water Treatment and Distribution, Szczyrk, 2009, p. 347–358 (in Polish).
[8] KULICZKOWSKI A., Gaz, Woda i Technika Sanitarna, 1995, 2, 58 (in Polish).
[9] KAPCIA J., Rynek Instalacyjny, 2006, 5, 50 (in Polish).
[10] KRÓLIKOWSKA J., KRÓLIKOWSKI A., INSTAL, 2008, 10, 74 (in Polish).
[11] KULICZKOWSKI A., Gaz, Woda i Technika Sanitarna, 1988, 6, 127 (in Polish).
[12] *Water Supply and Sewage Systems in Poland. Tradition and Modernity*, M.M. Sozański (Ed.), Polska Fundacja Ochrony Zasobów Wodnych, Poznań–Bydgoszcz, 2002 (in Polish).
[13] BIEDUGNIS S., SMOLARKIEWICZ M., PODWÓJCI P., CZAPCZUK A., Rocznik Ochrony Środowiska, 2007, (9), 303 (in Polish).
[14] RAK J., Ochr. Środ., 2003, 2, 33 (in Polish).
[15] DROZDOWSKI Ł., *Operation of the Sewage System in the City of Cracow*, MS dissertation under the supervision of J. Kapcia, Institute of Water Supply and Environmental Protection , Cracow University of Technology, Cracow, 2004 (in Polish).

Environment Protection Engineering

Vol. 37 2011 No. 4

N. GAMZE TURAN*, BASAK MESCI**

# ADSORPTION OF COPPER(II) AND ZINC(II) IONS BY VARIOUS AGRICULTURAL BY-PRODUCTS. EXPERIMENTAL STUDIES AND MODELLING

Effective removal of heavy metals from aqueous solutions belongs to the most important issues for many industrialized countries. Removal of copper(II) and zinc(II) ions from leaching solution of industrial waste were studied using hazelnut, almond and walnut shells. Batch adsorption experiments were performed in function of pH, contact time and adsorbent dosage. Adsorption kinetics was investigated using the pseudo-first and pseudo-second order, Elovich equations and intraparticle diffusion models. The results indicate that the second order model best describes adsorption kinetic data and the agricultural by products investigated may be used for removal of copper(II) and zinc(II) ions from leaching solution of industrial waste.

## 1. INTRODUCTION

The landfill method continues to be widely used for both municipal and industrial solid waste due to its economic advantages in the world. One of the problems arising from landfilling of the waste is generation of leachate [1]. Landfill leachate is the most complicated and costly wastewater to treat due to its high content of organic and inorganic pollutants [2–4]. Whereas the characterization and treatment of leachate from municipal solid waste has been widely studied, the leachate from security landfills for industrial waste has been studied to a much lesser degree [5].

Heavy metal is one of the most common groups of contaminants in landfill leachate. Heavy metals may constitute an environmental problem, if the leachate migrates into surface water or groundwater, or a treatment issue where leachate is col-

*Ondokuz Mayis University, Engineering Faculty, Department of Environmental Engineering, 55139 Kurupelit, Samsun, Turkey, e-mail: gturan@omu.edu.tr

**Ondokuz Mayis University, Engineering Faculty, Department of Material Science and Engineering, 55139 Kurupelit, Samsun, Turkey, e-mail: basakm@omu.edu.tr (corresponding author).

lected and treated prior to discharge. The presence of heavy metal ions in the environment is of major concern due to their toxicity to many life forms. Unlike organic pollutants, the majority of which are susceptible to biological degradation, metal ions do not degrade into harmless end products [6, 7].

Many industries such as metal fishing, electroplating, plastics, pigments and mining contain several heavy metals. Copper(II) and zinc(II) are among the most common heavy metals in these industries. While the accumulation of copper(II) in human body causes brain, skin, pancreas and hearth diseases, zinc(II) being in the list of priority pollutants proposed by Environmental Protection Agency gives rise to serious poisoning cases. The main symptoms of zinc(II) poisoning are dehydration, electrolyte imbalance, stomach ache, nausea, dizziness and incoordination in muscles [8].

Numerous processes exist for removing heavy metals such as adsorption, ion exchange, precipitation, phytoextraction, ultrafiltration, reverse osmosis and electrodialysis. Among them, adsorption receives considerable interest with the high efficiency in heavy metal removal. The most respective and widely used adsorbent material in the adsorption processes is activated carbon. Even though it has a high adsorption capacity, surface area and microporous structure; it is restricted to use due to its relatively high price; high operation costs, and problems with regeneration for the industrial scale applications. This led to a search directed to developing low-cost and locally available adsorbent materials with the maximum adsorption capacity [9].

In recent years, biosorbents have been widely studied for heavy metal removal from aqueous solution. These include peanut shells [10, 11], hazelnut shells [12], banana pith [13], peat [14], wood [15], pine bark [16], rice bran, soybean and cottonseed hulls [17], rice husk [18], sawdust [19], wool [20], orange peel and compost [21], and leaves [22]. Most of these studies have shown that natural products can be good sorbents for heavy metals.

Variety biosorbents have been shown to exhibit some affinity for heavy metals. Biosorbent choice should be inexpensive and readily available locally. Turkey is one of the top hazelnut, almond and walnut exporting countries in the world. Their shells are abundant and inexpensive in Turkey. Moreover, these products can be put in use directly without elaborate preparation; thus they could provide an economical source of biosorbents for heavy metal removal. However, microorganism based and other biomasses often need to be cultured and/or tediously prepared before application. This would increase the cost of the overall wastewater treatment processes [23].

The aim of this study is to investigate adsorption studies of hazelnut, walnut and almond shells for the removal of Cu(II) and Zn(II) ions from leaching solution of industrial waste. The effects of pH, adsorbent dosage and contact time on adsorption efficiency were analyzed, and the optimum values were determined from the experimental studies. Adsorption kinetics models were applied in order to determine adsorption mechanism and adsorption characteristic constants.

## 2. MATERIALS AND METHODS

*Materials*. Three agricultural by-products, hazelnut, walnut and almond shells (HS, WS and AS, respectively, were used from the Black Sea Region of Turkey. Hazelnut, walnut and almond shells were obtained from species of *Corylus pontica*, *Juglans regia* and *Prunus dulcis,* respectively. Fresh shells were washed several times with distilled water to remove surface impurities and dried at 373 K for 24 h. Then samples were crushed by means of a grinder and sieved to obtain the particles of the average diameter of 0.5 mm.

*Leachate preparation.* Industrial waste used for this study was obtained from the Elektrosan Electrocopper Industry in Samsun, Turkey. Standard 1:4 (w/w extractant to sample), 48 h leachings were performed using leaching procedure with deionized water [24]. 1 $dm^3$ of deionized water and 250 g of waste were mixed in a Teflon bottle. Bottles were shaken for 48 h at 25 °C on an end-over-end rotary shaker rotating at 200 rpm. Leachates were filtered (0.22 μm openings) and used as leaching solution in the adsorption experiments.

*Adsorption experiment.* Adsorption of copper(II) and zinc(II) ions from aqueous leachate of industrial wastes onto agricultural by-products was performed using batch equilibrium technique. All batch experiments were conducted with 100 $cm^3$ adsorbent samples. Erlenmeyer flasks closed with glass stoppers were used at constant temperature (25±1 °C) in a shaking waterbath.

In order to investigate the effect of pH, agricultural by-product of the concentration of 1.0 $g \cdot dm^{-3}$ was used at pH ranging from 2 to 10. Samples were shaken at 200 rpm for 2 h. pH was carefully adjusted using 0.1 M HCl and 0.1 M NaOH solutions and measured using a Mettler Toledo-MP 220 pH-meter. The effect of adsorbent concentration was investigated by using adsorbent samples of the concentrations ranging from 2.0 to 10.0 $g \cdot dm^{-3}$. Once the optimum pH and adsorbent dosage had been attained, contact time was determined for increasing periods of time (10–120 min) and temperatures of 20, 40 and 60 °C, until no more copper(II) and zinc(II) ions were removed from the aqueous phase and equilibrium had been achieved. After reaching the equilibrium, the suspension was filtered. Samples were digested with high-purity nitric acid to remove the organic matrix and leave the elements dissolved in the solution. The concentrations of copper(II) and zinc(II) ions were analyzed by an atomic absorption spectrophotometer (UNICAM model 929). Appropriate replicates were used for controls and blanks (as applicable) and for the treated samples.

To test the system at equilibrium such parameters as sorption capacity of the substrate ($q_e$) expressed in terms of metal amount adsorbed on the unitary natural sorbent mass ($mg \cdot g^{-1}$) and sorption efficiency of the system ($R_{em}$%) being the percentage of removed metal ions relative to the initial amount were used. These parameters have been calculated from the equations:

$$q_e = \frac{C_i - C_e}{W} V \tag{1}$$

$$R_{em}\% = \frac{100(C_i - C_e)}{C_i} \tag{2}$$

where $C_i$ is the initial concentration of metal ions in solution (mg·dm$^{-3}$), and $C_e$ is their final concentration (mg·dm$^{-3}$), $V$ is the volume of the solution (dm$^3$) and $W$ is the mass of adsorbate (g).

## 3. RESULTS AND DISCUSSION

### 3.1. EFFECT OF PH

Figure 1 shows the effect of pH on the removal of copper(II) and zinc(II) ions onto three agricultural by-products from the leachate of industrial waste. The maximum percent removal the ions were observed at pH > 6, and significantly decreased at lower pH values.

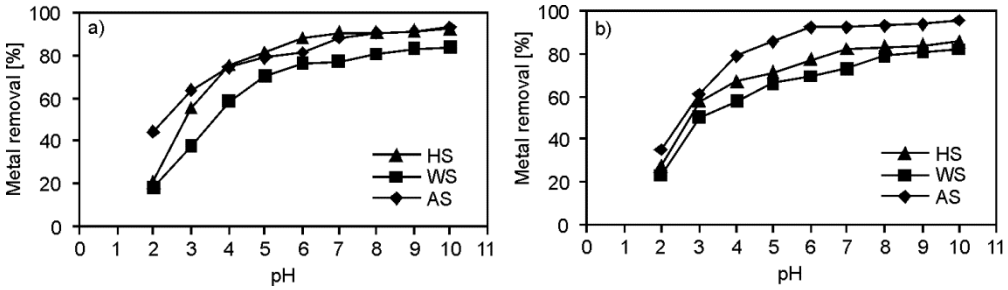


Fig. 1. Effect of pH on the removal of copper(II) (a) and zinc(II) (b) ions in industrial waste leachate by agricultural by-products

According to Low et al., little sorption at lower pH could be ascribed to hydrogen ions competing with metal ions for sorption sites [25]. This means that at higher $H^+$ concentration, the adsorbent surface becomes more positively charged, thus, reducing the attraction between adsorbent and metal ions. In contrast as the pH increases, more negatively charged surface becomes available, thus, facilitating greater metal uptake [4]. In this study, optimum pH values determined for the copper(II) and zinc(II) removal were 7 and 8, respectively (Fig. 1). At higher pH, the copper(II) and zinc(II) ions precipitated as hydroxides which decreased the rate of adsorption and subsequently the percent removal of metal ions.

### 3.2. EFFECT OF ADSORBENT DOSAGE

Figure 2 shows the effect of agricultural by-product dosages on the removal of copper(II) and zinc(II) ions. Upon increasing the agricultural by-product concentration, the amount of copper(II) and zinc(II) ions removed increased, as the number of binding sites would be increased. When the adsorbent concentrations increased from 2.0 to 12.0 g·dm$^{-3}$, the percentages of sorbed copper(II) for hazelnut, walnut and almond shells increased from 45.55% to 92.11%, from 30.21% to 78.55% and from 40.21% to 89.70%, respectively.

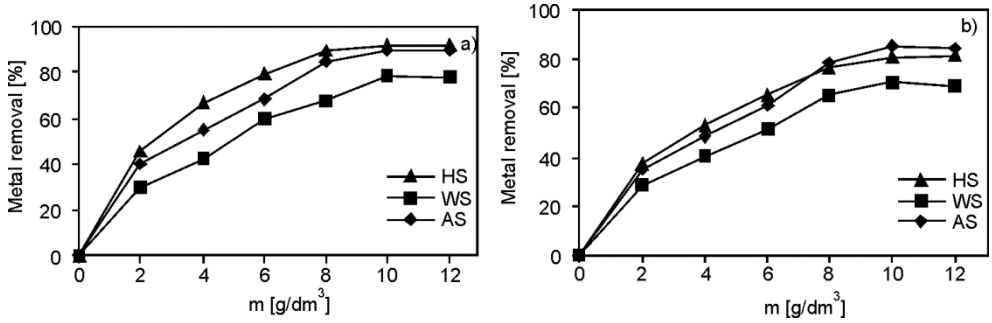


Fig. 2. Effect of adsorbent dosage on the removal of copper(II) (a) and zinc(II) (b) ions in industrial waste leachate by agricultural by-products

The percentages of sorbed zinc(II) for hazelnut, walnut and almond shells increased from 37.67% to 81.21%, from 28.91% to 70.41% and from 35.41% to 85.22, respectively. It was observed that there was not much change in removal efficiency at adsorbent concentrations higher than 10.0 g·dm$^{-3}$ and such concentration was used in further adsorption experiments.

### 3.3. EFFECT OF CONTACT TIME

The effect of contact time on copper(II) and zinc(II) adsorption with agricultural by-products was also evaluated. In the experiments, optimum values of pH and adsorbent dosage were used for the copper(II) and zinc(II) removal. The effect of contact time is shown in Fig. 3. The results reveal that the metal removal is higher at the beginning. That is probably due to the greater number of available reactive sorption sites of agricultural by-products used at the beginning for the adsorption of heavy metal ions. As the surface adsorption sites become exhausted, the uptake rate is controlled by the rate at which the adsorbate is transported from the exterior to the interior sites of the adsorbent particles [26, 27]. The optimum contact time determined for both copper(II) and zinc(II) removal was 10 min. It is seen that the two metals showed a fast rate of sorption onto agricultural by-products.

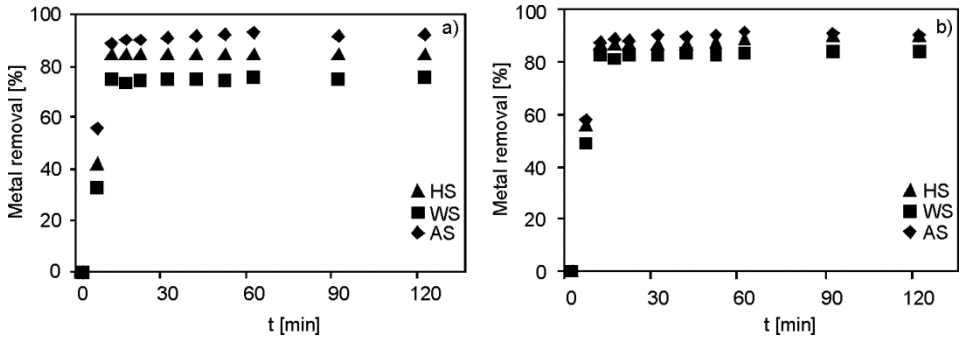


Fig. 3. Effect of contact time on the removal of copper(II) (a) and zinc(II) (b) ions in industrial waste leachate by agricultural by-products

### 3.4. ADSORPTION KINETICS

In order to examine the controlling mechanism of sorption process, several kinetic models were used to test the experimental data. Figure 4 shows the effect of contact time for the adsorption of the metal ions onto three agricultural by-products.

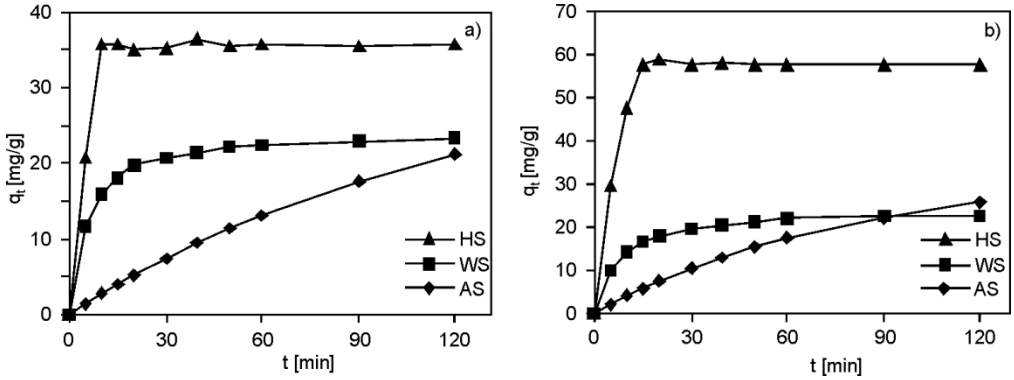


Fig. 4. Time dependences of sorption capacities of copper (II) (a) and zinc (II) (b) ions in industrial waste leachate by agricultural by-products

The examination of the kinetic curves reveals a rapid adsorption to attain the equilibrium stages of the leaching solutions. In all cases, two staged were observed. The former one, where the contact time is lower than 10 min, corresponds to rapid retention. The latter stage, with the contact time between 10 min and 120 min, represents a progressive fixation which is stabilized after 10 min of contact time, implying that equilibrium was reached. The pseudo first order, Elovich and the intraparticle diffusion equations were considered to interpret the time dependence of the experimental data.

PSEUDO FIRST ORDER KINETIC MODEL

A widely used Lagergreen model was employed to study the pseudo first order kinetics [28]:

$$\frac{dq_t}{d_t} = k_1\left(q_e - q_t\right) \tag{3}$$

where $q_e$ and $q_t$ refer to the amounts of heavy metal (mg·g$^{-1}$) adsorbed at equilibrium time and time $t$ (d) and $k_1$ is the Lagergreen rate constant (d$^{-1}$), respectively.

The integration of Eq. (3) gives the following expression:

$$\ln\left(q_e - q_t\right) = -k_1 t + C_1 \tag{4}$$

where $C_1$ is the integration constant for the reaction of the first order and

$$\ln\left(q_e - q_t\right) = \ln q_e - k_1 t \qquad \text{for} \qquad q = 0 \text{ at } t = 0 \tag{5}$$

The pseudo first order kinetic model considers the rate of occupation of adsorption sites to be proportional to the number of unoccupied sites. A straight line of $\ln(q_e - q_t)$ vs. $t$ indicates the application of the first order kinetic model (Fig. 5). The rate constants ($k_1$) are obtained from slope of the plots.

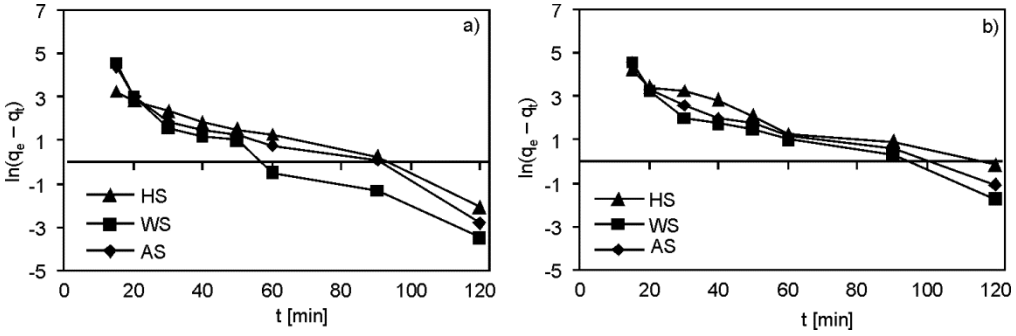


Fig. 5. Pseudo-first order reaction kinetics for the adsorption of copper(II) (a) and zinc(II) (b) ions

PSEUDO SECOND ORDER KINETIC MODEL

Adsorption data was also evaluated according to the pseudo second order kinetic proposed by [28]:

$$\frac{dq_t}{dt} = k_2\left(q_e - q_t\right)^2 \tag{6}$$

where $q_e$ and $q_t$ are the amounts of heavy metal (mg·g$^{-1}$) adsorbed at equilibrium time and time $t$ (d), respectively, and $k_2$ is the second order reaction constant (g·mg$^{-1}$·d$^{-1}$). Integration of Eq. (6) leads to the following expression:

$$\frac{1}{q_e - q_t} = k_2\ t + C_2 \tag{7}$$

In Equation (7), $C_2$ is the integration constant of the second order reaction kinetic. After rearrangement, the following equation is obtained:

$$\frac{t}{q_t} = \frac{1}{k_2 q_e^{\ 2}} + \frac{1}{q_e} \tag{8}$$

A straight line of $t/q_t$ vs. $t$ indicates the application of the second order kinetic model (Fig. 6). The values of $k_2$ are determined from the slope of the plots.

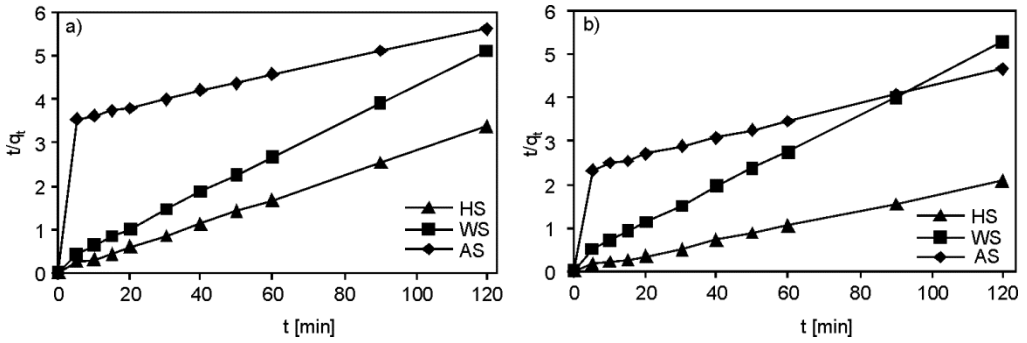


Fig. 6. Pseudo-second order reaction kinetics for the adsorption of copper(II) ions (a) and zinc(II) (b) ions

ELOVICH MODEL

The Elovich equation has the form [29]:

$$\frac{dq_t}{dt} = \alpha \exp\left(-\beta q_t\right) \tag{9}$$

where $\alpha$ is the initial adsorption rate (mg·g$^{-1}$·min$^{-1}$) and $\beta$ is the desorption constant (g·mg$^{-1}$). To simplify the Elovich equation, Chien and Clayton [30] assumed $\alpha\beta_t >> 1$, and for the boundary conditions $q_t = 0$ at $t = 0$ and $q_t = q_t$ at $t = t$, we arrive at [31]:

$$q_t = \frac{1}{\beta}\ln(\alpha\beta) + \frac{1}{\beta}\ln t \tag{10}$$

A straight line plot of $q_t$ vs. ln$t$ indicates the application of Elovich model (Fig. 7). The values of constants can be obtained from the slopes and intercepts of the plots.

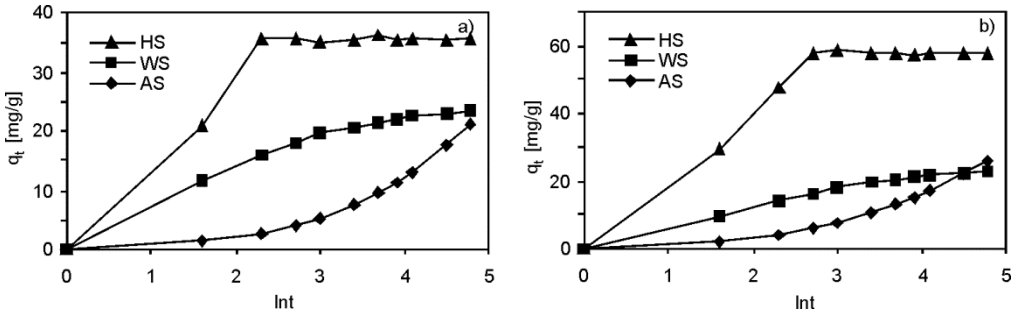


Fig. 7. Elovich kinetics for the adsorption of copper(II) (a) and zinc(II) (b) ions

INTRAPARTICLE DIFFUSION MODEL

Transport of the adsorbate from the solution to the surface of the adsorbent particles occurs in several steps. Generally, the process is diffusion controlled, if its rate is dependent on the rate at which components diffuse towards one another. The possibility of intraparticle diffusion was explored by using the intraparticle diffusion model as follows [32]:

$$q_t = K_{id}\ t^{1/2} + C \tag{11}$$

where $K_{id}$ is the intraparticle diffusion rate constant ($mg \cdot g^{-1} \cdot min^{-1/2}$) and $C$ is the intercept. Values of $C$ give an idea about thickness of the boundary layer, i.e., the larger intercept, the greater the boundary layer effect is [7].

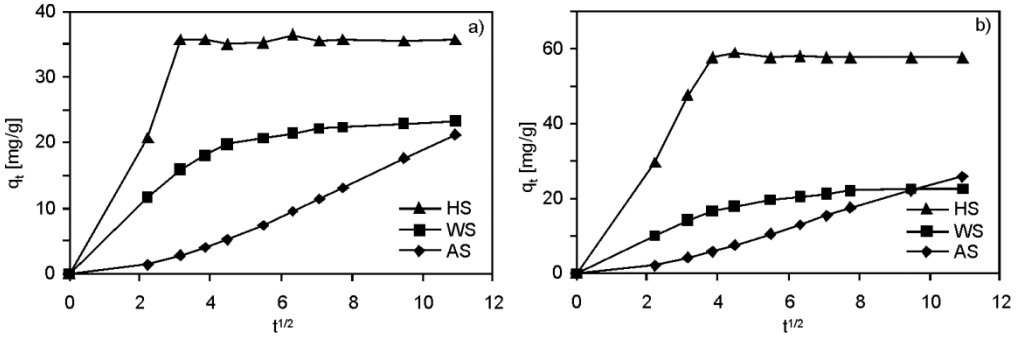


Fig. 8. Intraparticle diffusion kinetics for the adsorption of copper(II) (a) and zinc(II) (b) ions

The plot of $q_t$ versus $t^{1/2}$ indicates the application of the intraparticle diffusion model. The values of $K_{id}$ were determined from the slope of the plots. If the intraparticle diffusion is involved in the adsorption process, the plot of the amount of heavy metal adsorbed per unit mass of adsorbent ($q_t$) against square root of time ($t^{1/2}$) formed a straight line. The particle diffusion would be the controlling step if the line inter-

sected the origin [33]. Figure 8 presents the plots of the amount of Cu(II) and Zn(II) ions adsorbed per unit mass of the adsorbent vs. $t^{1/2}$. The deviation of straight lines from the origin indicates that intraparticle transport is not the rate limiting step. As seen from Fig. 7, the intraparticle diffusion rate equation fits well to the initial stages of the adsorption process for all the tested metal ions with the agricultural by-products.

The kinetic parameters of Cu(II) and Zn(II) ions onto agricultural by-products (Table 1) were calculated from the plots.

Table 1

Kinetic parameters of adsorption of copper(II) and zinc(II) in leaching solution of industrial waste by agricultural by-products[a]

| Kinetic equation and parameter | HS | WS | AS | Kinetic equation and parameter | HS | WS | AS |
|---|---|---|---|---|---|---|---|
| Cu(II) | | | | Zn(II) | | | |
| First order kinetic equation | | | | | | | |
| $k_1$ [min$^{-1}$] | 0.046 | 0.067 | 0.057 | $k_1$ [min$^{-1}$] | 0.040 | 0.050 | 0.046 |
| $q_1$ [mg·g$^{-1}$] | 46.512 | 73.259 | 70.401 | $q_1$ [mg·g$^{-1}$] | 77.254 | 68.252 | 73.215 |
| $R^2$ | 0.975 | 0.927 | 0.913 | $R^2$ | 0.975 | 0.906 | 0.924 |
| Second order kinetic equation | | | | | | | |
| $k_2$ [g·mg$^{-1}$·min$^{-1}$] | 0.037 | 0.010 | 0.968 | $k_2$ [g·mg$^{-1}$·min$^{-1}$] | 0.014 | 0.008 | 1.766 |
| $q_2$ [mg·g$^{-1}$] | 35.842 | 23.981 | 54.645 | $q_2$ [mg·g$^{-1}$] | 58.480 | 23.641 | 50.000 |
| $R^2$ | 0.999 | 0.999 | 0.999 | $R^2$ | 0.999 | 0.997 | 0.999 |
| Elovich equation | | | | | | | |
| $\alpha$ [mg·g$^{-1}$·min$^{-1}$] | 30.239 | 9.462 | 12.215 | $\alpha$ [mg·g$^{-1}$·min$^{-1}$] | 35.456 | 9.462 | 15.336 |
| $\beta$ [g·mg$^{-1}$] | 0.148 | 0.210 | 0.229 | $\beta$ [g·mg$^{-1}$] | 0.086 | 0.207 | 0.183 |
| $R^2$ | 0.710 | 0.927 | 0.799 | $R^2$ | 0.780 | 0.960 | 0.843 |
| Intraparticle diffusion equation | | | | | | | |
| $K_{id}$ [mg·g$^{-1}$·min$^{-1/2}$] | 2.363 | 1.835 | 2.076 | $K_{id}$ [mg·g$^{-1}$·min$^{-1/2}$] | 4.182 | 1.895 | 2.550 |
| $R^2$ | 0.462 | 0.729 | 0.965 | $R^2$ | 0.533 | 0.786 | 0.979 |

[a]HS– hazelnut shells, WS – walnut shells, AS – almond shells.

It can be easily seen from Table 1 that the correlation coefficients ($R^2$) for the pseudo-second order kinetic model is much higher than the corresponding values of the other kinetic models. Moreover, the calculated $q_e$ values are agree with experimental $q_e$ values for the pseudo-second order kinetic model, pointing to the applicability of this model to description of the adsorption model.

### 3.5. FITTING THE POLYNOMIAL EQUATIONS AND STATISTICAL ANALYSIS

In Table 2, the effect of initial pH is presented and basic statistical solutions and experimental ranges of the removal capacities for the use of hazelnut (HS), almond (AS) and walnut shells (WS) are given for further analysis.

Table 2

One factor experimental design and its related descriptive statistics for the effect of initial pH[a]

| Adsorbent | Responses | Min | Max | Average $R_{em}$ [%] | Std $R_{em}$ [%] | $R$ |
|---|---|---|---|---|---|---|
| HS | removal of Cu(II) | 21.2 | 90.91 | 71.90 | 25.53 | 4.28 |
| HS | removal of Zn(II) | 27.5 | 83.43 | 66.79 | 19.43 | 3.03 |
| WS | removal of Cu(II) | 18.4 | 80.6 | 59.88 | 23.60 | 4.38 |
| WS | removal of Zn(II) | 23.4 | 78.8 | 60.05 | 18.77 | 3.36 |
| AS | removal of Cu(II) | 45.5 | 90.8 | 74.65 | 15.95 | 2.04 |
| AS | removal of Zn(II) | 35.4 | 93.4 | 77.07 | 21.57 | 2.63 |

[a]Number of run – 7, range – 2–8, Min – minimum value, Max – maximum value, Std – standard deviation, $R$ – the ratio of Max/Min. If $R$ >10, a transformation such as square root, natural log, base 10log, inverse square, etc. is usually required for ANOVA.

Table 3

One factor experimental design and its related descriptive statistics for the effect of adsorbent dosage[a]

| Adsorbent | Responses | Min | Max | Average $R_{em}$ [%] | Std $R_{em}$ [%] | $R$ |
|---|---|---|---|---|---|---|
| HS | removal of Cu(II) | 45.55 | 92.21 | 74.74 | 19.12 | 2.02 |
| HS | removal of Zn(II) | 37.67 | 81.21 | 62.79 | 17.68 | 2.15 |
| WS | removal of Cu(II) | 30.21 | 78.55 | 55.71 | 19.35 | 2.60 |
| WS | removal of Zn(II) | 28.90 | 70.41 | 51.27 | 17.25 | 2.43 |
| AS | removal of Cu(II) | 40.20 | 89.70 | 67.90 | 20.65 | 2.23 |
| AS | removal of Zn(II) | 35.40 | 85.20 | 61.78 | 20.56 | 2.40 |

[a]Number of run – 5, range – 2–10.

Table 4

One factor experimental design and its related descriptive statistics for the effect of contact time[a]

| Adsorbent | Responses | Min | Max | Average $R_{em}$ [%] | Std $R_{em}$ [%] | $R$ |
|---|---|---|---|---|---|---|
| HS | removal of Cu(II) | 41.80 | 84.90 | 80.39 | 13.56 | 2.03 |
| HS | removal of Zn(II) | 55.60 | 90.30 | 84.72 | 10.33 | 1.62 |
| WS | removal of Cu(II) | 33.20 | 75.50 | 70.49 | 13.11 | 2.27 |
| WS | removal of Zn(II) | 48.88 | 84.20 | 79.61 | 10.82 | 1.72 |
| AS | removal of Cu(II) | 55.60 | 92.90 | 87.76 | 11.36 | 1.67 |
| AS | removal of Zn(II) | 58.24 | 91.88 | 86.71 | 10.07 | 1.57 |

[a]Number of run – 10, range – 5–120.

In Table 3, the effect of adsorbent dosage is shown and basic statistical solutions and experimental ranges of the removal capacities for t HS, AS and WS are given for further analysis. Similarly, in Table 4, the effect of contact time is presented and basic statistical solutions and experimental ranges of the removal capacities for the adsorbents used are given for further analysis. The experiments are repeated as twice to increase the reliability and average values of removal capacities are used for analysis.

In order to make a decision which of various models (linear, quadratic, or cubic) is better to describe removal capacities of Cu(II) and Zn(II) ions by HS, AS and WS, statistical calculations were carried out. Their results are given in Tables 5–7.

Table 5

Model summary statistics of HS for selecting the adequacy of the models

| | The effect of initial pH | | | | | | | | | |
|---|---|---|---|---|---|---|---|---|---|---|
| | Removal of Cu(II) | | | | | Removal of Zn(II) | | | | |
| Source | Std. Dev | $R^2$ | Adju. $R^2$ | Pre. $R^2$ | PRESS | Std. Dev | $R^2$ | Adj. $R^2$ | Pre. $R^2$ | PRESS |
| Linear | 13.25 | 0.7757 | 0.7308 | 0.3965 | 2360.70 | 9.45 | 0.8028 | 0.7634 | 0.4440 | 1259.36 |
| Quadratic | 4.90 | 0.9755 | 0.9632 | 0.8430 | 614.09 | 5.52 | 0.9462 | 0.9194 | 0.6633 | 762.65 |
| Cubic | 2.11 | 0.9966 | 0.9932 | 0.9543 | 178.67 | 3.73 | 0.9815 | 0.9630 | 0.5601 | 996.51 |
| Quartic | 1.67 | 0.9986 | 0.9957 | 0.9541 | 179.64 | 1.05 | 0.9990 | 0.9971 | 0.8886 | 252.32 |
| Fifth | 2.23 | 0.9987 | 0.9924 | –1.419 | 9465.01 | 0.77 | 0.9997 | 0.9984 | 0.4965 | 1140.50 |
| | The effect of adsorbent dosage | | | | | | | | | |
| | Removal of Cu(II) | | | | | Removal of Zn(II) | | | | |
| Source | Std. Dev | $R^2$ | Adj. $R^2$ | Pre. $R^2$ | PRESS | Std. Dev | $R^2$ | Adj. $R^2$ | Pre. $R^2$ | PRESS |
| Linear | 6.22 | 0.9205 | 0.8941 | 0.6482 | 514.71 | 3.59 | 0.9692 | 0.9589 | 0.8637 | 170.39 |
| Quadratic | 0.81 | 0.9991 | 0.9982 | 0.9940 | 8.75 | 0.75 | 0.9991 | 0.9982 | 0.9893 | 13.40 |
| Cubic | 1.09 | 0.9992 | 0.9968 | 0.8781 | 178.27 | 0.72 | 0.9996 | 0.9983 | 0.9376 | 78.02 |
| | The effect of contact time | | | | | | | | | |
| | Removal of Cu(II) | | | | | Removal of Zn(II) | | | | |
| Source | Std. Dev | $R^2$ | Adj. $R^2$ | Pre. $R^2$ | PRESS | Std. Dev | $R^2$ | Adj. $R^2$ | Pre. $R^2$ | PRESS |
| Linear | 13.32 | 0.1417 | 0.0344 | –0.451 | 2401.66 | 9.57 | 0.2370 | 0.1416 | –0.306 | 1254.85 |
| Quadratic | 12.62 | 0.3260 | 0.1334 | –1.032 | 3362.97 | 9.04 | 0.4044 | 0.2342 | –0.686 | 1619.77 |
| Cubic | 11.64 | 0.5086 | 0.2630 | –8.309 | 15405.9 | 8.58 | 0.5401 | 0.3102 | –7.399 | 8067.66 |
| Quartic | 9.71 | 0.7149 | 0.4868 | –140.8 | 2.347E5 | 7.21 | 0.7291 | 0.5123 | –143.0 | 1.384E5 |
| Fifth | 7.38 | 0.8685 | 0.7042 | –2681 | 4.439E6 | 5.31 | 0.8826 | 0.7357 | –2310 | 2.220E6 |
| Sixth | 5.33 | 0.9486 | 0.8457 | | | 3.92 | 0.9520 | 0.8559 | | |

Values corresponding to suggested models are underlined in the tables. The effect of initial pH can be modelled as cubic for HS, cubic for AS and quadratic for WS for removal of Cu(II) ions. Similarly, the effect of initial pH can be modelled as quartic for HS, cubic for AS and cubic for WS for removal of Zn(II) ions. The effect of adsorbent dosage can be modelled as quadratic for HS, linear for AS and linear for WS for removal of Cu(II) ions. Similarly, the effect of adsorbent dosage can be modelled as quadratic for HS, linear for AS and linear for WS for removal of Zn(II) ions. The effect of contact time can be modelled as fifth for HS, fifth for AS and fifth for WS for removal of Cu(II). Similarly, the effect of contact time can be modelled as fifth for HS, fifth for AS and fifth for WS for removal of Zn(II).

Table 6

Model summary statistics of AS for selecting the adequacy of the models

| | The effect of initial pH | | | | | | | | | |
|---|---|---|---|---|---|---|---|---|---|---|
| | Removal of Cu(II) | | | | | Removal of Zn(II) | | | | |
| Source | Std. Dev | $R^2$ | Adj. $R^2$ | Pre. $R^2$ | PRESS | Std. Dev | $R^2$ | Adj. $R^2$ | Pre. $R^2$ | PRESS |
| Linear | 6.08 | 0.8790 | 0.8548 | 0.6749 | 496.62 | 10.61 | 0.7986 | 0.7583 | 0.4656 | 1492.57 |
| Quadratic | 3.48 | 0.9684 | 0.9225 | 0.8138 | 284.40 | 2.92 | 0.9878 | 0.9817 | 0.9201 | 223.19 |
| Cubic | 1.76 | 0.9939 | 0.9878 | 0.8716 | 196.10 | 1.17 | 0.9985 | 0.9971 | 0.9938 | 17.34 |
| Quartic | 1.20 | 0.9981 | 0.9943 | 0.7429 | 392.78 | 1.32 | 0.9988 | 0.9963 | 0.9771 | 64.05 |
| Fifth | 0.56 | 0.9998 | 0.9988 | 0.6044 | 604.40 | 1.86 | 0.9988 | 0.9926 | –1.362 | 6598.20 |
| | The effect of adsorbent dosage | | | | | | | | | |
| | Removal of Cu(II) | | | | | Removal of Zn(II) | | | | |
| Source | Std. Dev | $R^2$ | Adj. $R^2$ | Pre. $R^2$ | PRESS | Std. Dev | $R^2$ | Adj. $R^2$ | Pre. $R^2$ | PRESS |
| Linear | 3.73 | 0.9755 | 0.9674 | 0.9019 | 167.34 | 2.59 | 0.9881 | 0.9841 | 0.9602 | 67.26 |
| Quadratic | 2.92 | 0.9900 | 0.9800 | 0.8693 | 222.90 | 2.76 | 0.9910 | 0.9819 | 0.8866 | 191.84 |
| Cubic | 2.45 | 0.9965 | 0.9859 | 0.4696 | 904.70 | 2.46 | 0.9964 | 0.9857 | 0.4601 | 913.55 |
| | The effect of contact time | | | | | | | | | |
| | Removal of Cu(II) | | | | | Removal of Zn(II) | | | | |
| Source | Std. Dev | $R^2$ | Adj. $R^2$ | Pre. $R^2$ | PRESS | Std. Dev | $R^2$ | Adj. $R^2$ | Pre. $R^2$ | PRESS |
| Linear | 10.85 | 0.1887 | 0.0873 | –0.391 | 1616.57 | 9.59 | 0.1944 | 0.0937 | –0.398 | 1277.92 |
| Quadratic | 9.92 | 0.4072 | 0.2379 | –0.891 | 2196.80 | 8.70 | 0.4208 | 0.2553 | –0.767 | 1615.94 |
| Cubic | 8.96 | 0.5853 | 0.3780 | –6.333 | 8519.25 | 8.00 | 0.5801 | 0.3701 | –6.532 | 6885.59 |
| Quartic | 7.61 | 0.7505 | 0.5508 | –129.6 | 1.518E5 | 6.74 | 0.7518 | 0.5532 | –139.3 | 1.283E5 |
| Fifth | 5.62 | 0.8911 | 0.7549 | –2311 | 2.686E6 | 4.82 | 0.8985 | 0.7716 | –1846 | 1.689E6 |
| Sixth | 3.96 | 0.9596 | 0.8788 | | | 3.69 | 0.9554 | 0.8662 | | |

Table 7

Model summary statistics of WS for selecting the adequacy of the models

| | The effect of initial pH | | | | | | | | | |
|---|---|---|---|---|---|---|---|---|---|---|
| | Removal of Cu(II) | | | | | Removal of Zn(II) | | | | |
| Source | Std. Dev | $R^2$ | Adj. $R^2$ | Pre. $R^2$ | PRESS | Std. Dev | $R^2$ | Adj. $R^2$ | Pre. $R^2$ | PRESS |
| Linear | 9.56 | 0.8632 | 0.8358 | 0.6697 | 1103.84 | 7.93 | 0.8514 | 0.8217 | 0.5941 | 858.05 |
| Quadratic | 2.34 | 0.9934 | 0.9901 | 0.9737 | 87.87 | 4.65 | 0.9591 | 0.9387 | 0.7148 | 602.86 |
| Cubic | 2.47 | 0.9945 | 0.9891 | 0.8660 | 447.65 | 2.52 | 0.9910 | 0.9819 | 0.8581 | 300.06 |
| Quartic | 1.09 | 0.9993 | 0.9979 | 0.9279 | 240.84 | 2.42 | 0.9945 | 0.9834 | 0.4373 | 1189.68 |
| Fifth | 0.94 | 0.9997 | 0.9984 | 0.4941 | 1690.68 | 2.08 | 0.9979 | 0.9877 | –2.9174 | 8282.02 |
| | The effect of adsorbent dosage | | | | | | | | | |
| | Removal of Cu(II) | | | | | Removal of Zn(II) | | | | |
| Source | Std. Dev | $R^2$ | Adj. $R^2$ | Pre. $R^2$ | PRESS | Std. Dev | $R^2$ | Adj. $R^2$ | Pre. $R^2$ | PRESS |
| Linear | 2.67 | 0.9857 | 0.9810 | 0.9661 | 50.81 | 2.50 | 0.9842 | 0.9790 | 0.9436 | 67.19 |
| Quadratic | 2.34 | 0.9927 | 0.9854 | 0.9598 | 60.30 | 2.46 | 0.9898 | 0.9796 | 0.8644 | 161.52 |
| Cubic | 3.28 | 0.9928 | 0.9713 | –0.079 | 1618.58 | 2.01 | 0.9966 | 0.9864 | 0.48880 | 609.77 |
| | The effect of contact time | | | | | | | | | |
| | Removal of Cu(II) | | | | | Removal of Zn(II) | | | | |
| Source | Std. Dev | $R^2$ | Adj. $R^2$ | Pre. $R^2$ | PRESS | Std. Dev | $R^2$ | Adj. $R^2$ | Pre. $R^2$ | PRESS |
| Linear | 12.79 | 0.1548 | 0.0492 | –0.4262 | 2209.11 | 10.42 | 0.1770 | 0.0741 | –0.4041 | 1481.94 |
| Quadratic | 12.18 | 0.3291 | 0.1374 | –1.0085 | 3111.19 | 9.80 | 0.3636 | 0.1818 | –0.8699 | 1973.57 |
| Cubic | 11.31 | 0.5042 | 0.2563 | –7.9652 | 13886.9 | 9.12 | 0.5273 | 0.2910 | –8.2769 | 9791.31 |
| Quartic | 9.59 | 0.7034 | 0.4661 | –144.50 | 2.254E5 | 7.56 | 0.7295 | 0.5130 | –122.84 | 1.307E5 |
| Fifth | 7.41 | 0.8584 | 0.6814 | –2352.1 | 3.645E6 | 6.00 | 0.8633 | 0.6925 | –2313.8 | 2.443E6 |
| Sixth | 5.93 | 0.9319 | 0.7956 | | | 4.78 | 0.9352 | 0.8055 | | |

An empirical relationship expressed by polynomial equations with the main effects (known as input variables) was fitted between the experimental results and the input variables. The final equations obtained in terms of actual factors as follows:

- The use of HS:

$$Y_{\text{Cu(II)}} = -99.83 + 82.95A - 12.32A^2 + 0.61A^3 \tag{12}$$

$$Y_{\text{Zn(II)}} = -186.76 + 188.75A - 52.65A^2 + 6.52A^3 - 0.29A^4 \tag{13}$$

$$Y_{\text{Cu(II)}} = 19.87 + 14.39B - 0.71B^2 \tag{14}$$

$$Y_{\text{Zn(II)}} = 18.32 + 10.40B - 0.40B^2 \tag{15}$$

$$Y_{\text{Cu(II)}} = 0.86 + 11.64C - 0.53C^2 + 0.01C^3 + 9.53^{-5}C^4 + 3.06^{-7}C^5 \tag{16}$$

$$Y_{\text{Zn(II)}} = 25.24 + 8.62C + 0.40C^2 + 8.12^{-3}C^3 - 7.24^{-5}C^4 + 2.33^{-7}C^5 \tag{17}$$

- The use of AS:

$$Y_{\mathrm{Cu(II)}} = -24.99 + 48.57A - 7.65A^2 + 0.42A^3 \tag{18}$$

$$Y_{\mathrm{Zn(II)}} = -53.72 + 59.31A - 8.09A^2 + 0.37A^3 \tag{19}$$

$$Y_{\mathrm{Cu(II)}} = 29.20 + 6.45B \tag{20}$$

$$Y_{\mathrm{Zn(II)}} = 22.99 + 6.46B \tag{21}$$

$$Y_{\mathrm{Cu(II)}} = 22.72 + 9.28C - 0.42C^2 + 8.54^{-3}C^3 - 7.61^{-5}C^4 + 2.45^{-7}C^5 \tag{22}$$

$$Y_{\mathrm{Zn(II)}} = 28.60 + 8.32C - 0.38C^2 + 7.73^{-3}C^3 - 6.89^{-5}C^4 + 2.22^{-7}C^5 \tag{23}$$

- The use of WS:

$$Y_{\mathrm{Cu(II)}} = -38.66 + 32.91A - 2.27A^2 \tag{24}$$

$$Y_{\mathrm{Zn(II)}} = -64.85 + 62.44A - 10.02A^2 + 0.55A^3 \tag{25}$$

$$Y_{\mathrm{Cu(II)}} = 19.24 + 6.07B \tag{26}$$

$$Y_{\mathrm{Zn(II)}} = 51.27 + 21.65B \tag{27}$$

$$Y_{\mathrm{Cu(II)}} = -5.94 + 11.20C - 0.51C^2 + 0.01C^3 - 9.28^{-5}C^4 + 2.97^{-7}C^5 \tag{28}$$

$$Y_{\mathrm{Zn(II)}} = 17.76 + 8.89C - 0.40C^2 + 8.09^{-3}C^3 - 7.14^{-5}C^4 + 2.28^{-7}C^5 \tag{29}$$

In Equations (12)–(29), the coefficients $A$, $B$ and $C$ represent the effect of initial pH, adsorbent dosage and contact time, respectively.

Based on the $R^2$ value, the performance of the fitted curves is almost near the performance of the second order kinetic equation. Equations (20), (21), (26), and (27) are only expressed by linear regression. These equations occur in a linear form due to the PRESS value (abbr. prediction error sum of squares). As seen in Table 6 and 7, the PRESS values of these equations are smaller than of other ones. The statistical significance of the ratio of mean square variation due to regression and mean square residual error was tested by the ANOVA method. The results showed that the equations adequately represented the actual relationship between the response and significant variables. The values of initial pH, adsorbent dosage and contact time are optimized by the Simplex algorithm [34]. The optimized values are presented in Table 8. Table 9 and 10 present the comparison of biosorption capacity (mg/g) of HS, WS, AS biomass from the Elovich isotherm for Cu(II) and Zn(II) with that of various biomass reported in literature.

Table 8

Optimized values of initial pH, adsorbent dosage and contact time

| Agricultural by-products | Removal efficiency [%] | |
|---|---|---|
| | Cu(II) | Zn(II) |
| The use of AS | | |
| Initial pH 6.29 | 80.81 | 88.75 |
| Adsorbent dosage 8.21 mg/dm$^3$ | 79.47 | 69.59 |
| Contact time 15.41 min | 93.61 | 91.88 |
| The use of HS | | |
| Initial pH 6.85 | 87.45 | 75.71 |
| Adsorbent dosage 8.77 mg/dm$^3$ | 88.49 | 74.52 |
| Contact time 15.99 min | 89.38 | 90.3 |
| The use of WS | | |
| Initial pH 6.53 | 73.74 | 68.44 |
| Adsorbent dosage 8.10 mg/dm$^3$ | 69.51 | 65.05 |
| Contact time 15.67 min | 76.77 | 84.20 |

Table 9

Biosorption capacities of various biosorbents for Cu(II) removal

| Biosorbent | $q_{max}$ [mg·g$^{-1}$] | Reference |
|---|---|---|
| Hazelnut shells | 35.61 | this study |
| Almond shells | 23.35 | this study |
| Walnut shells | 21.28 | this study |
| Peanut shells | 25.4 | [11] |
| Hyacinth roots | 22.7 | [35] |
| Crab shell biomass | 38.62 | [36] |
| Arca shell biomass | 17.64 | |
| Fungal biomass *Botrytis cinerea* | 9.23 | [37] |
| Wheat shell | 8.34 | [38] |
| Cone biomass *Thuja orientalis* | 19.23 | [39] |
| Orange residue | 23.47 | [40] |
| *Pinus silvestris* biomass | 28.83 | [41] |
| Sawdust | 4.9 | [42] |
| Brown alga *Fucus vesiculosus* | 23.4 | |
| Terrestrial moss *Pleurozium schreberi* | 11.1 | |
| Sugar beet pulp | 31.4 | [43] |
| Herbaceous | 4.84 | [44] |
| Dehydrated wheat bran | 51.5 | [45] |
| Wheat straw | 4.48 | [46] |
| Soybean straw | 5.44 | |
| Crab shell | 44.94 | |
| Rice bran | 27.81 | |
| *Focus vesiculosus* | 23.4 | [42] |
| Arca shell | 26.88 | |

Table 10

Biosorption capacities of various biosorbents for Zn(II) removal

| Biosorbent | $q_{max}$ [mg·g$^{-1}$] | Reference |
|---|---|---|
| Hazelnut shells | 57.69 | this study |
| Almond shells | 22.6 | this study |
| Walnut shells | 25.7 | this study |
| *Padina* sp. | 35.1 | [47] |
| *Sargassum* sp. | 29.8 | |
| *Laminaria hyperborea* | 19.2 | [48] |
| *Sargassum muticum* | 34.1 | [49] |
| *Fucus spiralis* | 34.3 | [50] |
| *Bifurcaria bifurcata* | 30.3 | |
| *Ceratophyllum demersum* | 13.98 | [51] |
| *Fontinalis antipyretica* | 15 | [52] |
| Cork ($C_0$ = 10 mg/dm$^3$) | 3.4 | [53] |
| Cork ($C_0$ = 70 mg/dm$^3$) | 7.5 | |
| Cork ($C_0$ = 150 mg/dm$^3$) | 12,4 | |
| *Myriophyllum spicatum* | 15.59 | [54] |
| *Streptomyces noursei* | 1.6 | [55] |
| *Chlorella kessleri* ($C_0$ = 9 mg/dm$^3$) | 4.15 | [56] |
| *Chlorella kessleri* ($C_0$ = 68 mg/dm$^3$) | 20.53 | |
| *Chlorella kessleri* ($C_0$ = 150 mg/dm$^3$) | 40.38 | |

## 4. CONCLUSIONS

The study revealed that agricultural by-products such as hazelnut, walnut and almond shells, could be used to remove copper(II) and zinc(II) ions from aqueous leachate of industrial waste.

The adsorption of copper(II) and zinc(II) ions on the agricultural by-products is found to be pH, contact time and adsorbent dosage dependent. The maximum adsorption capacity of agricultural by-products was obtained at pH 6 for copper(II) and at pH 8 for zinc(II) ions. The amount of copper(II) and zinc(II) ions removed increased upon increasing the agricultural by-product dosages.

The equilibrium established within the first 10 min. The pseudo second order kinetic model agrees very well with the dynamic behaviour of the adsorption of copper(II) and zinc(II) ions from aqueous leachate of industrial waste onto agricultural by-products.

The shells under investigation had relatively high capacities for the removal of copper(II) and zinc(II) ions from aqueous leachate of industrial waste. Furthermore, as seen from Tables 9 and 10, the removal efficiencies of the proposed agricultural by products are higher than those of various bio-sorbents reported in the literature.

## REFERENCES


[1] FERNÁNDEZ Y., MARAÑÓN E., CASTRILLÓN L., VÁZQUEZ I., J. Hazar. Mat., 2005, 126, 169.
[2] ŚLĘZAK R., KRZYSTEK L., LEDAKOWICZ S., Environ. Prot. Eng., 2009, 35 (3), 81.
[3] BOHDZIEWICZ J., KWARCIAK A., NECZAJ E., Environ. Prot. Eng., 2005, 31 (3-4), 61.
[4] BILGILI M.S., DEMIR A., □NCE M., ÖZKAYA B., J. Hazar. Mater., 2007, 145, 186.
[5] RODRÍGUEZ J., CASTRILLÓN L., MARAÑÓN E., SASTRE H., FERNÁNDEZ E., Water Resour., 2004, 38, 3297.
[6] GUPTA V.K., SHRIVASTAVA A.K., JAIN N., Water Resour., 2001, 35, 4079.
[7] EL-ASHTOUKHY E.-S.Z., AMIN N.K., ABDELWAHAB O., Desalination, 2008. 223, 162.
[8] JAIN C.K., SINGHAL D.C., SHARMA M.K., J. Hazar. Mater., 2004, 114, 231.
[9] SÖLENER M., TUNALI S., ÖZCAN A.S., ÖZCAN A., GEDIKBEY T., Desalination, 2008, 223, 308.
[10] WAFWOYO W., SEO C.W., MARSHALL S.E., J. Chem. Technol. Biotechnol., 1999, 74, 1117.
[11] WITEK-KROWIAK A., SZAFRAN R.G., MODELSKI S., Desalination, 2011, 265(1-3), 126.
[12] CIMINO G., PASSERINI A., TOSCANO G., Water Resour., 2000, 34, 2955.
[13] LOW K.S., LEE C.K., LEO A.C., Biores. Technol., 1995, 51, 227.
[14] HO Y.S., MCKAY G., Water Resour., 2000, 34, 735.
[15] POOTS V.J.P., MC KAY G., HEALY J.J., J. Water Pollut. Control Feder., 1978, 50, 926.
[16] AL-ASHEH S., DUVNJAK Z., Adv. Environ. Res., 1997, 2, 194.
[17] MARSHALL W.E., JOHNS M.M., J. Chem. Technol. Biotechnol., 1996, 66, 192.
[18] MISHRA S.P., TIWARI D., DUBEY R.S., Appl. Radiat. Isotopes., 1997, 48, 877.
[19] YU B., ZHANG Y., SHUKLA A., SHUKLA S.S., DORRIS K.L., J. Hazar. Mater., 2000, 84, 83.
[20] BALKÖSE D., BALTACIOĞLU H., J. Chem. Technol. Biotechnol., 1992, 54, 393.
[21] AZAB M.S., PETERSON P.J., Water Sci. Technol., 1989, 21, 1705.
[22] ZAGGOUT F.R., Asian J. Chem., 2001, 13, 639.
[23] DANG V.B.H., DOAN H.D., DANG-VU T., LOHI A., Biores. Technol., 2009, 100, 211.
[24] *Shake Extraction of Solid Waste with Water*, Am. Soc. Test. Mater., ASTM 3987-85, [In:] *Annual Book of ASTM Standards*, West Conshohocken, 1990, PA.
[25] LOW K.S., LEE C.K., LEE K.P., Biores. Technol., 1993, 44, 109.
[26] DORRLS K.L., YU B., ZHANG Y., SHUKLA A., SHUKLA S.S., J. Hazar. Mater., 2000, 80, 33.
[27] BULUT Y., TEZ Z., J. Hazar. Mater., 2007, 149, 35.
[28] HO Y.S., Scientometrics, 2004, 59, 171.
[29] LOW M.J.D., Chem. Rev., 1960, 6, 267.
[30] CHIEN S.H., CLAYTON W.R., Soil Sci. Soc. Am. J., 1980, 44, 265.
[31] SPARKS D.L., *Kinetics and Mechanisms of Chemical Reactions at the Soil Mineral/Water Interface*, [In:] *Soil Physical Chemistry*, CRC Press, Boca Raton, 1999, Florida.
[32] SRIHARI V., DAS A., Desalination, 2008, 225, 220.
[33] AL-ASHEH S., BANAT F., ABU-AITAH L., Sep. Purif. Technol., 2003, 33, 1.
[34] CHVATAL V., *Linear Programming*, W.H. Freeman Comp., New York, 1983.
[35] ZHENG J.-C., FENG H.-M., LAM M.H.-W., J. Hazar. Mater., 2009, 171, 780.
[36] DAHIYA S., TRIPATHI R.M., HEGDE A.G., J. Hazar. Mater., 2008, 150, 376.
[37] AKAR T., TUNALI S., MIneral. Eng., 2005, 18, 1099.
[38] BASCI N., KOCADAGISTAN E., KOCADAGISTAN B., Desalination, 2004, 164, 135.
[39] NUHOGLU Y., OGUZ E., Process Biochem., 2003, 38, 1627.
[40] KHORMAEI M., NASERNEJAD B., EDRISI M., J. Hazar. Mater., 2007, 149, 269.
[41] UCUN H., AKSAKAL O., YILDIZ E., J. Hazar. Mater., 2009, 161, 1040.
[42] GRIMM A., ZANZI R., BJÖRNBOM E., Bioresour. Technol., 2008, 99, 2559.
[43] ZÜMRIYE AKSU Z., ISAOĞLU I.A., Process Biochem., 2005,40, 3031.

[44] GÜNDOGAN R., ACEMIOGLU B., ALMA M.H., J. Colloid Interface Sci., 2004, 269, 303.
[45] ÖZER A., ÖZER D., ÖZER A., Process Biochem., 2004, 39, 2183.
[46] SCIBAN M., KLASNJA M., SKRBIC B., Desalination, 2008, 229, 170.
[47] SHENG P.X., TING Y.P., CHEN P., HONG L., J. Colloid Interface Sci., 2004, 275, 131.
[48] PURANIK P.R., PAKNICAR K.M., Bioresour. Technol., 1999, 70, 269.
[49] YU Q., MATHEICKAL J.T., YIN P., KAEWSARN P., Water Res., 1999, 33(6), 1534.
[50] PRASAD M.N.V., FREITAS H., Environ. Pollut., 2000, 110, 277.
[51] KESKINKAN O., GOKSU M.Z.L., BASIBUYUK M., FORSTER C.F., Biores. Technol., 2004, 92, 197.
[52] MARTINS R.J.E., PARDO R., BOAVENTURA R.A.R., Water Res., 2004, 38, 693.
[53] CHUBAR N., CARVALHO J.R., CORREIA M.J.N., Physicochem. Eng. Aspects, 2004, 230, 57.
[54] KESKINKAN O., GOKSU M.Z.L., YUCEER A., BASIBUYUK M FORSTER C.F., Process Biochem., 2003, 39, 179.
[55] RUIZ C.G., TIRADO V.R., GIL B.G., Biores. Technol., 2008, 99, 3864.
[56] HORVATHOVA H., MRAZIKOVA A., KADUKOVA J., STOFKO M., *Zinc Removal from Model Solution by Biosorption*, 4th European Bioremediation Conference, Chania, Crete, Greece, September 3–8, 2008.